

---

**mgr Emilia Balcer**

**Badania nad wybranymi metodami potencjalnie  
poprawiającymi skuteczność terapeutyczną  
4-borono-L-fenyloalaniny w terapii borowo-  
neutronowej**

**Rozprawa na stopień doktora nauk medycznych i nauk o zdrowiu  
w dyscyplinie nauki farmaceutyczne**

Promotorzy: dr hab. Joanna Giebułtowicz, prof. dr hab. Ewa Bulska

Promotor pomocniczy: dr Monika Sobiech

Zakład Chemii Leków, Analizy Farmaceutycznej i Biomedycznej

Wydział Farmaceutyczny Warszawskiego Uniwersytetu Medycznego



**WYDZIAŁ  
FARMACEUTYCZNY  
WUM**

Obrona rozprawy doktorskiej przed Radą Dyscypliny Nauk Farmaceutycznych  
Warszawskiego Uniwersytetu Medycznego

Warszawa 2023

---

**Słowa kluczowe:** 4-borono-L-fenylalanina, polimery wdrukowane molekularnie, ICP-MS pojedynczej komórki, nośniki boru, terapia borowo-neutronowa, L-fenylalanina, L-tyrozyna, wstępna ekspozycja na L-aminokwasy

**Keywords:** *4-borono-L-phenylalanine, molecularly imprinted polymers, Single Cell ICP-MS, boron carriers, boron neutron capture therapy, L-phenylalanine, L-tyrosine, L-amino acid preloading*

---

**Radiofarmaceutyki dla ukierunkowanej molekularnie diagnostyki i terapii medycznej,  
RadFarm.**

Projekt w ramach konkursu Narodowego Centrum Badań i Rozwoju POWER Nr POWR.03.02.00-00-I009/17-00 (Program Operacyjny Wiedza Edukacja Rozwój 2014-2020 współfinansowany ze środków Europejskiego Funduszu Społecznego).

---

Serdecznie dziękuję moim promotorkom, dr hab. Joannie Giebułtowicz, prof. dr hab. Ewie Bulskiej oraz dr Monice Sobiech, za zaangażowanie, nieustanne wsparcie oraz ogromną pomoc okazaną w trakcie wykonywania niniejszej pracy.

Dziękuję dr hab. Piotrowi Lulińskiemu, dr Małgorzacie Sochackiej, dr Annie Ruszczyńskiej oraz mgr Magdalenie Muszyńskiej za nieocenioną pomoc w pracy badawczej i współpracę naukową.

Szczególnie podziękowania składam filarom mojego życia prywatnego: rodzicom, Elżbiecie i Tadeuszowi, babciom, Zofii i Mariannie, krewnym – Agnieszce, Tomkowi, Annie, Wojtkowi, Uli i Andrzejowi, Monice Ładzie, bliskim przyjaciołom i współpracownikom – Lidii, Natalii, Kasi i Izie, a także mojej drugiej rodzinie – Annie, Mateuszowi, Kaziowi i Feli, bez których ta praca by nie powstała.



---

## Wykaz publikacji stanowiących pracę doktorską

1) **Balcer E.**, Sobiech M., Luliński P., *Molecularly Imprinted Carriers for Diagnostics and Therapy – A Critical Appraisal*. Pharmaceutics, 2023, 15(6), 1647. Punkty IF: 5,4; Punkty MEiN: 140;

2) **Balcer E.**, Sobiech M., Giebułtowicz J., Sochacka M., Luliński P., *Molecularly Imprinted Polymers Specific towards 4-Borono-L-Phenylalanine – Synthesis Optimization, Theoretical Analysis, Morphology Investigation, Cytotoxicity, and Release Studies*, Polymers, 2023, 15(14), 3149. Punkty IF: 5,0; Punkty MEiN: 100;

3) **Balcer E.**, Giebułtowicz J., Sochacka M., Ruszczyńska A., Muszyńska M., Bulska E., *Investigation of the Impact of L-Phenylalanine and L-Tyrosine Pre-Treatment on the Uptake of 4-Borono-L-Phenylalanine in Cancerous and Normal Cells Using an Analytical Approach Based on SC-ICP-MS*, Molecules, 2023, 28(18), 6552. Punkty IF: 4,6; Punkty MEiN: 140.

---

## Spis treści

Wykaz publikacji stanowiących pracę doktorską .....	5
Wykaz skrótów i symboli.....	7
Streszczenie .....	8
1. Wstęp.....	12
2. Założenia i cel pracy .....	15
3. Kopie opublikowanych prac.....	17
3.1. Molecularly Imprinted Carriers for Diagnostics and Therapy – A Critical Appraisal..	17
3.2. Molecularly Imprinted Polymers Specific towards 4-Borono-L-Phenylalanine – Synthesis Optimization, Theoretical Analysis, Morphology Investigation, Cytotoxicity, and Release Studies .....	36
3.3. Investigation of the Impact of L-Phenylalanine and L-Tyrosine Pre-Treatment on the Uptake of 4-Borono-L-Phenylalanine in Cancerous and Normal Cells Using an Analytical Approach Based on SC-ICP-MS .....	55
4. Podsumowanie i wnioski.....	66
5. Oświadczenia współautorów prac .....	68
6. Bibliografia.....	82

---

## Wykaz skrótów i symboli

<b>BNCT</b>	(ang. <i>boron neutron capture therapy</i> ) terapia borowo-neutronowa
<b>BPA</b>	(ang. <i>4-borono-L-phenylalanine</i> ) 4-borono-L-fenyloalanina
<b>MIP</b>	(ang. <i>molecularly imprinted polymer</i> ) polimer wdrukowany molekularnie
<b>ICP-MS</b>	(ang. <i>inductively coupled plasma mass spectrometry</i> ) spektrometria mas sprzężona z plazmą wzbudzaną indukcyjnie
<b>SC-ICP-MS</b>	(ang. <i>single cell inductively coupled plasma mass spectrometry</i> ) spektrometria mas pojedynczej komórki sprzężona z plazmą wzbudzaną indukcyjnie
<b>LAT-1</b>	(ang. <i>L-amino acid transporter-1</i> ) transporter-1 L-aminokwasów

---

## Streszczenie

Leczenie chorób nowotworowych wciąż pozostaje jednym z największych wyzwań współczesnej medycyny. Obiecującą alternatywą dla konwencjonalnych metod terapeutycznych jest terapia borowo-neutronowa (BNCT), przeżywająca obecnie renesans, dzięki postępom w rozwoju akceleratorów. Zasada działania BNCT opiera się na wykorzystaniu reakcji jądrowej zachodzącej pomiędzy izotopem boru  $^{10}\text{B}$ , dostarczającym do miejsca zmienionego nowotworowo, a neutronami termicznymi z zewnętrznej wiązki dostarczanej przez akceleratory lub reaktory jądrowe. Produktami tej reakcji są ciężkie jony, które niszczą komórki nowotworowe. Istotnym ograniczeniem terapii jest jednak brak odpowiednio efektywnego nośnika boru. Zmodyfikowanie używanego już w praktyce klinicznej związku boru np. poprzez zastosowanie nowoczesnych systemów dostarczania leków, może być obiecującym rozwiązaniem w uzyskaniu nośnika boru dla BNCT.

W niniejszej pracy skupiłam się na metodach potencjalnie poprawiających skuteczność terapeutyczną 4-borono-L-fenyloalaniny (BPA), związku boru stosowanego w praktyce klinicznej w BNCT, badając dwa aspekty. Pierwszy koncentrował się na opracowaniu i charakterystyce polimerów wdrukowanych molekularnie (MIPs), nowoczesnych materiałów polimerowych, jako systemów dostarczania BPA. Drugi aspekt, oparty na badaniach komórkowych, dotyczył zastosowania aminokwasowych analogów BPA układu L, w celu zwiększenia ilości BPA dostarczanej do komórek. L-aminokwasy są transportowane poprzez mechanizm antyportowy sprzężony z substratem, co powoduje, że przedekspozycyjne narażenie (ang. *preloading*) na wybrany analog nasila wychwyt BPA. W celu oceny tego wychwytu opracowałam nową metodę oznaczania stężenia boru w komórkach z wykorzystaniem spektrometrii mas pojedynczej komórki sprzężonej z plazmą wzbudzaną indukcyjnie (SC-ICP-MS).

Z powodzeniem zsyntetyzowałam MIPs specyficzne wobec BPA o strukturze tzw. plastra miodu metodą polimeryzacji rodnikowej. Nie wykazały one cytotoksyczności w stosunku do zbadanych nowotworowych i prawidłowych linii komórkowych. Przedekspozycyjne narażenie na L-tyrozinę pokazało istotnie statystyczny wpływ na wychwyt BPA zarówno w komórkach niedrobnokomórkowego raka płuc, jak i prawidłowych fibroblastach płuc. Zastosowanie SC-ICP-MS do oznaczania boru dostarczyło nowych informacji na temat jego dystrybucji w komórkach i podkreśliło niejednorodność zawartości boru w przypadku komórek nowotworowych.

Badania dowiodły, że zaprojektowane MIPs mają potencjał do dalszych zastosowań *in vivo* jako nośniki BPA dla BNCT, natomiast przedekspozycyjne narażenie na L-tyrozinę

---

wyduje się być obiecującym dodatkowym narzędziem w użyciu BPA w BNCT. Ponadto, opracowana nowa metoda analizy boru z zastosowaniem SC-ICP-MS, może stać się znaczącą techniką w dalszych badaniach nad terapiami opartymi na wykorzystaniu boru.

---

## Abstract

### **Title: Studies on the selected methods potentially improving the therapeutic effectiveness of 4-borono-L-phenylalanine in boron neutron capture therapy**

Treatment of cancerous diseases still remains one of the biggest challenges of modern medicine. A promising alternative to conventional therapeutic modalities is boron neutron capture therapy (BNCT), a method currently experiencing a renaissance, due to the latest advances in the development of accelerators. The principle of BNCT is the use of a nuclear reaction occurring between  $^{10}\text{B}$  isotope, specifically delivered to the tumour site, and thermal neutrons from the external beam, provided by accelerators or nuclear reactors. The products of this reaction are heavy ions that destroy cancerous cells. A significant limitation, however, is the lack of appropriately effective boron carrier. The modification of a boron compound already implemented in clinical practice with e.g. the use of modern drug delivery systems, may be a promising solution to obtaining an appropriate boron carrier for BNCT.

In this study, I focused on the methods potentially improving the therapeutic effectiveness of 4-borono-L-phenylalanine (BPA), a boron compound already used in clinical practice in BNCT, by investigating two aspects. The first one concentrated on the design and characterization of molecularly imprinted polymers (MIPs), modern polymeric materials, as BPA delivery systems. The second, cellular-assay-based, concerned using the L-amino-acidic analogues of BPA in order to increase the BPA uptake in cells. L-amino acids are transported through an antiport mechanism coupled with a substrate, which causes the preloading with the chosen analogue to enhance BPA uptake. In order to assess this uptake, I developed a new method for the determination of boron concentration in cells using single cell inductively coupled plasma mass spectrometry (SC-ICP-MS).

I successfully synthesized MIPs of honeycomb-like structure using radical polymerization method, which were specific towards BPA and have shown no cytotoxicity towards tested cancerous and normal cell lines. Preloading with L-tyrosine has shown statistically significant effect on the BPA uptake in both non-small cell lung carcinoma cells and normal lung fibroblasts. The use of SC-ICP-MS in boron determination provided new information on its distribution in cells and highlighted the heterogeneity in boron content in the case of cancerous cells.

The research proved that the designed MIPs have the potential for further *in vivo* applications as BPA carriers in BNCT, and that preloading with L-tyrosine seems a promising additional tool in BNCT treatment using BPA. Moreover, the newly developed method of boron

---

analysis using SC-ICP-MS may become a significant technique in further research on boron-based therapies.

---

## 1. Wstęp

Konwencjonalne metody stosowane w leczeniu chorób nowotworowych, takie jak chemo- czy radioterapia, często nie są w stanie przynieść odpowiednio skutecznych odpowiedzi terapeutycznych, a ich efekty niepożądane mogą znacznie obniżyć jakość życia pacjentów. Jednym z relatywnie nowych rozwiązań tych problemów może być terapia borowo-neutronowa (ang. *boron neutron capture therapy*, BNCT), która dzięki znaczącemu postępowi w konstrukcji akceleratorów, przeżywa w ciągu ostatnich dwóch dekad renesans [1]. W BNCT wykorzystywana jest reakcja jądrowa zachodząca pomiędzy izotopem boru  $^{10}\text{B}$ , dostarczonym przez nośnik boru podawany pacjentowi przed napromienianiem, a neutronami termicznymi z zewnętrznego źródła. Główne produkty tej reakcji, cząstki alfa oraz jądro  $^7\text{Li}$ , to ciężkie cząstki naładowane, silnie jonizujące i o krótkim zasięgu, zdolne do efektywnego niszczenia komórek nowotworowych [1]. Obecnie, jednym z największych wyzwań BNCT, jest zapewnienie odpowiedniego nośnika boru, który powinien charakteryzować się m.in. zdolnością dostarczania odpowiednio dużej ilości boru (20-50  $\mu\text{g } ^{10}\text{B}$  na gram tkanki nowotworowej), specyficznym wiązaniem tylko z komórkami nowotworowymi, niską toksycznością, odpowiednio długą retencją w guzie i relatywnie szybkim usuwaniem z krwioobiegu [2]. Ze względu na wysokokosztową i technicznie problematyczną produkcję związków boru wzbogaconych w izotop  $^{10}\text{B}$  [3], skupienie się na tych już poznanych i stosowanych w praktyce klinicznej wydaje się być wysoce zasadne. Połączenie ich z nowoczesnymi systemami dostarczania leków to jeden z kierunków rozwoju nośników boru opisywany przez wielu naukowców [4].

Związkiem boru szeroko stosowanym w praktyce klinicznej jest 4-borono-L-fenyloalanina (BPA), pochodna L-fenyloalaniny, zawierająca jeden atom boru w cząsteczce [4]. Ze względu na niski stopień rozpuszczalności BPA w wodzie, substancja ta podawana jest w formie kompleksu z D-fruktozą [5]. BPA jest dostarczana do komórek w organizmie poprzez transport aktywny, z udziałem transporterów aminokwasów typu L, głównie transportera-1 (LAT-1) [6]. Intensywny wzrost komórek nowotworowych powoduje zwiększenie ich zapotrzebowania na aminokwasy, co prowadzi do nadekspresji transporterów aminokwasów, czyniąc z nich obiecujące cele molekularne [7]. W przypadku BPA, LAT-1 stanowi cel molekularny. Niekorzystnym zjawiskiem podczas terapii BPA jest konkurencyjny transport innych aminokwasów typu L do komórek, co może przyczyniać się do zbyt krótkiej retencji BPA w tkankach nowotworowych [8]. Grupa badawcza pod kierunkiem Nomoto wyjaśniła to zjawisko jako mechanizm antyportowy [8], powodujący ciągłą wymianę BPA



---

wewnątrz- i zewnątrzkomórkowego z L-aminokwasami. Uniemożliwia to osiągnięcie odpowiednio wysokiego stężenia BPA w komórkach i tym samym obniża efektywność terapii. Obecnie w badaniach klinicznych opracowuje się nowe protokoły dozowania BPA w połączeniu z podawaniem innego związku boru, pochodnej dodekaboranu, w celu utrzymania odpowiedniego stężenia boru w miejscu zmienionym nowotworowo [4]. Może się to jednak wiązać z niekomfortowym dla pacjenta przedłużeniem czasu infuzji dożylniej. W badaniach podstawowych i przedklinicznych proponowane są więc inne metody poprawy dostępności BPA.

Jedną z metod poprawy dostępności BPA opisała wspomniana już grupa Nomoto, która zastosowała kompleksowanie BPA poli(alkoholem winylowym) [8]. Utworzony kompleks został przetransportowany do komórek drogą endocytozy z wykorzystaniem LAT-1, co skutkowało wolniejszym usuwaniem BPA z komórek niż w przypadku standardowo podawanego kompleksu BPA z D-fruktozą. Zakładając uzyskanie podobnego efektu w przypadku użycia innych związków polimerowych, obiecującym rozwiązaniem może być zastosowanie polimerów wdrukowanych molekularnie (MIPs). MIPs należą do grupy nowoczesnych materiałów polimerowych, charakteryzujących się wysoką selektywnością wobec wybranej cząsteczki oraz stabilnością chemiczną i termiczną [9]. Synteza MIP, nazywana również drukowaniem molekularnym, jest trzyetapowa i obejmuje utworzenie kompleksu prepolimeryzacyjnego między wybranym monomerem funkcyjnym oraz cząsteczką szablonu (wdrukowywaną w strukturę polimeru), reakcję polimeryzacji, oraz usunięcie szablonu z otrzymanego MIP [10]. Co istotne, MIPs wykazują wysoką zdolność do integracji z innymi materiałami, czyniąc z nich obiecujące systemy dostarczania leków wzbogacone o elementy typu cząstki magnetyczne, fluorofory, czy domeny rozpoznające wybrane cele molekularne [11]. MIPs jako materiały do dostarczania związków boru nie były do tej pory opisane.

Kolejną metodą poprawy dostępności BPA może być zastosowanie jej analogów – innych aminokwasów typu L. Strategia ta wykorzystuje antyportowy, sprzężony z substratem mechanizm transportu L-aminokwasów [12]. Zwiększone wewnątrzkomórkowe stężenie L-aminokwasów stymuluje proces transportu zewnątrzkomórkowej BPA do komórek [13]. Wpływ tej metody na wychwyt BPA był badany zarówno na modelach komórkowych i zwierzęcych, jak i wycinkach tkanek ludzkich, skupiając się głównie na zastosowaniu takich aminokwasów jak L-tyrozyna, L-DOPA oraz L-fenylalanina, a badane modele obejmowały przede wszystkim nowotwory mózgu i czerniaka [13–22]. Choć wiele doniesień literaturowych potwierdza skuteczność tej metody [15–18], nie zawsze przynosi ona oczekiwane skutki

---

[13,14,19–21]. Według Yanga i in. [21], stymulujący efekt zależy od histologii i umiejscowienia nowotworu, przez co nie w każdym przypadku zauważalne będą korzystne z punktu widzenia skuteczności terapii rezultaty. Dlatego też zasadność zastosowania tej strategii, jako sposobu na zwiększenie efektywności dostarczania BPA, powinna być ustalana dla konkretnego nowotworu. Brak jest obecnie doniesień literaturowych o wpływie przedeksponowania na L-aminokwasy na wychwyt BPA w modelu raka płuc, a także o jego wpływie na wychwyt BPA w komórkach prawidłowych. Do badań zawartości i dystrybucji BPA w komórkach stosowano do tej pory przede wszystkim techniki oparte na spektroskopii mas [13,23–25] i emisyjnej spektroskopii atomowej [26,27], które z wyjątkiem spektrometrii mas jonów wtórnych (będącej jednak metodą o niskiej przepustowości) [13] nie pozwalają na przeanalizowanie dystrybucji boru na poziomie pojedynczej komórki oraz struktur subkomórkowych. Stąd też zapotrzebowanie na metodę, za pomocą której możliwe będzie określenie wychwytu BPA na poziomie komórki, co pozwoli na udoskonalenie protokołów terapeutycznych stosowanych w BNCT. Odpowiedzią na tę potrzebę może być technika ICP-MS pojedynczej komórki (SC-ICP-MS), mierząca stężenie określonego pierwiastka na poziomie pojedynczych komórek, dzięki czemu uzyskiwane są dane różnicujące badaną populację komórek [28]. SC-ICP-MS stanowi stosunkowo nową metodę, opisaną w relatywnie małej liczbie publikacji [29], a jej zastosowanie w określaniu zawartości boru nie było do tej pory udokumentowane.

---

## 2. Założenia i cel pracy

Celem niniejszej pracy było zbadanie metod potencjalnie prowadzących do poprawienia skuteczności terapeutycznej BPA w BNCT. W szczególności zaproponowałam dwa aspekty: MIP jako system dostarczania BPA do komórek, oraz zastosowanie przedeksponowanego narażenia na aminokwasowe analogi BPA typu L na modelu niedrobnokomórkowego raka płuc. W celu oznaczenia stężenia i dystrybucji boru w populacji komórek opracowałam także nową metodę analityczną na bazie techniki SC-ICP-MS. Ze względu na istotne ograniczenia BNCT, związane z brakiem efektywnych nośników boru oraz wysokokosztowym i technicznie problematycznym procesem otrzymywania związków boru wzbogaconych w izotop  $^{10}\text{B}$ , w pracy skupiłam się na badaniach mających na celu polepszenie działania stosowanego obecnie w BNCT związku boru.

Cel badawczy zrealizowałam w poniżej opisanych etapach:

- Przygotowanie przeglądu piśmiennictwa na temat zastosowania MIP w terapii i diagnostyce (teranostyce) chorób nowotworowych (**Publikacja 1**);
- Opracowanie i optymalizacja syntezy MIP oraz polimerów kontrolnych, specyficznych wobec BPA (**Publikacja 2**);
- Charakterystyka otrzymanych polimerów pod względem parametrów fizykochemicznych, morfologii i struktury, w celu dokładnego opisu i potwierdzenia uzyskania zaprojektowanego materiału (**Publikacja 2**);
- Zbadanie właściwości adsorpcyjnych otrzymanych polimerów wobec BPA w układach modelowych. Pozwoliło to na wyselekcjonowanie polimeru o największej specyficzności i pojemności adsorpcyjnej wobec BPA, do dalszych badań uwalniania i cytotoksyczności (**Publikacja 2**);
- Zbadanie uwalniania BPA z otrzymanych polimerów w środowisku soli fizjologicznej buforowanej fosforanami, w różnym pH, w celu określenia możliwości zastosowania uzyskanego materiału w układach biologicznych, w warunkach koniecznych dla prowadzenia terapii BNCT (**Publikacja 2**);
- Określenie cytotoksyczności otrzymanych polimerów *in vitro* za pomocą testu redukcji bromku 3-(4,5-dimetylotiazol-2-yl)-2,5-difenylotetrazoliowego wobec dwóch wybranych linii komórkowych – niedrobnokomórkowego raka płuc, linia A549, oraz prawidłowych fibroblastów płuc, linia V79-4. Informacja ta jest niezbędna dla wstępnego oszacowania bezpieczeństwa stosowania uzyskanego materiału w modelach *in vivo* (**Publikacja 2**);

- 
- Zbadanie wpływu przedekspozycyjnego narażania na L-fenylalaninę i L-tyrozinę na wychwyt BPA *in vitro* w komórkach niedrobnokomórkowego raka płuc (linia A549) i prawidłowych fibroblastach płuc (linia V79-4) za pomocą techniki ICP-MS, w celu oszacowania efektywności tej metody w niedrobnokomórkowym raku płuc (**Publikacja 3**);
  - Zastosowanie techniki SC-ICP-MS do określenia zawartości boru w komórkach linii A549 i V79-4 po ekspozycji na BPA i przedekspozycyjnym narażaniu na L-tyrozinę. Badanie to miało na celu poszerzenie informacji o sposobie dystrybucji boru w komórkach na skutek ekspozycji na BPA, o dane niedostępne w standardowych pomiarach ICP-MS. W metodzie ICP-MS badane komórki mineralizuje się łącznie, więc tracone są informacje o heterogeniczności badanej populacji (**Publikacja 3**).

### 3. Kopie opublikowanych prac

#### 3.1. Molecularly Imprinted Carriers for Diagnostics and Therapy – A Critical Appraisal



Review

## Molecularly Imprinted Carriers for Diagnostics and Therapy—A Critical Appraisal

Emilia Balcer <sup>1</sup>, Monika Sobiech <sup>2,\*</sup> and Piotr Luliński <sup>2</sup>

<sup>1</sup> Department of Drug Chemistry, Faculty of Pharmacy, Medical University of Warsaw, Banacha 1, 02-097 Warsaw, Poland; emilia.balcer@wum.edu.pl

<sup>2</sup> Department of Organic and Physical Chemistry, Faculty of Pharmacy, Medical University of Warsaw, Banacha 1, 02-097 Warsaw, Poland; piotr.lulinski@wum.edu.pl

\* Correspondence: monika.sobiech@wum.edu.pl; Tel.: +48-22-5720950

**Abstract:** Simultaneous diagnostics and targeted therapy provide a theranostic approach, an instrument of personalized medicine—one of the most-promising trends in current medicine. Except for the appropriate drug used during the treatment, a strong focus is put on the development of effective drug carriers. Among the various materials applied in the production of drug carriers, molecularly imprinted polymers (MIPs) are one of the candidates with great potential for use in theranostics. MIP properties such as chemical and thermal stability, together with capability to integrate with other materials are important in the case of diagnostics and therapy. Moreover, the MIP specificity, which is important for targeted drug delivery and bioimaging of particular cells, is a result of the preparation process, conducted in the presence of the template molecule, which often is the same as the target compound. This review focused on the application of MIPs in theranostics. As an introduction, the current trends in theranostics are described prior to the characterization of the concept of molecular imprinting technology. Next, a detailed discussion of the construction strategies of MIPs for diagnostics and therapy according to targeting and theranostic approaches is provided. Finally, frontiers and future prospects are presented, stating the direction for further development of this class of materials.

**Keywords:** molecularly imprinted polymer; diagnostic agent; targeted delivery; cancer therapy; theranostic



**Citation:** Balcer, E.; Sobiech, M.; Luliński, P. Molecularly Imprinted Carriers for Diagnostics and Therapy—A Critical Appraisal. *Pharmaceutics* **2023**, *15*, 1647. <https://doi.org/10.3390/pharmaceutics15061647>

Academic Editors: Ortensia Ilaria Parisi, Manuel A. N. Coelho and Sílvia Castro Coelho

Received: 27 April 2023

Revised: 24 May 2023

Accepted: 1 June 2023

Published: 3 June 2023



**Copyright:** © 2023 by the authors. Licensee MDPI, Basel, Switzerland. This article is an open access article distributed under the terms and conditions of the Creative Commons Attribution (CC BY) license (<https://creativecommons.org/licenses/by/4.0/>).

### 1. Introduction

Along with the growing number of emerging new methods of combating cancerous diseases, a certain information noise can be observed in the scientific literature. Numerous advancements in analytical and synthetic techniques of the past decades allowed researchers to design limitless amounts of potential therapeutic or diagnostic agents. While this increases the chances of significant discoveries, the primary focus in all such studies should always continue to improve the quality of life of patients. Regarding that, one of the most-promising fields in current medical research is personalized medicine, closely related to targeted therapy and diagnostics, which simultaneously may provide a valuable theranostic approach.

Conventional methods in cancer therapy, such as chemotherapy or radiotherapy while still used as first-choice options, very often exhibit dose-limiting toxicity. The result of such a treatment is an ineffective therapy and further deterioration of the physical and psychological well-being of a patient, which often crucially affects therapeutic success or failure. Targeted therapy promises a solution to that problem by the ability to precisely reach the neoplastic cells in the tumor microenvironment. Therapeutic agents delivered to the sites of interest possess the ability to more effectively inhibit cell proliferation and destroy cancerous tissues. Direct drug binding and the possibility of increasing the dosage of a medicine that no longer reaches normal cells reduce the adverse side

effects of therapy. While very promising in theory, many studies have shown that the efficacy of targeted therapy can significantly fluctuate in different groups of patients on an individual level [1]. The explanation for that phenomenon is the heterogeneity of tumors. Diversity in their genome and phenotype causes the choice of a molecular target to be a long and complicated process, often resulting in changing targets at different stages of therapy. To overcome this obstacle, the choice of therapeutic agents should be preceded by routine genome screenings in order to obtain accurate characterizations of tumors on the microenvironmental level. That operation will lead to the appropriate selection of biomarkers further used for treatment planning and monitoring [2].

Here, one of the important aspects is therapeutic agents that exhibit a molecular recognition ability and have been identified as being of special importance in targeted therapy. Apart from the agents consisting of the drug itself, a strong focus is put on the development of drug carriers for which the introduction to the market dates back the mid-Twentieth Century [3]. The use of drug carriers allows for utilizing other types of recognizing molecules that could not be individually used as drugs due to, e.g., an insufficient toxic effect on cancer cells, as well as opens the way to the design of theranostic agents for simultaneous diagnostics and treatment or combination therapies, where the synergistic effect can improve the efficacy of the treatment.

Taking into account that fact, the idea of theranostics was implemented in medicine [4]. Over the years, the concept expanded beyond nuclear medicine, where it initially started, and became an area of interest for other fields in medical studies. The development of the field of theranostics is closely related to the many new solutions introduced in material sciences. A significant part of research concerning theranostic platforms currently focuses on nanomedical devices, mostly in regard to cancerous diseases. Nanoscale materials in medical studies offer a number of advantages that make these kinds of composites a perfect fit for reaching the tumor environment. One such quality is the ability to modify the structure or surface of nanomaterials, especially nanoparticles, in various ways and with many different compounds including targeting ligands, linkers, and drug molecules. This feature seems particularly important as it allows utilizing the active targeting approach, in addition to the enhanced permeability and retention effect (selective accumulation of nanoparticles observed due to the characteristics of tumor tissues [5]) that is demonstrated by nanomaterials and used as a passive targeting method (liposomes, polymeric micelles, dendrimers, quantum dots, and metallic, inorganic, and protein-based nanoparticles) [6–8]. Above that, one of the very promising branches of nanomedicine in regard to theranostic applications is radiopharmacy [9]. Current limitations that slow down the process of the clinical translation of all nanomedical platforms are mostly related to the toxicity triggered by the response of the immune system, which leads to the instability of the compound and its rapid clearance. Another containment is the manufacturing process, which should allow for the cost-effective production of materials of controlled and desired qualities, while maintaining Good Manufacturing Practice standards required by supervisory agencies and their established regulations [10].

The exploration of new drug delivery materials that offer improved transport properties, provide optimized pharmacokinetic profiles, control the drug release rate, and maintain the drug concentration within its therapeutic window, as well as enhance delivery efficacy by increasing diffusivity and biodistribution is currently one of the hot topics in medicine. Here, strong attention has been drawn to those based on molecularly imprinted polymers (MIPs) because of their advantages such as high selectivity, chemical and thermal stability, and capability to integrate with other materials, which is very important in the case of diagnostics and therapy.

In this review, the concept of molecular imprinting and its potential in therapy will be presented prior to the construction strategies of MIPs for diagnostics and therapy according to targeting and theranostic approaches. Finally, a critical outlook of synthetic feasibility and applications emphasizing the frontiers together with future prospects for that class of materials is pointed out.



## 2. Concept of Molecular Imprinting and Its Potential in Therapy

MIPs are a class of polymeric materials prepared during a three-step synthetic process (Figure 1). In the first step, a template molecule (an imprinted compound) creates a prepolymerization complex with selected functional monomer(s), involving non-covalent interactions (non-covalent strategy) [11] or a chemical reaction is carried out to form bonds between the template and the functional monomer, resulting in a functionalized template (covalent strategy) [12]. Then, the prepolymerization complex or functionalized template is cross-linked during the polymerization process, and in the final stage, the template is removed from the polymeric matrix, either by extraction or chemical cleavage, leading to the surface modification of the resulting polymer [13].

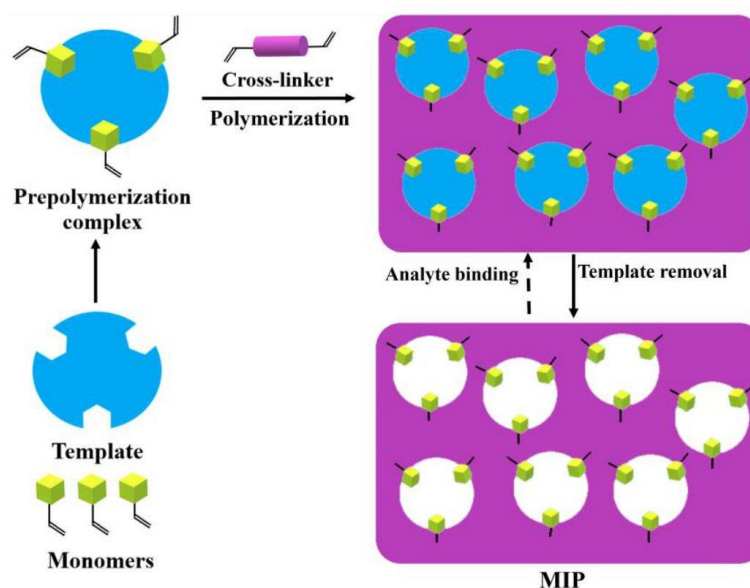


Figure 1. Concept of molecular imprinting.

The route to obtain a specific MIP involves the use of a template molecule that is the same compound as the target one. This means that the MIP is dedicated to the chemical compound that was imprinted, and to this compound, it should possess the highest specificity. Alternatively, the close structural analog of the compound to which the MIP shall possess specificity is often used as a template in the synthesis of MIPs. A plethora of papers describe the effectiveness of such an approach, and here, paclitaxel could be an example [14]. In the case of low stable macromolecules used as the templates, the “epitope-imprinting” process is a good alternative [15,16]. It assumes the use of a peptide as a template to form a MIP with desired specificity towards a protein. Although multiple peptides have been used as templates, the choice of peptide should be carefully screened, taking into account the antigenic domain of the corresponding therapeutic antibody that targets the receptor [17]. Moreover, the process has been adopted in the surface imprinting technique, allowing obtaining MIPs with more proper characteristics of mass transfer and sorption kinetics [18].

Up to date, MIPs are considered to be a very mature class of materials that have found widespread application in separation science and in the detection of molecules, mostly because of their properties such as high selectivity, thermal and chemical stability, and reusability [19,20]. The facile preparation together with relatively low costs have resulted in the enormous utilization of materials in the field of analytical chemistry as stationary

phases in solid phase extraction and as parts of the receptor elements coupled with different detection systems [21–23]. It is extremely important to emphasize the advantages of MIP sensors prepared as the nanocomposites of molecularly imprinted polypyrrole film, gold nanoparticles, functionalized black phosphorus nanosheets [24], or as the molecularly imprinted polypyrrole film-coated poly(3,4-ethylenedioxythiophene)-polystyrene sulfonate-functionalized black phosphorene composite [25].

The potential of MIPs for therapy was recognized in early 2000s [26] with the idea of “intelligent drug release” and “magic bullet” drug targeting, opening significant future opportunities for the application of MIPs. Since that time, a few important papers have been published, describing the possible applications of MIPs for ocular, transdermal, or oral routes of administration. Those studies were comprehensively discussed in recent reviews [27–29]. It should be underlined that some ideas such as the use of molecularly imprinted soft contact lenses for ocular therapy [30–32], the construction of transdermal patches with MIPs for nicotine prolonged delivery [33], or studies of floating molecularly imprinted gastroretentive carriers [34] have contributed significantly to the field.

It should be mentioned that the nature of the molecularly imprinted matrix plays a crucial role in the drug release profile. Since the imprinting process itself is considered to be very complex in nature, the mechanisms of the release of drugs from MIPs could be complex, as well. Here, the swelling controlled systems such as low cross-linked hydrogels or non-swelling controlled systems such as more rigid polymer networks could be considered. In the latter systems, the relaxation of the polymer matrix governs the penetration of physiological fluid inside the net, and the transport is characterized by Fick’s laws of diffusion [35]. However, in various molecularly imprinted systems, anomalous transport mechanisms are observed because multiple complementary or sterically oriented functional residues interact with the drug, delaying its release despite the swelling degree of the polymer [36–38]. Finally, the mechanism that involves the release of a drug in a physical stimuli-responsive manner, for instance as a consequence of the response to a shift of physical (thermo-, solvent-, magnetic-responsive or photo-/radiation-sensitive) or chemical factors [15,34,39–44], is also considered.

Since MIPs are often described as “synthetic antibodies”, the comparison to monoclonal antibodies or aptamers should be mentioned. The biggest issue concerning MIPs in regard to the differences between these materials is still the insufficient amount of data regarding the behavior of MIPs in the biological environment. Despite that, the advantageous low cost of production, physical and chemical stability, and the wide choice of monomers for the imprinting process of MIPs altogether present a strong argument for further studies and development of MIPs for theranostics [45]. As an additional advantage compared to other drug delivery forms, such as those based on metallic nanoparticles, MIPs imprinted with epitopes, as prepared, do not require functionalization with other targeting compounds, which significantly simplifies the preparation process.

Therefore, one of the most important MIP advances is their capability for integration with various materials that could disclose additional properties such as magnetic or photochemical ones. This has opened MIPs to a broad perspective for new applications in the field of diagnostics and therapy, a field that has recently become a scientific hot topic for the exploration of MIPs [46]. Thus, the enormous progress of concepts brought the idea of “intelligent drug release” and “magic bullet” drug targeting into realization.

### 3. Construction Strategies of MIPs for Diagnostics and Therapy

The capability for the integration of MIPs with various materials has been widely adopted in the construction of MIPs for diagnostics and therapy. Here, we would like to present recent approaches in the construction of MIP-based devices for diagnostics and therapy taking into account the targeting and theranostic aspects. It has to be underlined that the presence of a MIP as an integrated part of the device (or platform) gives the opportunity to serve as the drug carriers (for instance, in cancer therapy) or to serve as



ligands that recognize specific domains on the cell surface (for instance, glycoproteins overexpressed by the cancer process) [47].

### 3.1. Targeting Approaches

Since the majority of recent platforms for drug (and other compounds) delivery focus on some form of targeting strategy, two separate approaches should be highlighted, viz. active targeting, which refers to specific molecular recognition of a chosen domain that is overexpressed on cancer cells (for this purpose, different ligands binding to these domains are used), and the passive strategy, which relies mostly on the enhanced permeability and retention effect, which allows small molecules to accumulate in tumor sites. Since the terminology of passive and active targeting refers to the biological activity of a compound, here, the delivery of platforms based on their magnetic properties will be considered a different passive targeting method.

#### 3.1.1. MIPs for Active Targeting

The concept of personalized medicine emphasizes that the choice of the specific target should be based on the genetics of individual tumors, but only a finite amount of targets can be found in the recent literature. Some of the most-commonly studied cancer biomarkers such as the epidermal growth factor receptors EGFR and HER2 or folate receptor were already thoroughly described in other reviews in regard to MIPs [29,46,48]. Here, other targets recently considered in the design of MIP-based platforms are discussed.

CD59 is a protein overexpressed in different types of tumors such as breast, lung, and ovarian cancer [49], and some recent papers on its use as a target for MIP-based composites can be found. In an excellent paper, published by Peng and co-workers [15], gadolinium-doped silicon nanocrystals were synthesized to serve as a fluorescent/magnetic resonance (MR) dual-imaging agent. Subsequently, the material was combined with (7*S*,8*S*)-3-carboxy-5-(carboxymethyl)-13-ethenyl-18-ethyl-7,8-dihydro-2,8,12,17-tetramethyl-21*H*,23*H*-porphine-7-propanoic acid (chlorin e6) prior to modification by tetraethyl orthosilicate and 3-(trimethoxysilyl) propyl methacrylate. Chlorin e6 is recognized as one of the most-commonly used photosensitizers applied in photodynamic therapy. Finally, the MIP layer was conjugated, containing two kinds of cavities after elution. The first cavity type was left by the CD59 protein's epitope, while the other one was left to load an appropriate amount of doxorubicin, a commonly used anti-neoplastic drug for chemotherapy. In another paper, the tumor-sensitive biodegradable MIP particles with a fluorescent component based on zeolitic imidazolate framework-8 were constructed for targeted imaging and delivery of doxorubicin (Figure 2) [50]. During the construction process, fluorescent particles—carbon dots—were encapsulated together with doxorubicin in the zeolitic imidazolate framework-8 through a one-pot method. In order to stabilize the prepared core and give it targeting ability, the MIP layer with the use of the *N*-terminal epitope of the CD59 glycoprotein as the template was synthesized on the core surface. After core modification with application of trifluoromethyl acrylate (monomer), the MIP shell was synthesized from dimethylaminoethyl methacrylate, *N*-isopropylacrylamide, *N*-tert-butylacrylamide (monomers), and *N,N'*-diacryloylcystamine (cross-linker). The use of *N,N'*-diacryloylcystamine introduced into the MIP matrix disulfide bridges, which were broken under the tumor microenvironment because of the high concentration of glutathione. Additionally, dimethylaminoethyl methacrylate, the main monomer used during synthesis, caused the protons in low pH to swell. Therefore, the MIP matrix degraded under the tumor microenvironment so that the internal part of the component containing the drug was exposed to a weak acidic environment to achieve drug release through further degradation.

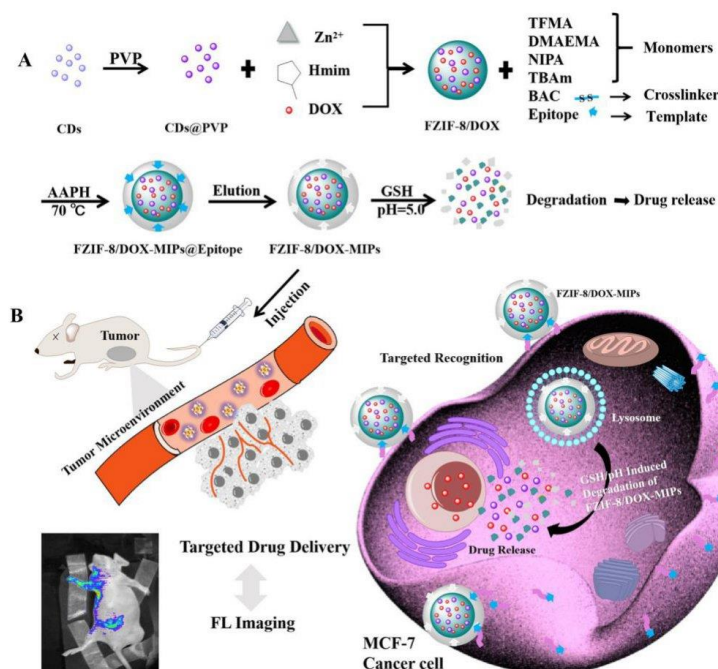


**Figure 2.** (A) Synthesis and glutathione/pH dual stimulation degradation route of doxorubicin MIP-stabilized fluorescent zeolitic imidazolate framework-8 (FZIF-8/DOX-MIPs); (B) schematic illustration of targeted imaging and glutathione/pH-responsive drug delivery of FZIF-8/DOX-MIPs [50]. Copyright 2020, American Chemical Society.

Another target worth mentioning is CD47, a protein overexpressed in various cancer cells [51]. Wang and co-workers [52] used an approach combining fluorescence imaging and targeted chemodynamic therapy—a method of oncotherapy based on the use of cytotoxic hydroxyl radical converted from  $\text{H}_2\text{O}_2$  by chemodynamic agents [53]. In this study, a composite consisting of fluorescent calcium peroxide as an imaging probe and a source of  $\text{H}_2\text{O}_2$  and epitope imprinted polymer as a recognition unit for targeting CD47 was prepared. The MIP matrix contained copper acrylate, *N*-isopropylacrylamide, 4-vinylpyridine (monomers), and *N,N'*-diacryloylcystamine (cross-linker) residues. As the template, the exposed peptide of the extracellular domain from CD47 was used. The MIP possessing specific recognition sites enabled targeting CD47-positive cells. The cross-linker, having disulphide bonds, was reduced under the cancer cell microenvironment, then the MIP was degraded gradually, and the fluorescent calcium peroxide could contact with water in a weak acidic environment to generate  $\text{H}_2\text{O}_2$ . Copper ions from the MIP matrix catalyzed the production of the hydroxyl radical from  $\text{H}_2\text{O}_2$  to eliminate the cancer cells. The therapeutic efficacy of the composite was tested in an in vitro model. The results showed promising biodegradable material properties, which should be further evaluated in cytotoxicity studies on cancerous and normal cells.

The carcino-embryonic antigen, a tumor marker used for diagnostic purposes in, i.e., colorectal cancer [54], was also considered in regard to MIPs for specific recognition. In a study by Han and co-workers [55], a successful synthesis of a composite based on graphene oxide, equipped with specific sites for molecular recognition of carcino-embryonic tumor markers and loaded with doxorubicin, was reported. During the preparation process, magnetic graphene oxide was obtained and functionalized with boronic acid residues. Next,

the MIP, produced from dopamine used as monomer and carcino-embryonic tumor markers used as the template, was grafted onto the surface of modified magnetic graphene oxide. Lastly, the prepared material was mixed with doxorubicin to prepare the final product. The designed carrier combines several therapeutic approaches to obtain molecularly and magnetically targeted chemotherapy. The presented results also showed the pH sensitivity of the platform, which could allow for the valuable possibility of controlled drug release and, most importantly, good biocompatibility, an advantageous aspect at this stage of research. While no imaging techniques were suggested to track the obtained material, the magnetic component may be considered as a potential contrast agent for MR imaging.

Targeting sialic acid moieties is another approach used in the treatment of cancer [56]. As an example with regard to MIPs, the synthesis of the derivative of poly(fluorene-*alt*-benzothiadiazole) and phenylboronic acid was carried out [57]. This compound was able to provide a fluorescence response due to the presence of the fluorene and benzothiazole units, possessed a specific region to interact with the sialic acid domain by the dihydroxyborate functional group, and showed adequate hydrophilicity by the presence of quaternary ammonium salts (Figure 3). It was also tested in an in vitro model, proving a selective uptake by cells exhibiting sialic-acid-overexpressed surfaces.

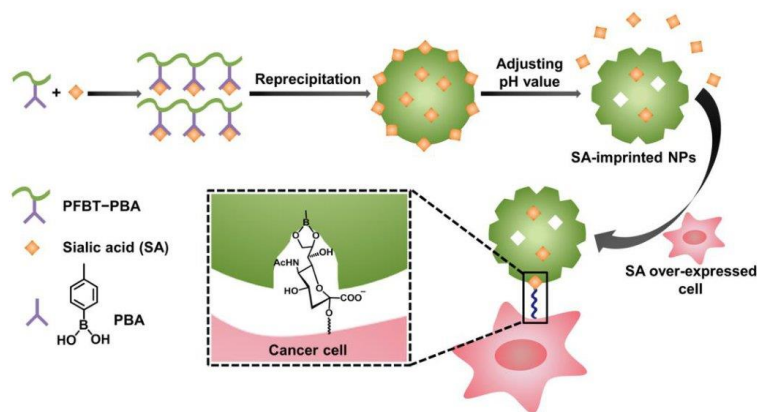


**Figure 3.** Schematic illustration of the preparation of sialic-acid-imprinted nanoparticles and mechanism of their selectivity toward cancer cells [57]. Copyright 2017, American Chemical Society.

### 3.1.2. MIPs for Passive Targeting

A well-described phenomenon of enhanced permeability and retention effect shown by different types of nanomaterials is a hallmark example of a passive targeting approach. While advantageous in many cases, it comes with its own challenges, such as tackling the issue of tumor heterogeneity [58]. Its utility in regard to MIPs has been described in a different review [46], yet considering the capability of MIPs to integrate with various materials and, hence, to design more promising platforms, it does not seem to be one of the more relevant approaches.

Here, the delivery of compounds utilizing their magnetic properties could be considered another passive targeting method. In this method, once the compound containing a magnetic element enters the bloodstream, an external magnetic field is applied in order to guide the compound to the tumor site [59]. MIPs are frequently conjugated to magnetically susceptible cores such as magnetite and/or maghemite, providing a platform that responds to an external magnetic field [60]. Additionally, such platforms could be used as contrast agents in MR imaging [61]. The conjugation of MIPs is mostly carried out on the magnetite surface, modified by tetraethyl orthosilicate and 3-(trimethoxysilyl)propyl methacrylate. This step additionally protects the magnetite core against oxidation and degradation, which could be considered also a very important problem. Here, the extended studies were



provided to reveal the effect of magnetic MIPs on cell survival or their degradation in a bioenvironment [62]. It was found that the degradation of maghemite MIPs in lysosome-like buffer evidenced the potential shielding effect of the polymer coating, but enzymes potentially present in the intracellular compartments modulated it. A very brilliant idea was proposed by Chen and co-workers [63], who prepared catalase-imprinted fibrous composite nanoparticles as an integrated platform for imaging and photothermal therapy. The ellipsoidal nanoplatform was composed of a magnetic  $\beta$ -FeOOH nanorod core and a catalase-imprinted fibrous siloxane/polydopamine composite shell. The comprehensive physicochemical analysis confirmed the structure and composition of the obtained composite. A study conducted by Parisi and co-workers [64] should also be highlighted as it proposed a new method of simplified synthesis by precipitation photo-polymerization in order to obtain magnetic imprinted nanospheres for the delivery of an anti-neoplastic drug, 9H-carbazole derivative. The magnetic element of the designed carrier,  $\text{Fe}_3\text{O}_4$  particles, was suggested to act as a vehicle for targeted delivery through the use of an external magnetic field. While the composite showed promising results, regarding binding capacity and selectivity for the chosen drug, as well as a cytotoxic effect in cancer cells, additional biological tests would have to be conducted to confirm the compound's safety required for potential experiments using animal models, such as stability and release studies in human plasma and viability studies on normal cell lines.

### 3.2. Theranostic Approaches

The recent progress of research on MIPs for biomedical applications creates numerous possibilities of using MIPs as theranostic platforms aiming for various techniques (Figure 4). Current studies, concerning the above-mentioned topic to a large extent, focus on the exploitation of various MIP-based theranostic agents for fluorescent bioimaging [17,40,50,65–69] and were already thoroughly described in other reviews [45,46,70]. While the use of fluorescent materials in the preliminary studies on cell cultures and small animal models ensures a relatively feasible imaging method and allows investigating biodistribution in these models, the clinical application of this method for the common practice of whole-body imaging in humans is yet to be implemented. Thus, it is of great importance to explore other diagnostic methods, especially those already translated into clinical practice, regarding MIP-based theranostic platforms. Another important factor to consider is ensuring the possibility of real-time imaging during the course of treatment, which would guarantee a higher value in terms of diagnostic utility. A fitting example of such a method is MR imaging, beyond being non-invasive and offering excellent image resolution, for which numerous MIP-based composites, containing elements that may be used as contrast agents (such as iron oxide- or gadolinium-based), can be designed [71]. Additionally, MIP-based composites possessing a magnetic element can be used for precise delivery of a compound with the use of an external localized magnetic field and for utilizing the hyperthermia effect in therapy. In the case of MIP-based platforms using gold nanoparticles, another possibility is computed tomography, for which some studies have suggested utilizing gold nanoparticles as improved contrast agents [72]. Due to the significant functionalization potential of MIPs, there is also the possibility of designing composites imprinted with ligands and proteins that are feasible for radiolabeling. The presence of a radiolabeled ligand in a MIP matrix introduces the possibility of using radiotracer-based diagnostic tools such as positron emission tomography or single-photon emission tomography. Despite the potentially easy synthesis, an important issue in this case could be polymeric degradation caused by radiation emitted by the tracer; hence, radiation stability studies would have to be the first step in the evaluation of such a material. Regarding therapy, numerous reports can be found on using MIPs in delivery for chemotherapy drugs, but also as vehicles for photothermal and photodynamic therapy [29,46,73]. Here, some of the recent studies on MIP-based theranostic agents showing the possibilities of combining different therapeutic and diagnostic methods will be highlighted with a summary of chosen approaches of MIP-based theranostic platforms presented in Table 1.

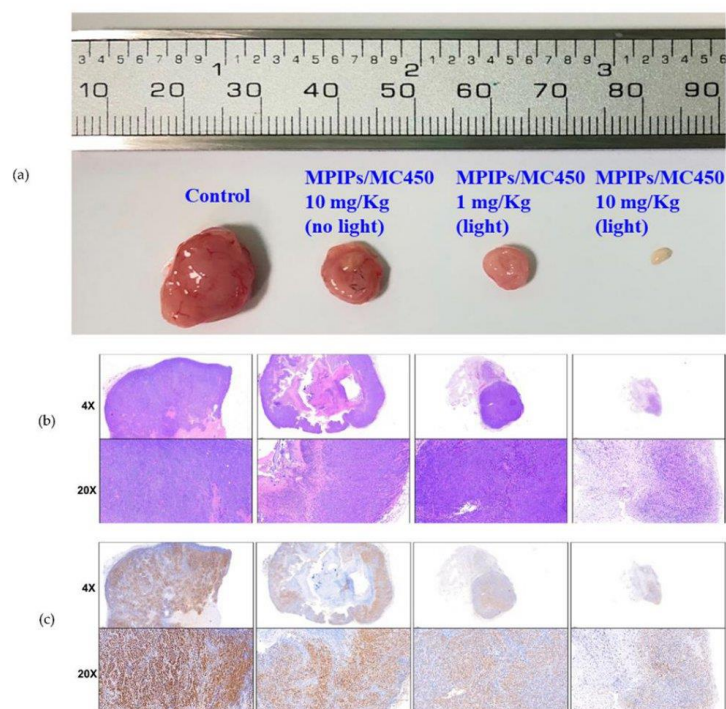


Figure 4. MIP application areas in theranostics.

Table 1. Chosen examples of different theranostic platforms utilizing MIPs.

Type of Formulation	Therapeutic Method	Diagnostic Method	Targeting Approach	Ref.
zeolitic nanoparticles as drug carriers	chemotherapy (doxorubicin)	fluorescence imaging	active targeting to CD59	[50]
Fe <sub>3</sub> O <sub>4</sub> /Fe nanorods	photothermal and radical therapy	MR imaging	magnetic-guided	[63]
core-shell nanoparticles as drug carriers	chemo- (doxorubicin) and photodynamic therapy	MR and fluorescence imaging	active targeting to CD59	[15]
gold nanorods	photothermal therapy	fluorescence imaging	active targeting to sialic acid	[67]
polymeric nanoparticles as drug carriers	chemotherapy (vinblastine)	fluorescence imaging	active targeting to folate	[69]
magnetic MIPs as drug carriers	chemotherapy (9H-carbazole derivative)	MR imaging (not considered in the paper)	magnetic-guided	[64]
graphene oxide-based composite	chemotherapy (doxorubicin)	MR imaging (not considered in the paper)	magnetic-guided and active targeting to carcinoembryonic antigen	[55]
magnetic nanoparticles	photodynamic and immunotherapy	MR imaging (not considered in the paper)	active targeting to programmed death-ligand 1 protein	[74]
silica nanoparticles-based composite	chemodynamic therapy	fluorescence imaging	active targeting to CD47	[52]
Au-embedded nanogels	X-ray radiotherapy	computed tomography (not considered in the paper)	passive targeting through enhanced permeability and retention effect	[75]

In the study conducted by Lee and co-workers, magnetic nanoparticles imprinted with the peptide sequence of programmed death-ligand 1 protein were synthesized with the additional element of immobilized photosensitizer, thus introducing a novel combination of targeted photodynamic and immunotherapy [74]. A significant advantage of this study, regarding all research on the use of MIPs for biomedical applications, was including an experiment on an animal tumor model, which proved that the highest treatment efficiency was observed in the case of combined therapy (Figure 5).



**Figure 5.** Pictures of tumor specimens from the xenograft models with the treatment of peptide-imprinted nanocomposite (a). Hematoxylin and eosin staining of the above tumor specimens (b). Immunohistochemical staining with anti-proliferating cell nuclear antigen primary antibodies (c) [74] (CC-BY 4.0).

Exploiting the magnetic properties of the composite could be another step in the research, possibly allowing for imaging of the synthesized material in an animal model. In a study conducted by the same scientific group [76], an imprinted magnetic platform of structure and application similar to that previously described was prepared, with additional embedded upconversion nanoparticles that permit using near-infrared light in order to activate the photosensitizer included in the composite (Figure 6). A disadvantage of the composite was the demonstrated elevated cytotoxicity in human hepatoblastoma cells (HepG2) in the absence of a near-infrared light source; although, as was pointed out, this effect could be reduced by modifying the nanoparticles' surface—a relatively easy method in the design of MIP-based materials. A different approach to combining MR imaging, fluorescence imaging, chemotherapy, and photodynamic therapy with molecular targeting was described in a study by Peng and co-workers [15]. The obtained composite was tested in vitro and in vivo on a tumor-bearing mice model, and the synergistic effect



of chemodynamic and photodynamic therapy was investigated, showing the highest therapeutic efficacy in the case of combined treatment (Figure 7). In order to confirm biocompatibility of the designed platform, a histopathological analysis was conducted, proving its safety for potential in vivo applications.

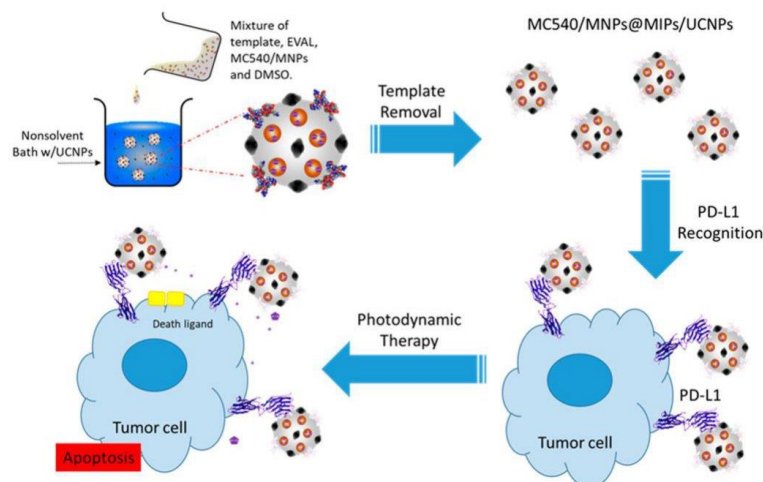


**Figure 6.** Preparation and administration of programmed death-ligand 1 peptide-imprinted composite nanoparticles [76] (CC-BY 4.0).

Although it was suggested that the composite could be used for MR imaging, no such experiments on animal models have been described, and it would be of benefit to consider such studies in the future. In one of the most-recent papers [75], an interesting approach was described by combining MIP hydrogel nanoparticles and gold nanoparticles. The MIP-based hydrogel possesses improved biocompatibility and the potential ability to cross natural barriers, as well as to express prolonged circulation in the blood [77]. At the same time, gold nanoparticles demonstrate potential in various diagnostic and therapeutic applications [78]. Due to the presence of the specific sites for the recognition of human serum albumin, a protein corona is formed around the composite upon exposure to human serum, which ensures a stealth effect and, thus, enhanced stability in vivo. This phenomenon leads to a lower accumulation of the nanomaterial in the spleen and liver, which is a common concern in nanomedicine platforms exploiting gold nanoparticles, and was proven in the study on the mouse model of pancreatic cancer. Here, the accumulation of Au in the organs was investigated with the use of inductively coupled plasma mass spectrometry; however, the properties of gold could allow for its biodistribution measurements through computed tomography, which may provide a potential research topic in future studies. The authors of the described report further highlighted the radiosensitizing properties of gold, which increased the therapeutic efficacy of X-ray radiotherapy, where the mechanism of passive targeting through an enhanced permeability and retention effect was utilized. The key advancement regarding this study is the possibility of creating stealth nanoplateforms for targeted therapy that do not trigger a response from the immune system, and this was also recently described regarding nanogels imprinted with the fragment crystallizable domain of immunoglobulin G [79].

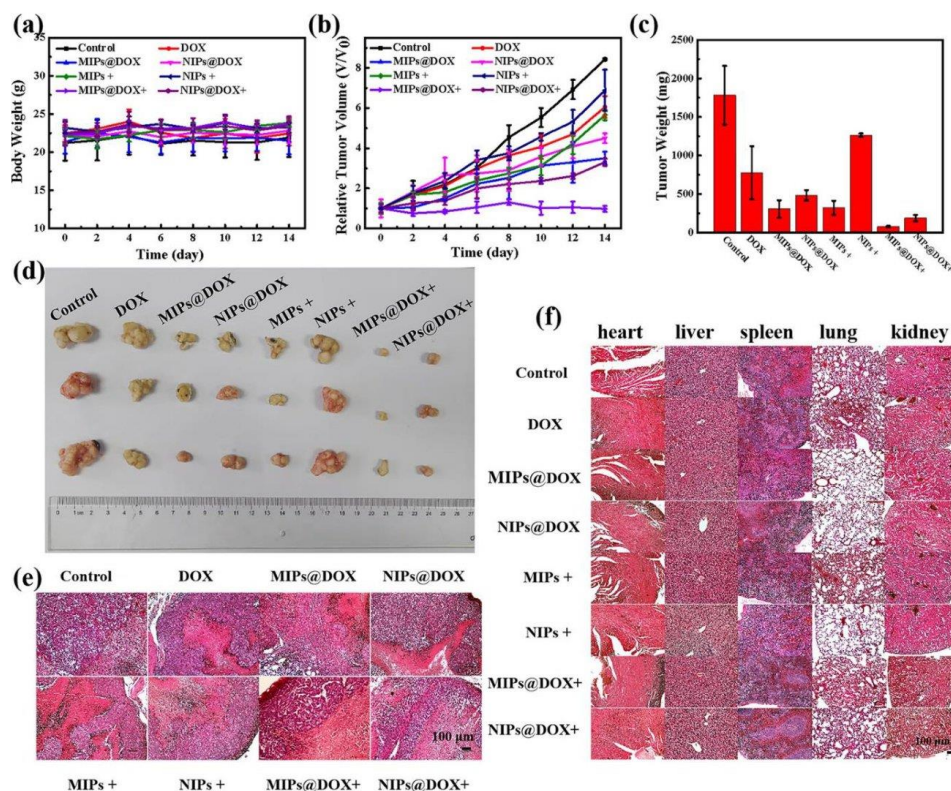


**Figure 7.** The effect of imprinted and non-imprinted drug carrier doxorubicin treatment of mice according to body weight changes (a), relative tumor volume (b), average tumor weight (c), and corresponding tumor tissues (d). Hematoxylin and eosin staining of tumor sections (e) and main organs (f). Reprinted with permission from [15]. Copyright 2020, American Chemical Society.

To sum up, the main advantages of MIPs include the possibility of producing them from various compounds and the capability of integrating them with different materials in order to create platforms with huge potential in diagnostics and therapy. More interestingly, due to the synthetic process, MIPs contain regions on their surface that are specific towards targeted domains, for instance on the cell surface. Thus, as prepared, MIPs do not have to be further functionalized with targeting ligands. This is a great advantage of MIPs that allows omitting additional steps of preparation, notably considering those materials for theranostics.

#### 4. Frontiers and Future Prospects

Taking into account the frontiers in the field of MIPs for theranostics, they could be related to the effectiveness of the imprinting process, the biosafety of materials (mostly for those at the nanosize scale), and the regulatory measures that allow them to be implemented in clinical practice.

It should be mentioned that, while the imprinting process of low-molecular weight compounds looks straightforward, the use of this technology for effective imprinting of high-molecular weight compounds and macromolecules is more complicated. The formation of prepolymerization complexes with small organic molecules was proven in



many studies by spectroscopic methods, such as proton nuclear magnetic resonance [80,81], and by theoretical analysis, which is a powerful tool used to support the stabilization of adducts, as well as to explain the nature of possible interactions [82]. It could be supposed that the prepolymerization complexes affect the extension of the surface of the resulting polymers, at least when highly cross-linked materials are synthesized, which was also proven by the porosity measurements [83,84]. Nevertheless, a few problems related to the conformational or isomeric stability of templates should be kept in mind while designing MIPs. Moreover, the harsh polymerization conditions, frequently used for the preparation of MIPs, can also affect the structural stability of the template [85]. Here, a careful choice of templates together with the application of more controllable polymerization techniques could be considered a solution. In our opinion, special attention should be paid to the previously mentioned epitope imprinting technique, seeming to be one of the most-promising approaches described thus far to effectively provide MIP systems specific towards macromolecules.

The polymerizable components of the prepolymerization mixture play a crucial role in the formation of the MIP. Here, various functional monomers and cross-linkers are applied to serve as compounds, forming a polymer backbone of the MIP. These aspects were closely discussed in many reviews dedicated to MIPs and will be omitted here [19,46]. The application of vinyl-derived compounds, such as methacrylic acid, *N*-isopropylacrylamide, *N,N*-methylenebisacrylamide, and ethylene glycol dimethacrylate, was verified by many scientific groups, but, in our opinion, extended investigations of naturally derived compounds are still required. From our perspective, it is important to pay special attention not only to the biocompatibility of MIPs, but also (if possible) to the biodegradability of MIPs as materials for theranostics. For example, as components, carboxymethyl cellulose–chitosan/alginate composite [86], Konjac glucomannan extracted from Konjac tubers [87], tannic acid [88], fructose [89], and glucose [90] have been examined as the potential materials to form MIPs as drug carriers. Those naturally derived compounds can easily undergo reactions to provide specific functional groups, which are limited due to their low selectivity. The biodegradability of MIPs could be provided by the application of naturally derived components, but the resulting MIPs are characterized, in general, by low selectivity. The alternative could be an application of metal–organic frameworks to provide biodegradability. In a very interesting paper, biodegradable magnesium-ion-doped silica-based molecularly imprinted nanoparticles for targeting tumor cells and drugs' controlled release were described [91]. The construction involved a new degradable functional monomer prepared from glycerol and lactide, on magnesium-ion-doped stellated mesoporous silica nanoparticles, for the delivery of doxorubicin. The molecularly imprinted layer avoided premature drug leakage, which is considered to be an important problem of MIPs as drug carriers. Meanwhile, the large number of ester bonds contained in the functional monomers in the layer was degraded by protonation in the tumor microenvironment to expose the drugs, because of the Mg–O bond property to pH-sensitive breakage in the slightly acidic conditions [50]. Similarly, it is worth mentioning that zinc-based metal–organic frameworks can undergo complete biodegradation in an acidic environment. A different way to introduce biodegradability to the MIP is to use the well-known derivatives of poly( $\epsilon$ -caprolactone) [92] or poly(lactide-co-glycolide) [93]. However, this approach has been little investigated until now. Finally, the problem of the insufficient binding capacity of the MIP drug carrier should be discussed. Here, the use of a metal–organic framework was analyzed for targeted delivery of doxorubicin [94]. Porous zirconium-based metal–organic frameworks are characterized by a high specific surface area and extended porosity. Thus, conjugated with MIPs, they could provide satisfactory drug loading efficiency. Similarly, the use of polyhedral oligomeric silsesquioxanes, the organic–inorganic hybrids of a cage-like architecture, together with liquid crystal monomers was verified as efficient to provide an improvement of the physical and mechanical properties of the composite. The favorable material properties were a result of the reinforcement of the rigidity of the polymers at the molecular level [95].

Another aspect regarding the biosafety of MIPs is the very limited data related to the behavior of the material in the biological environment, a significant disadvantage compared to other competing drug delivery systems. Even though the design of novel composites of different structures brings valuable information and broadens the knowledge of the synthetic process of MIPs, it would be beneficial to focus on a thorough examination of already described materials regarding their biocompatibility and biodegradability on *in vitro* and *in vivo* models. Results from more extensive biological studies could potentially pinpoint the specific problems shared by all MIP-based platforms, which are not noticeable at the physicochemical characterization stage of research, providing the information about critical aspects of designing MIPs for medical applications.

The main challenge, in regard to designing novel theranostic agents based on MIPs but also other materials (such as nanoparticles, liposomes, proteins), remains the costly *in vivo* studies on animal models. Similar to any new pharmaceutical being introduced to the market, they need to be in compliance with appropriate drug administration agency standards and regulations, which means being subjected to all stages of pre-clinical and clinical trials [96]. Aside from the length and high cost of such studies, reproducibility and the ability to scale-up the whole manufacturing process are other important challenges that need to be overcome. It is preferable that all the possible issues related to production are described at the earlier stages of the new platform's design, to ensure that not only medical, but also the economic benefits would be significant. In the case of nanovehicles, many characteristics concerning clearance and, hence, biosafety can be considered at the initial design stage through a careful choice of the nanomaterial's size, shape, and its surface modification (leading to, for example, stealth nanoplateforms) [97]. For MIPs specifically, theoretical studies will be especially useful in this early phase. The complexity of all of the novel nanosystems seems to be currently on the rise. While the development process becomes often more complicated, it is also a trigger for new discoveries in the material sciences, and most importantly, it significantly increases the effectiveness of these materials. In regard to regulations, a big problem remains also an inefficient classification system for these new theranostic platforms, which, if revised and improved, could help in creating universal protocols, leading to better standardization of the studies involved in the new drug registration process for specific types of materials [98]. It is crucial to emphasize that, while the interdisciplinary cooperation of scientists is essential for the progress in MIP-based theranostic agents' design, the insights from industry specialists experienced in the commercialization of drugs may be the missing aspect that will push the field forward.

The safety measures and clinical studies of new carriers are often omitted together with the long-term compatibility and clinical performance of those materials. It should become a standard in future studies, allowing those materials to be marketed in the foreseeable future. It should be emphasized that the fabrication aspects such as the reproducibility and scale-up possibilities ought to be clarified. Thus, the regulatory affairs, as well as economic aspects could be identified here as a significant barrier to commercialization.

Despite that, a wide selection of carriers with different properties intended for several imaging techniques [99] and various imprinting techniques allowing for targeted drug delivery of high specificity [100] provide a substantial potential of MIP-based platforms in biomedical applications. In the end, it should be emphasized that the statement from the previously referred to review by Sellergren and Allender, "The future will tell how far the imprinting engineers can take MIPs, and whether the fully synthetic antibody is destined to become fact or fiction" [26], is currently being realized. We are the witnesses of a process that looks very promising for the future progress of MIPs in diagnostics and therapy.

**Author Contributions:** Conceptualization, P.L., E.B. and M.S.; resources, E.B., P.L. and M.S.; writing—original draft preparation, E.B., P.L. and M.S.; writing—review and editing, E.B., P.L. and M.S.; supervision, P.L. and M.S.; funding acquisition, E.B. All authors have read and agreed to the published version of the manuscript.



**Funding:** The contribution of Emilia Balcer was realized within the National Centre for Research and Development Project No. POWR.03.02.00-00-I009/17-00 (Radiopharmaceuticals for molecularly targeted diagnosis and therapy, RadFarm. Operational Project Knowledge Education Development 2014–2020 co-financed by the European Social Fund).

**Conflicts of Interest:** The authors declare no conflict of interest.

## References

- Huang, M.; Shen, A.; Ding, J.; Geng, M. Molecularly Targeted Cancer Therapy: Some Lessons from the Past Decade. *Trends Pharmacol. Sci.* **2014**, *35*, 41–50. [\[CrossRef\]](#) [\[PubMed\]](#)
- van't Veer, L.J.; Bernards, R. Enabling Personalized Cancer Medicine through Analysis of Gene-Expression Patterns. *Nature* **2008**, *452*, 564–570. [\[CrossRef\]](#) [\[PubMed\]](#)
- Park, H.; Otte, A.; Park, K. Evolution of Drug Delivery Systems: From 1950 to 2020 and Beyond. *J. Control. Rel.* **2022**, *342*, 53–65. [\[CrossRef\]](#) [\[PubMed\]](#)
- Ehrhardt, J.D., Jr.; Güleç, S. A Review of the History of Radioactive Iodine Theranostics: The Origin of Nuclear Ontology. *Mol. Imaging Radionucl. Ther.* **2020**, *29*, 88–97. [\[CrossRef\]](#)
- Setua, S.; Jaggi, M.; Yallapu, M.M.; Chauhan, S.C.; Danilushkina, A.; Lee, H.; Choi, I.S.; Fakhrullin, R.; Esposti, L.D.; Tampieri, A.; et al. Targeted and Theranostic Applications for Nanotechnologies in Medicine. In *Nanotechnologies in Preventive and Regenerative Medicine*, 1st ed.; Uskoković, V., Uskoković, D.P., Eds.; Elsevier: Amsterdam, The Netherlands, 2018; pp. 399–511.
- Shete, M.B.; Patil, T.S.; Deshpande, A.S.; Saraogi, G.; Vasdev, N.; Deshpande, M.; Rajpoot, K.; Tekade, R.K. Current Trends in Theranostic Nanomedicines. *J. Drug. Deliv. Sci. Technol.* **2022**, *71*, 103280. [\[CrossRef\]](#)
- Alshehri, S.; Imam, S.S.; Rizwanullah, M.; Akhter, S.; Mahdi, W.; Kazi, M.; Ahmad, J. Progress of Cancer Nanotechnology as Diagnostics, Therapeutics, and Theranostics Nanomedicine: Preclinical Promise and Translational Challenges. *Pharmaceutics* **2020**, *13*, 24. [\[CrossRef\]](#)
- Xue, Y.; Gao, Y.; Meng, F.; Luo, L. Recent Progress of Nanotechnology-Based Theranostic Systems in Cancer Treatments. *Cancer Biol. Med.* **2021**, *18*, 336–351. [\[CrossRef\]](#)
- Shende, P.; Gandhi, S. Current Strategies of Radiopharmaceuticals in Theranostic Applications. *J. Drug. Deliv. Sci. Technol.* **2021**, *64*, 102594. [\[CrossRef\]](#)
- Singh, D.; Dilnawaz, F.; Sahoo, S.K. Challenges of Moving Theranostic Nanomedicine into the Clinic. *Nanomed.* **2020**, *15*, 111–114. [\[CrossRef\]](#)
- Arshady, R.; Mosbach, K. Synthesis of Substrate-Selective Polymers by Host-Guest Polymerization. *Macromol. Chem. Phys.* **1981**, *182*, 687–692. [\[CrossRef\]](#)
- Wulff, G.; Sarhan, A. Über die Anwendung von enzymanalogen gebauten Polymeren zur Racemattrennung. *Angew. Chem.* **1972**, *84*, 364. [\[CrossRef\]](#)
- Alvarez-Lorenzo, C.; Concheiro, A. *Handbook of Molecularly Imprinted Polymers*, 1st ed.; Smithers Rapra: Shrewsbury, UK, 2013.
- Tan, L.; Yang, L.-L.; Li, Y.-J.; Jiang, Z.-F.; Li, Q.-Y.; Ma, R.-R.; He, J.-Y.; Zhou, L.-D.; Zhang, Q.-H.; Yuan, C.-S. Investigating Two Distinct Dummy Templates Molecularly Imprinted Polymers as Paclitaxel Adsorbent in Synthesis System and Releaser in Biological Samples. *Microchem. J.* **2021**, *165*, 106042. [\[CrossRef\]](#)
- Peng, H.; Qin, Y.-T.; He, X.-W.; Li, W.-Y.; Zhang, Y.-K. Epitope Molecularly Imprinted Polymer Nanoparticles for Chemo-/Photodynamic Synergistic Cancer Therapy Guided by Targeted Fluorescence Imaging. *ACS Appl. Mater. Interfaces* **2020**, *12*, 13360–13370. [\[CrossRef\]](#) [\[PubMed\]](#)
- Qin, Y.-T.; Peng, H.; He, X.-W.; Li, W.-Y.; Zhang, Y.-K. Highly Effective Drug Delivery and Cell Imaging Using Fluorescent Double-Imprinted Nanoparticles by Targeting Recognition of the Epitope of Membrane Protein. *Anal. Chem.* **2019**, *91*, 12696–12703. [\[CrossRef\]](#)
- Canfarotta, F.; Lezina, L.; Guerreiro, A.; Czulak, J.; Petukhov, A.; Daks, A.; Smolinska-Kempisty, K.; Poma, A.; Piletsky, S.; Barlev, N.A. Specific Drug Delivery to Cancer Cells with Double-Imprinted Nanoparticles against Epidermal Growth Factor Receptor. *Nano Lett.* **2018**, *18*, 4641–4646. [\[CrossRef\]](#)
- Dong, C.; Shi, H.; Han, Y.; Yang, Y.; Wang, R.; Men, J. Molecularly Imprinted Polymers by the Surface Imprinting Technique. *Eur. Polym. J.* **2021**, *145*, 110231. [\[CrossRef\]](#)
- BelBruno, J.J. Molecularly Imprinted Polymers. *Chem. Rev.* **2019**, *119*, 94–119. [\[CrossRef\]](#)
- Janczura, M.; Luliński, P.; Sobiech, M. Imprinting Technology for Effective Sorbent Fabrication: Current State-of-Art and Future Prospects. *Materials* **2021**, *14*, 1850. [\[CrossRef\]](#)
- Ramanavicius, S.; Samukaite-Bubniene, U.; Ratautaite, V.; Bechelany, M.; Ramanavicius, A. Electrochemical Molecularly Imprinted Polymer Based Sensors for Pharmaceutical and Biomedical Applications (Review). *J. Pharm. Biomed. Anal.* **2022**, *215*, 114739. [\[CrossRef\]](#)
- Shahhoseini, F.; Azizi, A.; Bottaro, C.S. A Critical Evaluation of Molecularly Imprinted Polymer (MIP) Coatings in Solid Phase Microextraction Devices. *TrAC Trends Anal. Chem.* **2022**, *156*, 116695. [\[CrossRef\]](#)

23. Sobiech, M.; Luliński, P.; Wieczorek, P.P.; Marć, M. Quantum and Carbon Dots Conjugated Molecularly Imprinted Polymers as Advanced Nanomaterials for Selective Recognition of Analytes in Environmental, Food and Biomedical Applications. *TrAC Trends Anal. Chem.* **2021**, *142*, 116306. [\[CrossRef\]](#)
24. Li, G.; Qi, X.; Wu, J.; Xu, L.; Wan, X.; Liu, Y.; Chen, Y.; Li, Q. Ultrasensitive, Label-Free Voltammetric Determination of Norfloxacin Based on Molecularly Imprinted Polymers and Au Nanoparticle-Functionalized Black Phosphorus Nanosheet Nanocomposite. *J. Hazard. Mater.* **2022**, *436*, 129107. [\[CrossRef\]](#)
25. Li, G.; Wu, J.; Qi, X.; Wan, X.; Liu, Y.; Chen, Y.; Xu, L. Molecularly Imprinted Polypyrrole Film-Coated Poly(3,4-Ethylenedioxythiophene):Polystyrene Sulfonate-Functionalized Black Phosphorene for the Selective and Robust Detection of Norfloxacin. *Mater. Today Chem.* **2022**, *26*, 101043. [\[CrossRef\]](#)
26. Selligren, B.; Allender, C. Molecularly Imprinted Polymers: A Bridge to Advanced Drug Delivery. *Adv. Drug. Deliv. Rev.* **2005**, *57*, 1733–1741. [\[CrossRef\]](#) [\[PubMed\]](#)
27. Luliński, P. Molecularly Imprinted Polymers Based Drug Delivery Devices: A Way to Application in Modern Pharmacotherapy. A Review. *Mater. Sci. Eng. C.* **2017**, *76*, 1344–1353. [\[CrossRef\]](#) [\[PubMed\]](#)
28. Tuwahatu, C.A.; Yeung, C.C.; Lam, Y.W.; Roy, V.A.L. The Molecularly Imprinted Polymer Essentials: Curation of Anticancer, Ophthalmic, and Projected Gene Therapy Drug Delivery Systems. *J. Control. Rel.* **2018**, *287*, 24–34. [\[CrossRef\]](#)
29. He, S.; Zhang, L.; Bai, S.; Yang, H.; Cui, Z.; Zhang, X.; Li, Y. Advances of Molecularly Imprinted Polymers (MIP) and the Application in Drug Delivery. *Eur. Polym. J.* **2021**, *143*, 110179. [\[CrossRef\]](#)
30. Alvarez-Lorenzo, C.; Hiratani, H.; Gómez-Amoza, J.L.; Martínez-Pacheco, R.; Souto, C.; Concheiro, A. Soft Contact Lenses Capable of Sustained Delivery of Timolol. *J. Pharm. Sci.* **2002**, *91*, 2182–2192. [\[CrossRef\]](#)
31. Chu, Z.; Xue, C.; Shao, K.; Xiang, L.; Zhao, X.; Chen, C.; Pan, J.; Lin, D. Photonic Crystal-Embedded Molecularly Imprinted Contact Lenses for Controlled Drug Release. *ACS Appl. Bio. Mater.* **2022**, *5*, 243–251. [\[CrossRef\]](#)
32. Raesian, P.; Rad, M.S.; Khodaverdi, E.; Motamedshariaty, V.S.; Mohajeri, S.A. Preparation and Characterization of Fluorometholone Molecular Imprinted Soft Contact Lenses as Ocular Controlled Drug Delivery Systems. *J. Drug. Deliv. Sci. Technol.* **2021**, *64*, 102591. [\[CrossRef\]](#)
33. Ruela, A.L.M.; Figueiredo, E.C.; Pereira, G.R. Molecularly Imprinted Polymers as Nicotine Transdermal Delivery Systems. *Chem. Eng. J.* **2014**, *248*, 1–8. [\[CrossRef\]](#)
34. Zhang, L.-P.; Wang, X.-L.; Pang, Q.-Q.; Huang, Y.-P.; Tang, L.; Chen, M.; Liu, Z.-S. Solvent-Responsive Floating Liquid Crystalline-Molecularly Imprinted Polymers for Gastroretentive Controlled Drug Release System. *Int. J. Pharm.* **2017**, *532*, 365–373. [\[CrossRef\]](#)
35. Byrne, M.E.; Park, K.; Peppas, N.A. Molecular Imprinting within Hydrogels. *Adv. Drug. Deliv. Rev.* **2002**, *54*, 149–161. [\[CrossRef\]](#) [\[PubMed\]](#)
36. Venkatesh, S.; Saha, J.; Pass, S.; Byrne, M. Transport and Structural Analysis of Molecular Imprinted Hydrogels for Controlled Drug Delivery. *Eur. J. Pharm. Biopharm.* **2008**, *69*, 852–860. [\[CrossRef\]](#) [\[PubMed\]](#)
37. da Silva, M.S.; Viveiros, R.; Morgado, P.L.; Aguiar-Ricardo, A.; Correia, I.J.; Casimiro, T. Development of 2-(Dimethylamino)Ethyl Methacrylate-Based Molecular Recognition Devices for Controlled Drug Delivery Using Supercritical Fluid Technology. *Int. J. Pharm.* **2011**, *416*, 61–68. [\[CrossRef\]](#)
38. Matsumoto, K.; Kawamura, A.; Miyata, T. Conformationally Regulated Molecular Binding and Release of Molecularly Imprinted Polypeptide Hydrogels That Undergo Helix–Coil Transition. *Macromolecules* **2017**, *50*, 2136–2144. [\[CrossRef\]](#)
39. Javanbakht, S.; Saboury, A.; Shaabani, A.; Mohammadi, R.; Ghorbani, M. Doxorubicin Imprinted Photoluminescent Polymer as a pH-Responsive Nanocarrier. *ACS Appl. Bio Mater.* **2020**, *3*, 4168–4178. [\[CrossRef\]](#)
40. Jia, C.; Zhang, M.; Zhang, Y.; Ma, Z.-B.; Xiao, N.-N.; He, X.-W.; Li, W.-Y.; Zhang, Y.-K. Preparation of Dual-Template Epitope Imprinted Polymers for Targeted Fluorescence Imaging and Targeted Drug Delivery to Pancreatic Cancer BxPC-3 Cells. *ACS Appl. Mater. Interfaces* **2019**, *11*, 32431–32440. [\[CrossRef\]](#)
41. Li, L.; Chen, L.; Zhang, H.; Yang, Y.; Liu, X.; Chen, Y. Temperature and Magnetism Bi-Responsive Molecularly Imprinted Polymers: Preparation, Adsorption Mechanism and Properties as Drug Delivery System for Sustained Release of 5-Fluorouracil. *Mater. Sci. Eng. C.* **2016**, *61*, 158–168. [\[CrossRef\]](#) [\[PubMed\]](#)
42. Li, S.; Yang, K.; Deng, N.; Min, Y.; Liu, L.; Zhang, L.; Zhang, Y. Thermoresponsive Epitope Surface-Imprinted Nanoparticles for Specific Capture and Release of Target Protein from Human Plasma. *ACS Appl. Mater. Interfaces* **2016**, *8*, 5747–5751. [\[CrossRef\]](#)
43. Lu, H.; Xu, S.; Guo, Z.; Zhao, M.; Liu, Z. Redox-Responsive Molecularly Imprinted Nanoparticles for Targeted Intracellular Delivery of Protein toward Cancer Therapy. *ACS Nano* **2021**, *15*, 18214–18225. [\[CrossRef\]](#)
44. Yoshida, A.; Kitayama, Y.; Kiguchi, K.; Yamada, T.; Akasaka, H.; Sasaki, R.; Takeuchi, T. Gold Nanoparticle-Incorporated Molecularly Imprinted Microgels as Radiation Sensitizers in Pancreatic Cancer. *ACS Appl. Bio Mater.* **2019**, *2*, 1177–1183. [\[CrossRef\]](#)
45. Parisi, O.I.; Francomano, F.; Dattilo, M.; Patitucci, F.; Prete, S.; Amone, F.; Puoci, F. The Evolution of Molecular Recognition: From Antibodies to Molecularly Imprinted Polymers (MIPs) as Artificial Counterpart. *J. Funct. Biomater.* **2022**, *13*, 12. [\[CrossRef\]](#) [\[PubMed\]](#)
46. Haupt, K.; Medina Rangel, P.X.; Tse Sun Bui, B. Molecularly Imprinted Polymers: Antibody Mimics for Bioimaging and Therapy. *Chem. Rev.* **2020**, *120*, 9554–9582. [\[CrossRef\]](#)
47. Bărăian, A.-I.; Jacob, B.-C.; Bodoki, A.E.; Bodoki, E. *In Vivo* Applications of Molecularly Imprinted Polymers for Drug Delivery: A Pharmaceutical Perspective. *Int. J. Mol. Sci.* **2022**, *23*, 14071. [\[CrossRef\]](#) [\[PubMed\]](#)



48. Liu, R.; Poma, A. Advances in Molecularly Imprinted Polymers as Drug Delivery Systems. *Molecules* **2021**, *26*, 3589. [\[CrossRef\]](#) [\[PubMed\]](#)
49. Zhang, R.; Liu, Q.; Liao, Q.; Zhao, Y. CD59: A Promising Target for Tumor Immunotherapy. *Future Oncol.* **2018**, *14*, 781–791. [\[CrossRef\]](#) [\[PubMed\]](#)
50. Qin, Y.-T.; Feng, Y.-S.; Ma, Y.-J.; He, X.-W.; Li, W.-Y.; Zhang, Y.-K. Tumor-Sensitive Biodegradable Nanoparticles of Molecularly Imprinted Polymer-Stabilized Fluorescent Zeolitic Imidazolate Framework-8 for Targeted Imaging and Drug Delivery. *ACS Appl. Mater. Interfaces* **2020**, *12*, 24585–24598. [\[CrossRef\]](#)
51. Huang, C.-Y.; Ye, Z.-H.; Huang, M.-Y.; Lu, J.-J. Regulation of CD47 Expression in Cancer Cells. *Transl. Oncol.* **2020**, *13*, 100862. [\[CrossRef\]](#)
52. Wang, H.-Y.; Su, Z.-C.; He, X.-W.; Li, W.-Y.; Zhang, Y.-K. H<sub>2</sub>O<sub>2</sub> Self-Supplying Degradable Epitope Imprinted Polymers for Targeted Fluorescence Imaging and Chemodynamic Therapy. *Nanoscale* **2021**, *13*, 12553–12564. [\[CrossRef\]](#)
53. Li, S.; Jiang, P.; Jiang, F.; Liu, Y. Recent Advances in Nanomaterial-Based Nanoplatforams for Chemodynamic Cancer Therapy. *Adv. Funct. Mater.* **2021**, *31*, 2100243. [\[CrossRef\]](#)
54. Sørensen, C.G.; Karlsson, W.K.; Pommergaard, H.-C.; Burcharth, J.; Rosenberg, J. The Diagnostic Accuracy of Carcinoembryonic Antigen to Detect Colorectal Cancer Recurrence—A Systematic Review. *Int. J. Surg.* **2016**, *25*, 134–144. [\[CrossRef\]](#)
55. Han, S.; Teng, F.; Wang, Y.; Su, L.; Leng, Q.; Jiang, H. Drug-Loaded Dual Targeting Graphene Oxide-Based Molecularly Imprinted Composite and Recognition of Carcino-Embryonic Antigen. *RSC Adv.* **2020**, *10*, 10980–10988. [\[CrossRef\]](#)
56. Munkley, J.; Scott, E. Targeting Aberrant Sialylation to Treat Cancer. *Medicines* **2019**, *6*, 102. [\[CrossRef\]](#)
57. Liu, R.; Cui, Q.; Wang, C.; Wang, X.; Yang, Y.; Li, L. Preparation of Sialic Acid-Imprinted Fluorescent Conjugated Nanoparticles and Their Application for Targeted Cancer Cell Imaging. *ACS Appl. Mater. Interfaces* **2017**, *9*, 3006–3015. [\[CrossRef\]](#) [\[PubMed\]](#)
58. Prabhakar, U.; Maeda, H.; Jain, R.K.; Sevick-Muraca, E.M.; Zamboni, W.; Farokhzad, O.C.; Barry, S.T.; Gabizon, A.; Grodzinski, P.; Blakey, D.C. Challenges and Key Considerations of the Enhanced Permeability and Retention Effect for Nanomedicine Drug Delivery in Oncology. *Cancer Res.* **2013**, *73*, 2412–2417. [\[CrossRef\]](#)
59. Tietze, R.; Zaloga, J.; Unterwieser, H.; Lye, S.; Friedrich, R.P.; Janko, C.; Pöttler, M.; Dürr, S.; Alexiou, C. Magnetic Nanoparticle-Based Drug Delivery for Cancer Therapy. *Biochem. Biophys. Res. Commun.* **2015**, *468*, 463–470. [\[CrossRef\]](#)
60. Cui, Y.; Ding, L.; Ding, J. Recent Advances of Magnetic Molecularly Imprinted Materials: From Materials Design to Complex Sample Pretreatment. *TrAC Trends Anal. Chem.* **2022**, *147*, 116514. [\[CrossRef\]](#)
61. Nerantzaki, M.; Michel, A.; Petit, L.; Garnier, M.; Ménager, C.; Griffete, N. Biotinylated Magnetic Molecularly Imprinted Polymer Nanoparticles for Cancer Cell Targeting and Controlled Drug Delivery. *Chem. Commun.* **2022**, *58*, 5642–5645. [\[CrossRef\]](#)
62. Boitard, C.; Curcio, A.; Rollet, A.-L.; Wilhelm, C.; Ménager, C.; Griffete, N. Biological Fate of Magnetic Protein-Specific Molecularly Imprinted Polymers: Toxicity and Degradation. *ACS Appl. Mater. Interfaces* **2019**, *11*, 35556–35565. [\[CrossRef\]](#) [\[PubMed\]](#)
63. Chen, J.; Lei, S.; Zeng, K.; Wang, M.; Asif, A.; Ge, X. Catalase-Imprinted Fe<sub>3</sub>O<sub>4</sub>/Fe@fibrous SiO<sub>2</sub>/Polydopamine Nanoparticles: An Integrated Nanoplatforam of Magnetic Targeting, Magnetic Resonance Imaging, and Dual-Mode Cancer Therapy. *Nano Res.* **2017**, *10*, 2351–2363. [\[CrossRef\]](#)
64. Parisi, O.I.; Morelli, C.; Puoci, F.; Saturnino, C.; Caruso, A.; Sisci, D.; Trombino, G.E.; Picci, N.; Sinicropi, M.S. Magnetic Molecularly Imprinted Polymers (MMIPs) for Carbazole Derivative Release in Targeted Cancer Therapy. *J. Mater. Chem. B* **2014**, *2*, 6619–6625. [\[CrossRef\]](#) [\[PubMed\]](#)
65. Parisi, O.I.; Ruffo, M.; Malivindi, R.; Vattimo, A.F.; Pezzi, V.; Puoci, F. Molecularly Imprinted Polymers (MIPs) as Theranostic Systems for Sunitinib Controlled Release and Self-Monitoring in Cancer Therapy. *Pharmaceutics* **2020**, *12*, 41. [\[CrossRef\]](#)
66. Wang, H.-Y.; Cao, P.-P.; He, Z.-Y.; He, X.-W.; Li, W.-Y.; Li, Y.-H.; Zhang, Y.-K. Targeted Imaging and Targeted Therapy of Breast Cancer Cells via Fluorescent Double Template-Imprinted Polymer Coated Silicon Nanoparticles by an Epitope Approach. *Nanoscale* **2019**, *11*, 17018–17030. [\[CrossRef\]](#)
67. Yin, D.; Li, X.; Ma, Y.; Liu, Z. Targeted Cancer Imaging and Photothermal Therapy via Monosaccharide-Imprinted Gold Nanorods. *Chem. Commun.* **2017**, *53*, 6716–6719. [\[CrossRef\]](#) [\[PubMed\]](#)
68. Zhang, Y.; Deng, C.; Liu, S.; Wu, J.; Chen, Z.; Li, C.; Lu, W. Active Targeting of Tumors through Conformational Epitope Imprinting. *Angew. Chem.* **2015**, *127*, 5246–5249. [\[CrossRef\]](#)
69. Zhu, Y.; Liu, R.; Huang, H.; Zhu, Q. Vinblastine-Loaded Nanoparticles with Enhanced Tumor-Targeting Efficiency and Decreasing Toxicity: Developed by One-Step Molecular Imprinting Process. *Mol. Pharm.* **2019**, *16*, 2675–2689. [\[CrossRef\]](#)
70. Ali, M.M.; Zhu, S.; Amin, F.R.; Hussain, D.; Du, Z.; Hu, L. Molecular Imprinting of Glycoproteins: From Preparation to Cancer Theranostics. *Theranostics* **2022**, *12*, 2406–2426. [\[CrossRef\]](#)
71. Xiao, Y.-D.; Paudel, R.; Liu, J.; Ma, C.; Zhang, Z.-S.; Zhou, S.-K. MRI Contrast Agents: Classification and Application (Review). *Int. J. Mol. Med.* **2016**, *38*, 1319–1326. [\[CrossRef\]](#)
72. Cole, L.E.; Ross, R.D.; Tilley, J.M.; Vargo-Gogola, T.; Roeder, R.K. Gold Nanoparticles as Contrast Agents in X-Ray Imaging and Computed Tomography. *Nanomed.* **2015**, *10*, 321–341. [\[CrossRef\]](#) [\[PubMed\]](#)
73. Bodoki, A.E.; Jacob, B.-C.; Bodoki, E. Perspectives of Molecularly Imprinted Polymer-Based Drug Delivery Systems in Cancer Therapy. *Polymers* **2019**, *11*, 2085. [\[CrossRef\]](#)
74. Lee, M.-H.; Thomas, J.; Li, J.-A.; Chen, J.-R.; Wang, T.-L.; Lin, H.-Y. Synthesis of Multifunctional Nanoparticles for the Combination of Photodynamic Therapy and Immunotherapy. *Pharmaceutics* **2021**, *14*, 508. [\[CrossRef\]](#) [\[PubMed\]](#)

75. Kitayama, Y.; Yamada, T.; Kiguchi, K.; Yoshida, A.; Hayashi, S.; Akasaka, H.; Igarashi, K.; Nishimura, Y.; Matsumoto, Y.; Sasaki, R.; et al. In Vivo Stealthified Molecularly Imprinted Polymer Nanogels Incorporated with Gold Nanoparticles for Radiation Therapy. *J. Mater. Chem. B* **2022**, *10*, 6784–6791. [\[CrossRef\]](#)
76. Lin, C.-C.; Lin, H.-Y.; Thomas, J.L.; Yu, J.-X.; Lin, C.-Y.; Chang, Y.-H.; Lee, M.-H.; Wang, T.-L. Embedded Upconversion Nanoparticles in Magnetic Molecularly Imprinted Polymers for Photodynamic Therapy of Hepatocellular Carcinoma. *Biomedicines* **2021**, *9*, 1923. [\[CrossRef\]](#) [\[PubMed\]](#)
77. Tse Sum Bui, B.; Haupt, K. Molecularly Imprinted Polymer Hydrogel Nanoparticles: Synthetic Antibodies for Cancer Diagnosis and Therapy. *ChemBioChem* **2022**, *23*, e202100598. [\[CrossRef\]](#)
78. Gharatape, A.; Salehi, R. Recent Progress in Theranostic Applications of Hybrid Gold Nanoparticles. *Eur. J. Med. Chem.* **2017**, *138*, 221–233. [\[CrossRef\]](#) [\[PubMed\]](#)
79. Hayakawa, N.; Kitayama, Y.; Igarashi, K.; Matsumoto, Y.; Takano, E.; Sunayama, H.; Takeuchi, T. Fc Domain-Imprinted Stealth Nanogels Capable of Orientational Control of Immunoglobulin G Adsorbed In Vivo. *ACS Appl. Mater. Interfaces* **2022**, *14*, 16074–16081. [\[CrossRef\]](#) [\[PubMed\]](#)
80. López, A.S.; Ramos, M.P.; Herrero, R.; Vilariño, J.M.L. Design, Synthesis and HR – MAS NMR Characterization of Molecular Imprinted Polymers with Emerging Contaminants Templates. *Sep. Purif. Technol.* **2021**, *257*, 117860. [\[CrossRef\]](#)
81. Sánchez-González, J.; Peña-Gallego, A.; Sanmartín, J.; Bermejo, A.M.; Bermejo-Barrera, P.; Moreda-Piñeiro, A. NMR Spectroscopy for Assessing Cocaine-Functional Monomer Interactions When Preparing Molecularly Imprinted Polymers. *Microchem. J.* **2019**, *147*, 813–817. [\[CrossRef\]](#)
82. Maré, M.; Kupka, T.; Wiecezorek, P.P.; Namieśnik, J. Computational Modeling of Molecularly Imprinted Polymers as a Green Approach to the Development of Novel Analytical Sorbents. *TrAC Trends Anal. Chem.* **2018**, *98*, 64–78. [\[CrossRef\]](#)
83. Golker, K.; Olsson, G.D.; Nicholls, I.A. The Influence of a Methyl Substituent on Molecularly Imprinted Polymer Morphology and Recognition—Acrylic Acid versus Methacrylic Acid. *Eur. Polym. J.* **2017**, *92*, 137–149. [\[CrossRef\]](#)
84. Golker, K.; Nicholls, I.A. The Effect of Crosslinking Density on Molecularly Imprinted Polymer Morphology and Recognition. *Eur. Polym. J.* **2016**, *75*, 423–430. [\[CrossRef\]](#)
85. Klejn, D.; Luliński, P.; Maciejewska, D. Molecularly Imprinted Solid Phase Extraction in an Efficient Analytical Protocol for Indole-3-Methanol Determination in Artificial Gastric Juice. *RSC Adv.* **2016**, *6*, 108801–108809. [\[CrossRef\]](#)
86. Wang, P.; Zhang, A.; Jin, Y.; Zhang, Q.; Zhang, L.; Peng, Y.; Du, S. Molecularly Imprinted Layer-Coated Hollow Polysaccharide Microcapsules toward Gate-Controlled Release of Water-Soluble Drugs. *RSC Adv.* **2014**, *4*, 26063. [\[CrossRef\]](#)
87. An, K.; Kang, H.; Zhang, L.; Guan, L.; Tian, D. Preparation and Properties of Thermosensitive Molecularly Imprinted Polymer Based on Konjac Glucomannan and Its Controlled Recognition and Delivery of 5-Fluorouracil. *J. Drug. Deliv. Sci. Technol.* **2020**, *60*, 101977. [\[CrossRef\]](#)
88. Asadi, E.; Abdouss, M.; Leblanc, R.M.; Ezzati, N.; Wilson, J.N.; Azodi-Deilami, S. In Vitro/In Vivo Study of Novel Anti-Cancer, Biodegradable Cross-Linked Tannic Acid for Fabrication of 5-Fluorouracil-Targeting Drug Delivery Nano-Device Based on a Molecular Imprinted Polymer. *RSC Adv.* **2016**, *6*, 37308–37318. [\[CrossRef\]](#)
89. Asadi, E.; Abdouss, M.; Leblanc, R.M.; Ezzati, N.; Wilson, J.N.; Kordestani, D. Synthesis, Characterization and *in Vivo* Drug Delivery Study of a Biodegradable Nano-Structured Molecularly Imprinted Polymer Based on Cross-Linker of Fructose. *Polymer* **2016**, *97*, 226–237. [\[CrossRef\]](#)
90. Ali, Z.; Sajid, M.; Manzoor, S.; Ahmad, M.M.; Khan, M.I.; Elboughdiri, N.; Kashif, M.; Shanableh, A.; Rajhi, W.; Mersni, W.; et al. Biodegradable Magnetic Molecularly Imprinted Anticancer Drug Carrier for the Targeted Delivery of Docetaxel. *ACS Omega* **2022**, *7*, 28516–28524. [\[CrossRef\]](#)
91. Han, S.; Liu, S.; Song, Y.; Jiang, H. Biodegradable Magnesium Ion-Doped Silica-Based Molecularly Imprinted Nanoparticles for Targeting Tumor Cells to Drugs Controlled Release and Recognition Mechanism Research. *Colloids Surf. B. Biointerfaces* **2022**, *217*, 112665. [\[CrossRef\]](#)
92. Lee, K.-S.; Kim, D.S.; Kim, B.S. Biodegradable Molecularly Imprinted Polymers Based on Poly( $\epsilon$ -Caprolactone). *Biotechnol. Bioprocess. Eng.* **2007**, *12*, 152–156. [\[CrossRef\]](#)
93. Gagliardi, M.; Bertero, A.; Bifone, A. Molecularly Imprinted Biodegradable Nanoparticles. *Sci. Rep.* **2017**, *7*, 40046. [\[CrossRef\]](#)
94. Han, S.; Song, Y.; Liu, S.; Zhao, L.; Sun, R. Dual Responsive Molecularly Imprinted Polymers Based on UiO-66-DOX for Selective Targeting Tumor Cells and Controlled Drug Release. *Eur. Polym. J.* **2022**, *171*, 111219. [\[CrossRef\]](#)
95. Zhang, L.-P.; Tang, S.-H.; Mo, C.-E.; Wang, C.; Huang, Y.-P.; Liu, Z.-S. Synergistic Effect of Liquid Crystal and Polyhedral Oligomeric Silsesquioxane to Prepare Molecularly Imprinted Polymer for Paclitaxel Delivery. *Eur. Polym. J.* **2018**, *98*, 226–236. [\[CrossRef\]](#)
96. Eifler, A.C.; Thaxton, C.S. Nanoparticle Therapeutics: FDA Approval, Clinical Trials, Regulatory Pathways, and Case Study. *Methods Mol. Biol.* **2011**, *726*, 325–338. [\[CrossRef\]](#)
97. Bobo, D.; Robinson, K.J.; Islam, J.; Thurecht, K.J.; Corrie, S.R. Nanoparticle-Based Medicines: A Review of FDA-Approved Materials and Clinical Trials to Date. *Pharm. Res.* **2016**, *33*, 2373–2387. [\[CrossRef\]](#) [\[PubMed\]](#)
98. Etheridge, M.L.; Campbell, S.A.; Erdman, A.G.; Haynes, C.L.; Wolf, S.M.; McCullough, J. The Big Picture on Nanomedicine: The State of Investigational and Approved Nanomedicine Products. *Nanomedicine Nanotechnol. Biol. Med.* **2013**, *9*, 1–14. [\[CrossRef\]](#) [\[PubMed\]](#)

99. Fan, Z.; Fu, P.P.; Yu, H.; Ray, P.C. Theranostic Nanomedicine for Cancer Detection and Treatment. *J. Food Drug. Anal.* **2014**, *22*, 3–17. [[CrossRef](#)]
100. Fu, X.; Li, Y.; Gao, S.; Lv, Y. Selective Recognition of Tumor Cells by Molecularly Imprinted Polymers. *J. Sep. Sci.* **2021**, *44*, 2483–2495. [[CrossRef](#)] [[PubMed](#)]

**Disclaimer/Publisher's Note:** The statements, opinions and data contained in all publications are solely those of the individual author(s) and contributor(s) and not of MDPI and/or the editor(s). MDPI and/or the editor(s) disclaim responsibility for any injury to people or property resulting from any ideas, methods, instructions or products referred to in the content.



### 3.2. Molecularly Imprinted Polymers Specific towards 4-Borono-L-Phenylalanine – Synthesis Optimization, Theoretical Analysis, Morphology Investigation, Cytotoxicity, and Release Studies



Article

## Molecularly Imprinted Polymers Specific towards 4-Borono-L-phenylalanine—Synthesis Optimization, Theoretical Analysis, Morphology Investigation, Cytotoxicity, and Release Studies

Emilia Balcer <sup>1,2</sup> , Monika Sobiech <sup>3</sup> , Joanna Giebułtowicz <sup>1</sup> , Małgorzata Sochacka <sup>1</sup> and Piotr Luliński <sup>3,\*</sup>

- <sup>1</sup> Department of Drug Chemistry, Faculty of Pharmacy, Medical University of Warsaw, Banacha 1, 02-097 Warsaw, Poland; emilia.balcer@wum.edu.pl (E.B.); joanna.giebulutowicz@wum.edu.pl (J.G.); malgorzata.bogucka@wum.edu.pl (M.S.)  
<sup>2</sup> Radiochemistry Team, Reactor Research Division, Nuclear Facilities Operations Department, National Centre for Nuclear Research, Sołtana 7, Świerk, 05-400 Otwock, Poland  
<sup>3</sup> Department of Organic and Physical Chemistry, Faculty of Pharmacy, Medical University of Warsaw, Banacha 1, 02-097 Warsaw, Poland; monika.sobiech@wum.edu.pl  
\* Correspondence: piotr.lulinski@wum.edu.pl; Tel.: +48-22-5720643

**Abstract:** The aim of this study was to create molecularly imprinted polymers (MIPs) that are specific towards 4-borono-L-phenylalanine (BPA) to serve as boron compound carriers. The honeycomb-like MIPs were characterized in the matter of adsorption properties, morphology, structure, and cytotoxicity towards A549 and V79-4 cell lines. The honeycomb-like MIP composed from methacrylic acid and ethylene glycol dimethacrylate was characterized by a binding capacity of  $330.4 \pm 4.6 \text{ ng g}^{-1}$  and an imprinting factor of 2.04, and its ordered, porous morphology was confirmed with scanning electron microscopy. The theoretical analysis revealed that the coexistence of different anionic forms of the analyte in basic solution might lower the binding capacity of the MIP towards BPA. The release profiles from the model phosphate buffer saline showed that only 0 to 4.81% of BPA was released from the MIP within the time frame of two hours, furthermore, the obtained material was considered non-cytotoxic towards tested cell lines. The results prove that MIPs can be considered as effective BPA delivery systems for biomedical applications and should be investigated in further studies.

**Keywords:** 4-borono-L-phenylalanine; molecularly imprinted polymer; morphology; cytotoxicity; boron carrier



**Citation:** Balcer, E.; Sobiech, M.; Giebułtowicz, J.; Sochacka, M.; Luliński, P. Molecularly Imprinted Polymers Specific towards 4-Borono-L-phenylalanine—Synthesis Optimization, Theoretical Analysis, Morphology Investigation, Cytotoxicity, and Release Studies. *Polymers* **2023**, *15*, 3149. <https://doi.org/10.3390/polym15143149>

Academic Editor: Beom Soo Kim

Received: 28 June 2023

Revised: 17 July 2023

Accepted: 21 July 2023

Published: 24 July 2023



**Copyright:** © 2023 by the authors. Licensee MDPI, Basel, Switzerland. This article is an open access article distributed under the terms and conditions of the Creative Commons Attribution (CC BY) license (<https://creativecommons.org/licenses/by/4.0/>).

## 1. Introduction

Boron neutron capture therapy (BNCT) is a type of cancer treatment that uses nuclear capture and fission reactions, occurring when the atoms of boron-10 ( $^{10}\text{B}$ ) are irradiated with neutrons from an external beam. The products of this reaction,  $\alpha$  particles and lithium nuclei, in theory, kill only  $^{10}\text{B}$ -containing cells in the immediate vicinity of the reaction [1]. Thus, the effectiveness of BNCT is dependent on the selective delivery of  $^{10}\text{B}$  to the tumor site.

Providing the success of finding the appropriate boron carrier, BNCT has the potential to become not only an alternative treatment method but also a first-choice option in the case of inoperative or metastatic tumors. A significant advantage of BNCT in comparison to conventional methods, such as radio- or chemotherapy, is the possibility of limiting the exposition of healthy cells to an excessive dose of radiation due to the minimized interaction between the neutrons and the tissues with no deposited boron. Moreover, the nature of neutrons themselves allows the avoidance of damage that is caused by different types of ionizing radiation. This advantage is directly linked to the reduction in adverse effects of therapy, which further greatly influences the quality of life of the



patients—an aspect that should be prioritized in every case. One of the biggest obstacles in the widespread application and further development of BNCT remains the challenge of providing an ideal boron carrier. Such a compound should be characterized by a low toxicity and high biocompatibility, high specificity to tumor cells, sufficient capacity for the delivery of 20–50 µg of boron per g of tumor tissue, concentration ratio in tumor-healthy tissues and tumor-blood greater than 3:1, high and fast elimination from blood and normal cells, and retention in a tumor long enough for the duration of irradiation [2]. Additionally, the compounds dedicated to brain tumors should have the ability to penetrate the blood–brain barrier.

Despite the fact that various boron carriers have been designed and described, at the moment, only two compounds are used in clinical trials, 4-borono-L-phenylalanine (BPA) and sodium mercaptoundecahydro-closo-dodecaborate (BSH) [3]. Even though BSH shows the advantage of having 12 boron atoms per molecule, its use is limited due to the passive diffusion mechanism that governs its transport, which results in insufficiently selective delivery [1]. Thus, most of the scientific interest is focused on BPA since it is delivered to cancerous cells using the mechanism of active uptake mediated by L-amino acid transporters (primarily LAT1), providing more efficient therapy. However, the BPA solubility in water at blood pH level is insufficiently low. For that purpose, various alternative modifications were proposed to tackle this problem, e.g., the complex of BPA with D-fructose [4–6].

Recently, boron-based polymers, such as organoboranes, borazine (polymers with conjugated boron heterocyclic systems), boron quinolates, derivatives of boronic acid and functionalized boronic ester polymers, carborane, or borane clusters containing polymers, have attracted scientific attention because of their effectiveness in penetrating cancerous tissues and the homogeneous delivery of the boron clusters into tumor cells [7]. A very promising solution was proposed by Nomoto et al. [8], where BPA was complexed with poly(vinyl alcohol) (PVA), which caused the formulation to be transported into tumor cells by LAT1-mediated endocytosis and thus slowed the unwanted efflux. The formed PVA–BPA complex demonstrated a higher accumulation and longer retention in the tumor than the fructose–BPA complex, significantly improving the therapeutic effect. The application of boron-based polymers looks like a promising alternative for a BNCT-dedicated compound, but some synthetic routes and post-polymerization modifications could hamper their utility [9].

Thus, one of interesting options is to use the molecularly imprinted polymers (MIPs) as the carriers of boron with the potential for further application in BNCT. The MIPs are a class of polymeric materials formed during a three-step synthetic process which includes creating a prepolymerization complex with selected functional monomer(s) involving non-covalent interactions or a chemical reaction, the polymerization process, and in the last step, the template removal from the polymeric matrix. Today, MIPs are considered to be a well-known class of materials that are used in separation science and in the detection of molecules, mostly due to their beneficial properties such as high selectivity, thermal and chemical stability, and reusability [10,11]. The facile preparation and capability for their integration with other compounds or systems to fabricate composite devices became additional advantages of MIPs, causing their broad utilization in the field of analytical chemistry [12,13]. The potential of MIPs as drug delivery devices was also investigated [14,15]. However, it should be emphasized that a MIP being an integrated part of the device gives it the opportunity to not only serve as the drug carriers (for example, in the treatment of cancer) but also to act as ligands that are able to recognize specific domains on the surface of cells (for instance, glycoproteins overexpressed in the cancer process) [16].

In this paper, we are interested in investigating the MIP with potential capability in the delivery of boron. In order to achieve this goal, in the synthesis optimization step, the theoretical analysis was employed to reduce the costs at the step of functional monomer selection. Moreover, a cavity of the MIP generated *in silico* allowed us to explain the interactions between the BPA and the polymer matrix to prove the specificity. Comprehensive

morphological investigations of MIPs prepared from various cross-linking reagents were performed and compared to the results of the binding capacities. Biocompatibility studies were carried out, and the release of the target molecule was analyzed to verify the MIP's potential as a boron carrier. It has to be emphasized that to the best of our knowledge, the MIP for boron-containing molecule delivery has not been designed. Thus, it constitutes as a novelty of our study. It has to be underlined that the presented results comprise a preliminary stage of the investigations related to MIP-based boron delivery devices.

## 2. Materials and Methods

### 2.1. Reagents and Standards

A template molecule, L-phenylalanine, and the target molecule, BPA, were purchased from Sigma-Aldrich (Steinheim, Germany). The functional monomer: methacrylic acid; the cross-linkers: ethylene glycol dimethacrylate (1), poly(ethylene) glycol dimethacrylate (2), trimethylolpropane trimethacrylate (3), triethylene glycol dimethacrylate (4), and divinylbenzene (5); and the silane components: tetraethoxysilane and 3-(trimethoxysilyl)propyl methacrylate (MPS) were purchased from Sigma-Aldrich (Steinheim, Germany). The solvents: acetonitrile, methanol, ethanol, propan-2-ol, toluene, acetone, glacial acetic acid, trifluoroacetic acid, hydrofluoric acid (48–50%), hydrochloric acid (36%), formic acid (98%), acetic acid, and ammonium hydroxide (25%), and salts: ammonium acetate and sodium hydroxide, were brought from POCh (Gliwice, Poland). The polymerization reaction initiator, 1,1'-azobiscyclohexanecarbonitrile, was from Fluka (Steinheim, Germany). The HPLC gradient-grade methanol, acetic acid, and acetonitrile were purchased from Merck (Darmstadt, Germany). Ultra-pure water, delivered from a Hydrolab HLP 5 system (Straszyn, Poland), was used to prepare the water solutions.

The A549 (human non-small cell lung carcinoma) cell line was provided by the Department of Applied Toxicology, Faculty of Pharmacy, Medical University of Warsaw, and the V79-4 (Chinese hamster lung fibroblasts) cell line was provided by the Department of Environmental Health Science, Faculty of Pharmacy, Medical University of Warsaw. Dulbecco's Modified Eagle Medium (DMEM), Kaighn's Modification of Ham's F-12 Medium (F12-K), streptomycin, penicillin, fetal bovine serum (FBS), and phosphate buffered saline (PBS) were purchased from Gibco (Paisley, United Kingdom). The 3-(4,5-dimethylthiazol-2-yl)-2,5-diphenyltetrazolium bromide (MTT) was brought from Sigma-Aldrich (Steinheim, Germany).

### 2.2. Polymers

#### 2.2.1. Bulk Polymer

The radical bulk polymerization was performed to obtain a polymer from methacrylic acid and ethylene glycol dimethacrylate, coded as MIP1<sub>b</sub> (index b refers to bulk) in the presence of L-phenylalanine, acting as the template. The corresponding non-imprinted polymer, NIP1<sub>b</sub>, was prepared in the same way but without the template. The experimental amounts of reagents are provided in Table 1. Briefly, L-phenylalanine (0.35 mmol), methacrylic acid (2 mmol), and ethylene glycol dimethacrylate, were dissolved in a mixture of toluene, glacial acetic acid, and trifluoroacetic acid in a falcon-tube. The addition of glacial acetic acid and trifluoroacetic acid facilitates the dissolution of L-phenylalanine in the porogenic solvent of toluene [17]. Then, the polymerization initiator, 1,1'-azobiscyclohexanecarbonitrile, was added, and the homogeneous solution was purged with nitrogen for five minutes (min) before sealing the tube. Subsequently, the polymerization was carried out in a nitrogen atmosphere for 24 h at 88 °C. The bulk rigid polymer was then ground and wet-sieved into particles below 45 µm in diameter. Fine particles were separated by repeated decantation from acetone. The removal of L-phenylalanine was processed, using continuous extraction in a Soxhlet apparatus (24–36 h, 80 mL, methanol), followed by a washing sequence (in brackets, volumes of solvent per 10 mg of polymer are provided): methanol–1% aq. ammonium hydroxide (10 mL), methanol–1% aq. formic acid (10 mL), methanol–40 mmol L<sup>−1</sup> aq. ammonium acetate (70:30, v/v, 10 mL), and 80% aq. methanol (1 mL). The template removal

was monitored using liquid chromatography coupled with tandem mass spectrometry (LC-MS/MS). The particles were dried in a vacuum at room temperature.

**Table 1.** Amounts of SiO<sub>2</sub>@MPS and cross-linkers used in the polymerization of 172.6 mg (2 mmol) of methacrylic acid in the presence of L-phenylalanine, 57.8 mg (0.35 mmol), and 20 mg of 1,1'-azobiscyclohexanecarbonitrile as the initiator in a mixture of toluene (2.5 mL), glacial acetic acid (0.3 mL), and trifluoroacetic acid (0.2 mL).

Code of MIP	Cross-Linker (g, mmol)	SiO <sub>2</sub> @MPS (mg)
MIP1 <sub>b</sub>	ethylene glycol dimethacrylate (1), 1.98, 10	without
MIP1 <sub>h</sub>	ethylene glycol dimethacrylate (1), 1.98, 10	1000
MIP2 <sub>h</sub>	poly(ethylene) glycol dimethacrylate (2), 5.50, 10	1000
MIP3 <sub>h</sub>	trimethylolpropane trimethacrylate (3), 3.38, 10	1000
MIP4 <sub>h</sub>	triethylene glycol dimethacrylate (4), 2.86, 10	1000
MIP5 <sub>h</sub>	divinylbenzene (5), 1.30, 10	1000

### 2.2.2. Synthesis of Siloxane Particles

The siloxane particles were synthesized according to Stöber method [18]. For this purpose, a solution of 12.5 mL of tetraethoxysilane in 200 mL of anhydrous ethanol was added to two-neck round-bottom flask. Then, a solution of 12 mL of 25% aq. ammonium hydroxide in 20 mL of ultra-pure water was added dropwise. The reaction mixture was stirred at 150 rpm for 2 h at room temperature. The white precipitate was collected by centrifugation (700 rpm, 45 min) and was washed three times with anhydrous ethanol. Next, the siloxane particles were functionalized with MPS. For this purpose, an amount of 3.9 g of siloxane particles was dispersed in 195 mL of anhydrous toluene in a round-bottom flask. Then, 19.5 mL of MPS was added, and mixture was stirred at 400 rpm at room temperature for 24 h. Obtained functionalized siloxane particles coded as SiO<sub>2</sub>@MPS were centrifuged (700 rpm, 30 min) and were washed three times with anhydrous toluene prior to drying.

### 2.2.3. Honeycomb-like Polymers

The radical polymerization was performed to obtain the honeycomb-like polymers from methacrylic acid (2 mmol) and various cross-linkers, coded as MIP1<sub>h</sub>–MIP5<sub>h</sub> (index h refers to honeycomb-like) in the presence of L-phenylalanine (0.35 mmol), acting as the template. The corresponding non-imprinted polymers, NIP1<sub>h</sub>–NIP5<sub>h</sub>, were prepared in the same way but without the template. The experimental amounts of the reagents (moles, masses, and volumes) used for the preparation of the different types of polymers are listed in Table 1.

Briefly, L-phenylalanine, methacrylic acid, and a selected cross-linker, were dissolved in a mixture of toluene, glacial acetic acid, and trifluoroacetic acid in a falcon-tube prior to purging with nitrogen for five min and transferring to another falcon-tube with separately weighted particles of SiO<sub>2</sub>@MPS. Next, the content (pre-polymerization mixture together with functionalized siloxane particles) was placed into the ultrasonic bath for 15 min. After, the initiator of the polymerization reaction was added, the falcon-tube was purged with nitrogen once again for five min, and then put into the oil bath for 24 h, keeping the temperature at 94 °C and allowing the polymerization reaction to proceed. Next, the polymer was removed from falcon-tube and was gently crushed to obtain irregular particles of ca 2–5 mm of diameter which were put into the solution of 2.5% aq. hydrofluoric acid, keeping the proportion of five–ten particles per 5 mL of the solution. The etching of siloxane lasted for 3 days. Then, the solution of 2.5% aq. hydrofluoric acid was removed, and the particles were transferred to deionized water (5 mL) for 1 day. Finally, the water was removed, and the particles were washed twice with methanol (10 mL). Next, a washing sequence was carried out to remove the template (in brackets, volumes of solvent per 10 mg of polymer are provided): methanol–1% aq. ammonium hydroxide (1.5 mL), methanol–1% aq. formic acid (1.5 mL), methanol–40 mmol L<sup>−1</sup> aq. ammonium acetate (70:30, v/v, 1.5 mL), and



80% aq. methanol (1 mL). The sequence was repeated six times with intervals between the change of solution from 4 to 24 h. The template removal was monitored using LC-MS/MS. The particles were dried in a vacuum at room temperature.

### 2.3. Binding Studies

For binding studies, polypropylene tubes were filled with 10 mg of MIP1<sub>b</sub> and MIP1<sub>h</sub>-MIP5<sub>h</sub>, NIP1<sub>b</sub> and NIP1<sub>h</sub>-NIP5<sub>h</sub>, and a volume of 1 mL of methanol–water (85:15, *v/v*) standard solutions of BPA (concentration of 7.5 µg L<sup>−1</sup>) were added. The tubes were sealed, and for the MIP1<sub>b</sub> and NIP1<sub>b</sub> oscillated with a thermoshaker at 25 °C for 2 h, and for the MIP1<sub>h</sub>-MIP5<sub>h</sub> and NIP1<sub>h</sub>-NIP5<sub>h</sub>, were first manually, gently stirred and then left at room temperature for 2 h. Then, the aliquots of the supernatant were used to analyze the unbound amounts of compound using LC-MS/MS (for the MIP1<sub>b</sub> and NIP1<sub>b</sub>, the tubes were first centrifuged). All measurements were carried out in triplicate. The binding capacities (*B*, µg g<sup>−1</sup>) of MIP1<sub>b</sub>, NIP1<sub>b</sub>, MIP1<sub>h</sub>-MIP5<sub>h</sub>, and NIP1<sub>h</sub>-NIP5<sub>h</sub> were calculated according to Equation (1):

$$B = \frac{(c_i - c_f)V}{m} \quad (1)$$

and followed by the calculation of the distribution coefficients (*K<sub>D</sub>*, L g<sup>−1</sup>) for MIP1<sub>b</sub>, NIP1<sub>b</sub>, MIP1<sub>h</sub>-MIP5<sub>h</sub>, and NIP1<sub>h</sub>-NIP5<sub>h</sub> according to Equation (2):

$$K_D = \frac{(c_i - c_f)V}{c_f m} \quad (2)$$

where *V* represents a volume of solution (L), *c<sub>i</sub>* represents the initial solution concentration (µg L<sup>−1</sup>), *c<sub>f</sub>* represents the solution concentration after adsorption (µg L<sup>−1</sup>), and *m* represents the mass of the polymer sample (g). The imprinting factors (*IF*) were calculated according to Equation (3):

$$IF = \frac{K_D(\text{MIP})}{K_D(\text{NIP})} \quad (3)$$

### 2.4. Release Studies

For preliminary desorption studies, first, the soaking of MIP1<sub>h</sub> and NIP1<sub>h</sub> in the standard solution of BPA at the concentrations of 20 µg L<sup>−1</sup>, 200 µg L<sup>−1</sup>, or 1000 µg L<sup>−1</sup> in the methanol–water system (85:15, *v/v*) was performed, according to the procedure described in Section 2.3. The aliquots of the supernatant were used to analyze the unbound amounts of compound using LC-MS/MS. Then, to study the desorption process, the solutions of BPA were replaced with 1 mL of methanol–water (85:15, *v/v*) for each sample. At 20, 60, and 120 min after the replacement of solutions, aliquots of the supernatant were collected for LC-MS/MS analysis. After each aliquot collection, the volumes of methanol–water (85:15, *v/v*) solutions were adjusted to 1 mL. All measurements were carried out in triplicate.

For the release in PBS studies, first, the soaking of MIP1<sub>h</sub> and NIP1<sub>h</sub> in the standard solution of BPA at the concentration of 200 µg L<sup>−1</sup> in the methanol–water system (85:15, *v/v*)—in various pH values, viz. 2, 5, and 9.5—was performed, according to the procedure described in Section 2.3. The pH values of the standard solutions were adjusted with the use of 1 M aq. hydrochloric acid (for pH 2), methanol–1% aq. formic acid (for pH 5), and methanol–1% aq. ammonium hydroxide (for pH 9.5). The aliquots of the supernatant were used to analyze the unbound amounts of compound using LC-MS/MS. Then, to study the release process, the solutions of BPA were replaced with 1 mL of PBS for each sample. At 20, 60, and 120 min after the replacement of solutions, aliquots of the supernatant were collected for LC-MS/MS analysis. After each aliquot collection, the volumes of PBS solutions were adjusted to 1 mL. All measurements were carried out in triplicate.

## 2.5. Instrumentation

Instrumental analysis was performed using an Agilent 1260 Infinity System (Agilent Technologies, Santa Clara, CA, USA), equipped with a degasser, a thermostatted column compartment, an autosampler, and a binary pump, coupled to a QTRAP 4000 hybrid triple quadrupole/linear ion trap mass spectrometer (AB Sciex, Framingham, MA, USA). The turbo ion spray source was operated in positive mode. The curtain gas, ion source gas 1, ion source gas 2, and collision gas (all high purity nitrogen) were set at 241 kPa, 414 kPa, 276 kPa, and “medium” instrument units, respectively. The ion spray voltage and source temperature were 5500 V and 600 °C, respectively. The target compounds were analyzed in multiple reaction monitoring (MRM) mode. The quantitative MRM transitions, declustering potential (DP), and collision energy (CE) for BPA were ( $m/z$ ) 210/164 (DP = 66 V, CE = 18 V). Chromatographic separation was achieved with a Kinetex® EVO C18 column (100 mm × 4.6 mm, 2.6 µm) from Phenomenex (Torrance, CA, USA). The column was maintained at 40 °C at a flow rate of 0.5 mL min<sup>−1</sup>. The mobile phase consisted of water with 0.2% acetic acid as eluent A (90%) and acetonitrile with 0.2% acetic acid as eluent B (10%). The run lasted for 5 min. The injection volume was 10 µL.

The surface morphology analysis using scanning electron microscopy (SEM) with a Merlin FE-SEM (Zeiss, Oberkochen, Germany) was performed at the Faculty of Chemistry, University of Warsaw, Poland. The samples were Au/Pd-sputter-coated before SEM analysis. The infrared (FT-IR) spectra were recorded on Nicolet iS50 FT-IR (Thermo Fisher Scientific, Waltham, MA, USA) at the Biological and Chemical Research Centre, University of Warsaw, Poland.

## 2.6. Theoretical Analysis

Molecular modelling methodology was performed according to previous works [19,20]. Briefly, the optimized geometries of all compounds and the so-called ESP (electrostatic potential) atomic partial charges on the atoms were obtained using the density functional theory (DFT) with B3LYP/6-311pG (d,p) hybrid functional implemented in the Gaussian 16 program [21]. Random starting models of analyzed systems were created using the Packmol software [22]. A CHARMM force field [23] was applied during molecular mechanics (MM) and molecular dynamic (MD) simulations performed using the BIOVIA Discovery Studio 2021 software package [24]. The MM process consisted of two cycles of minimization—the first using 100 steps of steepest descent, and the second using 10,000 steps of conjugate gradient—and was applied until the RMS gradient of the structure reached below 0.01 kcal mol<sup>−1</sup> Å<sup>−1</sup>. The MD protocol contained a heating step (100 ps, time steps of 1 fs). The system was heated from 0 to 300 K. Prior to the production stage, isothermal equilibration was performed (100 ps, temperature of 300 K). The production run was conducted for 5 ns in the NVT ensemble (constant-volume/constant-temperature dynamics) at 300 K, and the coordinates were recorded every 10 ps. For the MD protocols, the Leapfrog Verlet integration and SHAKE [25] algorithms were applied. Trajectory file data generated from the NVT MD simulation have been used in all the calculations and analyses presented in this research.

The first step of the simulation process was performed to find the best monomer for synthetic procedure. Thirteen different monomer structures, viz. acrylamide, N-allylaniline, N-allylurea, 1-allylpiperazine, 2-acrylamido-2-methylpropane sulfonic acid, 2-(diethylamino)ethyl methacrylate, 1,1,1,3,3,3-hexafluoroisopropyl methacrylate, 2-hydroxyethyl methacrylate, acrylic acid, isopropenylbenzene, 2-(trifluoromethyl)acrylic acid, 4-vinylpyridine, and methacrylic acid were tested. During the studies, simple models of the pre-polymerization complexes were created from the template and the functional monomers. The boxes with the template molecule (cation of L-phenylalanine, cationic form was used because of the acidic solvent used during synthetic procedure) surrounded by six molecules of appropriate monomer molecules were prepared, and starting structures were created using Packmol. Then, the energy optimization procedure using MM was applied to obtain models of pre-polymerization systems with intermolecular interactions formed

between the template and monomers. The monomer that gave the lowest complexation energy value was selected for the construction of the MIP cavity model and for polymer synthesis. The complexation energies ( $\Delta EC$ , kcal mol<sup>−1</sup>) were calculated according to Equation (4):

$$\Delta EC = E_{\text{system}} - E_{\text{template}} - E_{\text{monomers}}, \quad (4)$$

where  $E_{\text{system}}$  is the potential energy of the pre-polymerization complex,  $E_{\text{template}}$  is the potential energy of the template molecule, and  $E_{\text{monomers}}$  is the potential energy of the monomers without the template.

In the next step of computational analysis, the model of the MIP cavity was built, constructed from the monomer (methacrylic acid) chosen in the previous step, and simulation of the BPA adsorption process on the MIP matrix was performed to analyze and define interactions responsible for molecular recognition of the analyte with MIP. The MIP cavity starting structure was obtained during the construction of the box with the template surrounded by methacrylic acid molecules, followed by the addition of the cross-linker (ethylene glycol dimethacrylate) and porogen molecules (67 molecules of toluene, 15 molecules of acetic acid, 6 molecules of trifluoroacetic acid, and 1 molecule of trifluoroacetic acid anion) using Packmol. Then, MM and MD procedures were applied. Next, the C atoms present in the monomer and cross-linker vinyl groups that were closest to each other were bonded, taking into account the fact that all molecules of the monomer and cross-linker in the studied system should create one cross-linked polymeric chain. The operation described mimicked the polymerization reaction in the synthetic process. The so-called ESP atomic partial charges were calculated for the created polymeric chain structure, and the MM and MD procedures were repeated for the system constructed from the polymeric chain, the template and the solvent, to form a specific binding site in the polymer.

The obtained model of the MIP chain was applied during the modelling of the BPA adsorption process. The template was removed, and the empty space was proposed as the computer model of recognition site. The molecule of the analyte was inserted into the MIP cavity model (replacing the template). Different forms of the analyte, viz. cationic, anionic, and zwitterion, were analyzed according to different pH values of the adsorption process. Then, the MD simulation was carried out using the dielectric constant value of the methanol–water (85:15, v/v) solution,  $\epsilon = 36\epsilon_{\text{rj}}$  [26], mimicking the experimental conditions of adsorption.

## 2.7. Cytotoxicity Tests

In order to assess the cytotoxicity of the most promising composite, MIP1<sub>h</sub>, the MTT assay was used on V79-4 and A549 cell lines. The growth media used for V79-4 and A549 cell lines were, respectively, DMEM with a 10% addition of FBS and two antibiotics: 0.1 mg mL<sup>−1</sup> of streptomycin and 100 IU mL<sup>−1</sup> of penicillin, as well as F-12K with a 10% addition of FBS and two antibiotics: 0.1 mg mL<sup>−1</sup> of streptomycin and 100 IU mL<sup>−1</sup> of penicillin. Briefly, V79-4 and A549 cells were seeded in culture media on 96-well microplates at a density of  $8 \times 10^3$  and  $1 \times 10^4$ , respectively, and incubated for 48 h in controlled conditions at 36.8 °C, 5% CO<sub>2</sub>, and 95% humidity. At the end of the incubation, each well was examined under a microscope to confirm the 90% confluency of cells. After that, the medium was discarded and replaced with extracts of the MIP1<sub>h</sub> sample. To obtain the extracts for the experiment, samples were incubated for 24 h in the cell culture media (50 g L<sup>−1</sup>) with FBS concentration reduced to 5% at 36.8 °C, then gently stirred and sterilized by filtration using 0.22 µm syringe filters. The cells were exposed to different dilutions of the extracts in a twofold dilution series for 20 h at 36.8 °C, 5% CO<sub>2</sub>, and 95% humidity (twelve data points for each dilution). Afterwards, the extracts were removed, and the cells were washed with PBS and then treated with fresh media containing MTT (final concentration of 0.25 g L<sup>−1</sup>) and incubated for another 3 h. Then, cells were treated with acidified propan-2-ol (0.04 M HCl) to stop the reaction and dissolve purple formazan crystals. The absorbance of the solution in each well was colorimetrically assessed at



570 nm using the Epoch™ microplate reader (Agilent Technologies, Santa Clara, CA, USA), and the optical density (OD) values were obtained. The viability of the cells was evaluated by comparing the OD<sub>570</sub> results with the mean result of the control group (cells incubated in the same conditions as the experimental group without the added MIP1<sub>h</sub> extract). The MIP1<sub>h</sub> material was considered non-cytotoxic in the tested range of concentrations if the cell viability was not reduced to below 70%.

### 3. Results and Discussion

#### 3.1. Synthesis of the Materials

##### 3.1.1. Theoretical Choice of Functional Monomer

Firstly, computational modelling was used to choose the monomer that would be able to form the polymer with the highest binding affinity towards the analyte—BPA. To simplify and make the synthetic and simulation procedures cost- and time-effective, simple models of pre-polymerization complexes consisting of monomers and template molecules were constructed. As the template, L-phenylalanine (structure resembling the analyte) was used in experimental and theoretical studies to avoid the analyte bleeding phenomenon. It was expected that the functional monomer which showed the lowest complexation energy towards the template should produce the polymer with the highest affinity [27]. Potential functional monomers that could possibly form complexes with the template due to non-covalent interactions were tested for their complexation energy. Thirteen different molecules possessing polymerizable groups and residues that could interact with the template via non-covalent interactions were studied. The results are presented in Table 2.

**Table 2.** Screening of functional monomers on their interaction with L-phenylalanine.

Functional Monomer	Complexation Energy ( $\Delta EC$ , kcal mol <sup>−1</sup> )
Methacrylic acid	−75.13
Acrylic acid	−75.07
2-(Diethylamino)ethyl methacrylate	−72.00
2-Hydroxyethyl methacrylate	−68.26
N-Allylurea	−61.37
Acrylamide	−60.62
1,1,1,3,3,3-Hexafluoroisopropyl methacrylate	−59.98
4-Vinylpyridine	−57.41
2-Acrylamido-2-methylpropane sulfonic acid	−56.55
N-Allylaniline	−49.63
2-(Trifluoromethyl)acrylic acid	−48.63
1-Allylpiperazine	−40.91
Isopropenylbenzene	−33.62

As one can see, two acidic monomers, methacrylic ( $\Delta EC = -75.13$  kcal mol<sup>−1</sup>) and acrylic acid ( $\Delta EC = -75.07$  kcal mol<sup>−1</sup>), were identified as the most promising monomers that could form strong interactions with the template (Table 2). The ability of the described two monomers to create a stable pre-polymerization complex was mainly associated with the formation of hydrogen bonds between the monomer  $-\text{COOH}$  group and the template  $-\text{COOH}$  or  $-\text{NH}_3^+$  groups.

##### 3.1.2. Verification of Effectiveness of MIP with Bulk Polymer

In the next step of our investigations, the experimental verification of results from the theoretical analysis was performed. For that purpose, the functional monomer that was characterized by the lowest energy of the stabilization of the pre-polymerization complex with the L-phenylalanine template was chosen, viz. methacrylic acid, and the synthesis of the MIP was carried out in the presence of ethylene glycol dimethacrylate as the cross-linking agent (the scheme is presented in Figure 1). Here, the bulk material was prepared, and its capability to adsorb the BPA was evaluated in order to assess the effectiveness of the

MIP system when compared to NIP, which was also synthesized. The effectiveness of the MIP was determined based on the binding capacity (Equation (1)), distribution coefficient (Equation (2)), and the specificity expressed by the imprinting factor (Equation (3)). The results are provided in Table 3.

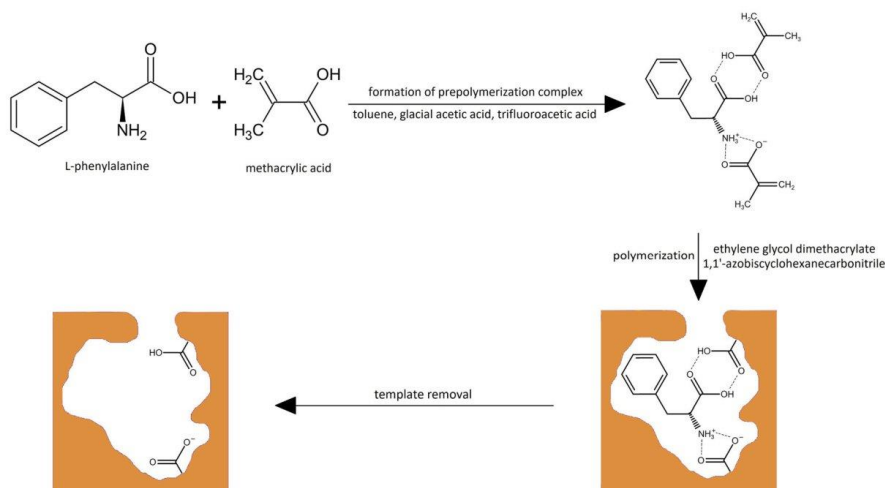


**Figure 1.** Scheme of MIP synthesis with a matrix based on L-phenylalanine as the template, methacrylic acid as the monomer, and ethylene glycol dimethacrylate as the cross-linker.

**Table 3.** Binding capacities of BPA on MIP1<sub>b</sub>–NIP1<sub>b</sub> and MIP1<sub>h</sub>–MIP5<sub>h</sub>/NIP1<sub>h</sub>–NIP5<sub>h</sub> (conc. 7.5 µg L<sup>−1</sup>, n = 3), KD and IFs.

No. of Polymer	Binding Capacities ± S.D. (B, ng g <sup>−1</sup> )		Distribution Ratio (KD, L g <sup>−1</sup> )		IF
	MIP	NIP	MIP	NIP	
1 <sub>b</sub>	269 ± 20	79.42 ± 0.26	0.041	0.009	4.36
1 <sub>h</sub>	330.4 ± 4.6	197.4 ± 1.9	0.055	0.027	2.04
2 <sub>h</sub>	225 ± 28	175 ± 24	0.032	0.023	1.38
3 <sub>h</sub>	208 ± 11	299 ± 47	0.029	0.047	0.61
4 <sub>h</sub>	176.9 ± 1.8	249 ± 18	0.023	0.036	0.64
5 <sub>h</sub>	130.4 ± 3.2	254 ± 34	0.016	0.037	0.44

As could be seen, the MIP prepared from methacrylic acid and ethylene glycol dimethacrylate was characterized by a nearly three-and-a-half-fold higher binding capacity of BPA than NIP. The comparison of distribution coefficients revealed high specificity with IF equal to 4.36. Although the capability of a methacrylic-acid-based MIP imprinted by L-phenylalanine was evaluated previously [28], to the best of our knowledge, the investigations of such a system for the specific adsorption of BPA has not been executed. Thus, it could be concluded that the MIP system synthesized from the methacrylic acid and ethylene glycol dimethacrylate in the presence of L-phenylalanine was effective for the adsorption of BPA. It should be underlined that the experimental results also confirmed the findings of the theoretical analysis, which could be used as the predictable and low-cost tools for the preselection of functional monomers for the MIP's synthesis.



### 3.1.3. Theoretical Explanation of Interactions in the MIP Cavity

On the basis of monomer selection results, the model of the polymer cavity was prepared, and the simulation of BPA adsorption was performed to identify the interactions responsible for the molecular recognition process on the MIP matrix. Different forms of the analyte were analyzed. In the optimized system with a zwitterionic form of BPA present in acidic-neutral solutions, three classical hydrogen bonds were observed: two between the H atoms of the  $\text{-B(OH)}_2$  group from the analyte molecule and the O atom of the cross-linker residue (length of 2.60 and 3.00 Å) and one between the H atom of the  $\text{-NH}_3^+$  group from the analyte and the O atom of the cross-linker residue (length of 2.47 Å). Additionally, one non-classical hydrogen bond was formed between the O atom of the  $\text{-COO}^-$  group from the analyte and the H atom of the  $\text{-CH}_2\text{-}$  group from the cross-linker residue (length of 2.38 Å), and three hydrophobic  $\pi$ -alkyl-type interactions were present between the aromatic ring of the analyte and the  $\text{-CH}_3$  groups of the cross-linker and monomer residues (lengths of 3.78, 4.58, and 4.68 Å, Figure 2). We observed that all three functional groups of the analyte ( $\text{-B(OH)}_2$ ,  $\text{-COO}^-$ , and  $\text{-NH}_3^+$ ) were involved in interactions with the polymeric matrix, and those interactions were important in the molecular recognition mechanism observed in the studied MIP system.

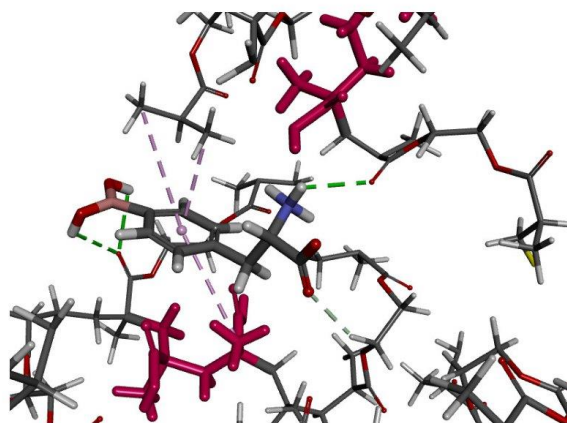


**Figure 2.** The cavity of MIP with the analyte inside. Monomer residues are shown as the pink molecules. The classical hydrogen bonds are shown as the green dashed lines, the non-classical hydrogen bonds are shown as the gray dashed lines, and the hydrophobic interactions are shown as the pink dashed lines.

In acidic solutions, the main form of BPA is a cationic form with a protonated amine group. In the simulated system with analyte cation, three classical hydrogen bonds were formed: two between the H atoms of the  $\text{-NH}_3^+$  group from the analyte and the O atom of the  $\text{-COOH}$  group from the monomer residue (length of 2.12 and 2.63 Å) and one between the O atom of the  $\text{-COOH}$  group from the analyte and the H atom of the  $\text{-COOH}$  group from the monomer residue (length of 2.37 Å). Also, two non-classical hydrogen bonds were observed between the O atom of the  $\text{-COOH}$  group from the analyte and the H atom of the  $\text{-CH}_2\text{-}$  group from the cross-linker residue (length of 2.76 Å), as well as between the H atom of the  $\text{-CH-}$  group from the analyte and the O atom from the cross-linker (length of 2.71 Å, Figure 3a). Only two functional groups ( $\text{-COOH}$  and  $\text{-NH}_3^+$ ) of BPA participated in the interactions' formations during the simulation of the adsorption process of the analyte cationic form on MIP material. No interactions of the analyte  $\text{-B(OH)}_2$  group with a polymeric matrix might be one of the reasons for a low MIP binding capacity of BPA from an acidic solution.

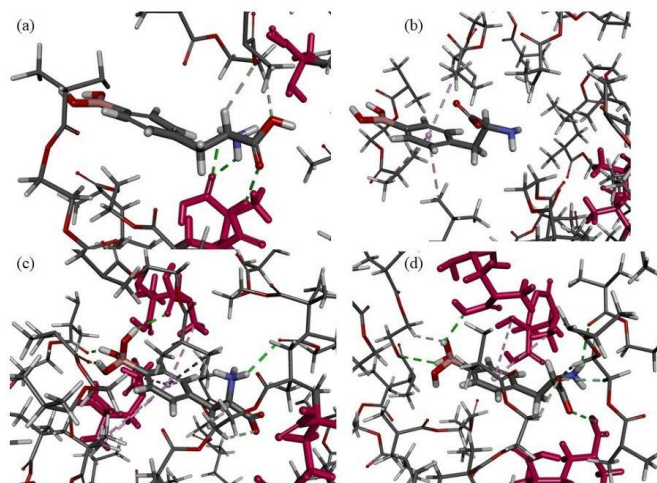


**Figure 3.** The cavity of MIP with different species of analyte inside: (a) cationic form; (b) anionic form with  $\text{COO}^-$  group; (c) zwitterion with  $\text{B(OH)}_3^-$  group; (d) anion with  $\text{COO}^-$  and  $\text{B(OH)}_3^-$  groups. Monomer residues are shown as the pink molecules. The classical hydrogen bonds are shown as the green dashed lines, the non-classical hydrogen bonds are shown as the gray dashed lines, and the hydrophobic interactions are shown as the pink dashed lines.

When the pH of an analyte solution is basic, anionic species of the analyte are present. Three different anions could be created: one with the  $\text{COO}^-$  group or zwitterion with the  $\text{B(OH)}_3^-$  group (charge of species is minus one) or one with both above mentioned groups (charge of form is minus two) [29]. In the system simulating the adsorption of an analyte anion with  $\text{COO}^-$  group, we observed only three hydrophobic  $\pi$ -alkyl-type interactions between the aromatic ring of the analyte and the  $\text{CH}_3$  groups of the cross-linker residues (lengths of 4.05, 4.10, and 4.89 Å, Figure 3b). No interactions were formed with the participation of the main functional groups of BPA, viz.  $\text{NH}_2$ ,  $\text{COO}^-$ , and  $\text{B(OH)}_2$ . On the other hand, when the systems modelling the adsorption process of two other anions (zwitterion with  $\text{B(OH)}_3^-$  group and the species with both  $\text{COO}^-$  and  $\text{B(OH)}_3^-$  groups) were analyzed, we could find interactions between all functional groups of the analyte and polymeric matrix. In the model of the  $\text{B(OH)}_3^-$  zwitterion adsorption, four classical hydrogen bonds were formed: three between the H atoms of the  $\text{B(OH)}_3^-$  group from the analyte molecule and the O atoms of the monomer or cross-linker residues (lengths of 2.19, 2.16, and 2.33 Å) and one between the H atom of the  $\text{NH}_3^+$  group from the analyte and the O atom of the cross-linker residue (length of 2.70 Å). Additionally, one non-classical hydrogen bond was formed between the O atom of the  $\text{COO}^-$  group from the analyte and the H atom of the  $\text{CH}_2$  group from the cross-linker residue (length of 2.58 Å), and seven hydrophobic  $\pi$ -alkyl-type interactions were present between the aromatic ring of the analyte and the  $\text{CH}_3$  groups of the cross-linker and monomer residues (length between 4.41 and 5.49 Å, Figure 3c). In the optimized system simulating the adsorption of an anion with two minus charges, we observed four classical hydrogen bonds: two between the H atoms of the  $\text{B(OH)}_3^-$  group from the analyte molecule and the O atoms of the monomer or cross-linker residues (lengths of 2.22 and 2.92 Å), one between the H atom of the  $\text{NH}_2$  group from the analyte and the O atom of the cross-linker residue (length of 2.55 Å), and one between the O atom of the  $\text{COO}^-$  group from the analyte and the H atom of the  $\text{COOH}$  group from the monomer residue (length of 2.82 Å). Also, four non-classical hydrogen bonds were formed: one between the O atom of  $\text{B(OH)}_3^-$  group from the analyte and the H atom of the  $\text{CH}_2$  group from the cross-linker residue (length of 2.43 Å) and

three between the O atom of the  $\text{-COO}^-$  group from the analyte and the H atoms of the  $\text{-CH}_2\text{-}$  groups from the cross-linker residues (lengths of 2.71, 2.75, and 2.80 Å). Moreover, two  $\pi$ -alkyl-type interactions were present between the aromatic ring of the analyte and the  $\text{-CH}_3$  groups of the monomer residues (lengths of 4.66 and 5.39 Å, Figure 3d). The types of interactions and functional groups of the analytes involved in the adsorption process on the MIP matrix in computational studies were similar when the zwitterion form and two anionic forms of BPA were analyzed. The coexistence of different anionic forms of the analyte in basic solution that could interact with the MIP in different ways might result in a lower specificity of MIP towards analyte in basic solution.

### 3.1.4. Fabrication of Honeycomb-like Polymer and Adsorption Capabilities

In the following step of the investigation, we aimed to construct the MIP with enhanced binding capacity. It is known from the literature survey that more sophisticated D- and L-phenylalanine imprinted systems, such as MIP conjugates with gold nanoparticles [30] or MIPs synthesized in the presence of chiral ionic liquids [31], could affect the binding capacity of the resulted materials, being promising sorbents for separation purposes. However, it should be emphasized that the application of those systems for BNCT could be limited due to biosafety reasons. Thus, we concluded that the use of well-known biocompatible components for the MIP synthesis will be beneficiary [32]. The previously optimized composition system based on methacrylic acid and ethylene glycol dimethacrylate was used in the synthesis of honeycomb-like structures with an extended surface area (the scheme is presented in Figure 1). The honeycomb-like structures have found applications in many diverse fields such as architecture or mechanical engineering, but most importantly, they are highly utilized in biomedicine [33].

In the fabrication process of the honeycomb-like structure, the siloxane particles that were functionalized with MPS were used to provide a support for the polymer matrix prior to the etching of siloxane material. It allowed us to obtain the structural periodic systems of a regular nature and an extended external surface. Moreover, we have expanded our investigation for the analysis of the cross-linker effect on the binding capacity of honeycomb-like MIPs towards BPA. For that purpose, five MIPs were composed from methacrylic acid and ethylene glycol dimethacrylate as well as four other cross-linkers, viz. poly(ethylene) glycol dimethacrylate, trimethylolpropane trimethacrylate, triethylene glycol dimethacrylate, and divinylbenzene. Although the last cross-linker cannot be considered as a biocompatible reagent, it was very interesting for us to explore the effect of the rigid molecular structure of divinylbenzene on the formation of honeycomb-like structure. The results of the binding capacities, distribution coefficients, and *IFs* are presented in Table 3.

As can be seen, the honeycomb-like structure of MIP1<sub>h</sub> was characterized by the higher binding capacity of BPA when compared to bulk MIP1<sub>b</sub>. It could be explained by the higher accessibility of the adsorption sites to the target molecule. However, simultaneously, we observed a decrease in the specificity of MIP1<sub>h</sub> when compared to bulk MIP1<sub>b</sub> due to significantly increased adsorption on the NIP1<sub>h</sub>. The specificity was reduced by more than double when compared to bulk material. We could suppose that the higher accessibility of the extended surface of the honeycomb-like structure resulted also with higher non-specific adsorption. This phenomenon was confirmed in the next analyzed systems that were characterized by higher non-specific adsorption of non-imprinted materials, and the specificities of those systems were unsatisfactory. The MIP2<sub>h</sub>, MIP3<sub>h</sub>, MIP4<sub>h</sub>, and MIP5<sub>h</sub> were characterized by the moderate binding capacity with a decreasing trend. As can be expected, the MIP5<sub>h</sub> synthesized from the rigid cross-linker, divinylbenzene, was characterized by the lowest binding capacity of BPA among all polymers.

## 3.2. Characterization of Honeycomb-like Polymer

### 3.2.1. Morphological Studies

In order to confirm the formation of the honeycomb-like structure, SEM analysis was employed, and the micrographs of the copolymers of methacrylic acid-co-ethylene glycol



dimethacrylate, MIP1<sub>h</sub>/NIP1<sub>h</sub> (Figure 4a–f), and methacrylic acid-co-poly(ethylene) glycol dimethacrylate, MIP2<sub>h</sub>/NIP2<sub>h</sub> (Figure 4g,h), were analyzed.

As can be seen, the micrographs of MIP1<sub>h</sub>/NIP1<sub>h</sub> in high magnification (Figure 4a–c) revealed an ordered porous, honeycomb-like structure. It was clearly detected that the polymer formed over the siloxane support possessed periodic intervals that were created after the etching of functionalized siloxane particles. We have found that internal layers of the polymer were more homogeneous (Figure 4a–c) than external layers (Figure 4d), but the honeycomb-like structure was still maintained. The diameter of the periodic structure of the honeycomb-like element was equal to  $487 \pm 23$  nm (Figure 4b). The external layer revealed multiple holes (Figure 4d), and their nature was investigated more deeply. We have found nestle-like regions with multiple polymer entities that were etched (Figure 4e). We could suppose that these holes in the polymeric spherical particles originated from the breaks in the polymeric layer, allowing aqueous hydrofluoric acid to be transferred into the internal siloxane core of the particles. These breaks could be a result of the conglomeration of siloxane functionalized particles during the polymerization process. Moreover, the effectiveness of the etching of internal siloxane cores was proved. We have also observed sunken, hollow-like structures (Figure 4f). As can also be seen, the micrographs of MIP2<sub>h</sub>/NIP2<sub>h</sub> in high magnification (Figure 4g,h) revealed an ordered, porous, honeycomb-like structure. However, the character of this structure differed when compared to the honeycomb-like structure of MIP1<sub>h</sub>/NIP1<sub>h</sub>. The remaining polymer skeleton after etching could be characterized by thicker layers with a smoother surface. We could only suppose that the higher viscosity of the poly(ethylene) glycol dimethacrylate component of the pre-polymerization mixture (approx. 70 mPa s) when compared to the ethylene glycol dimethacrylate (approx. 2 mPa s) component was responsible for the morphology of MIP2<sub>h</sub>/NIP2<sub>h</sub> [34,35].

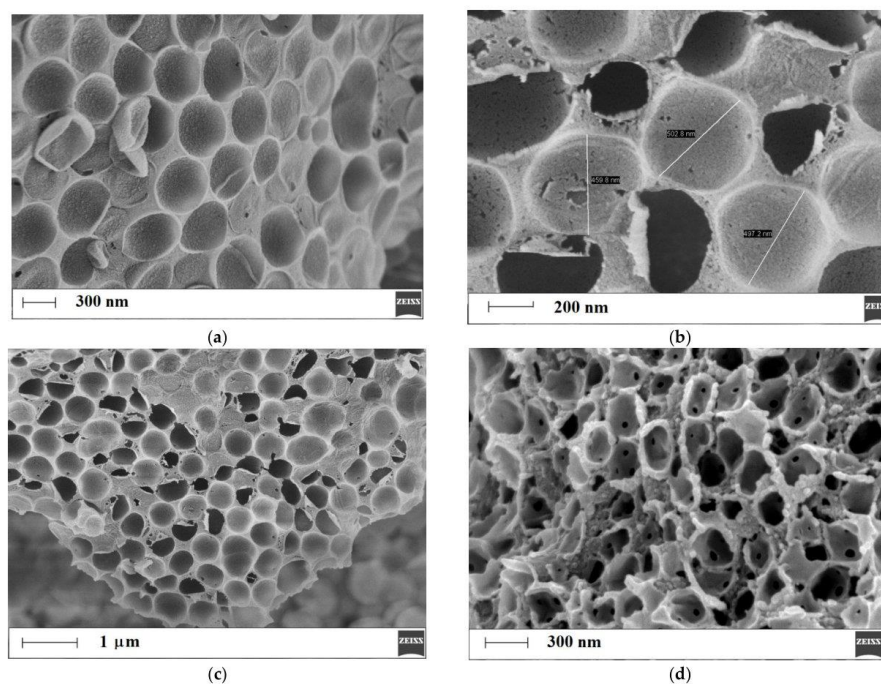


Figure 4. Cont.



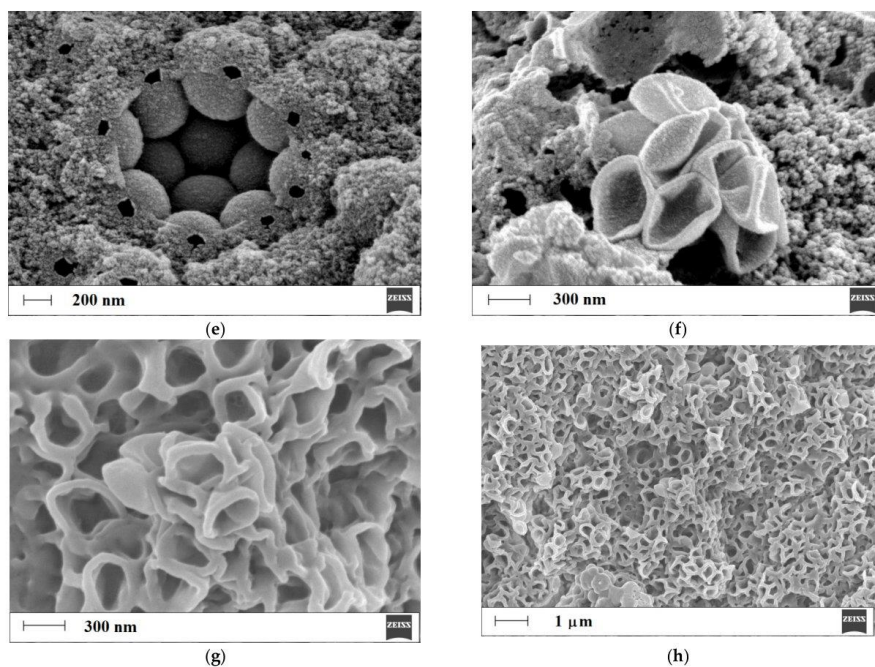


Figure 4. Micrographs of honeycomb-like structures of MIP1<sub>h</sub>/NIP1<sub>h</sub> (a–f) and MIP2<sub>h</sub>/NIP2<sub>h</sub> (g,h).

### 3.2.2. Structural Analysis

The FT-IR analysis was employed to prove the structure of the obtained MIP1<sub>h</sub> (Figure 5a). The MIP1<sub>h</sub> was analyzed after the synthesis and the extraction of the template molecule of L-phenylalanine. To reveal the predicted interactions between BPA and the MIP1<sub>h</sub>, the FT-IR analysis was extended to the sample of a polymer soaked in the standard solution of BPA and dried (Figure 5b).

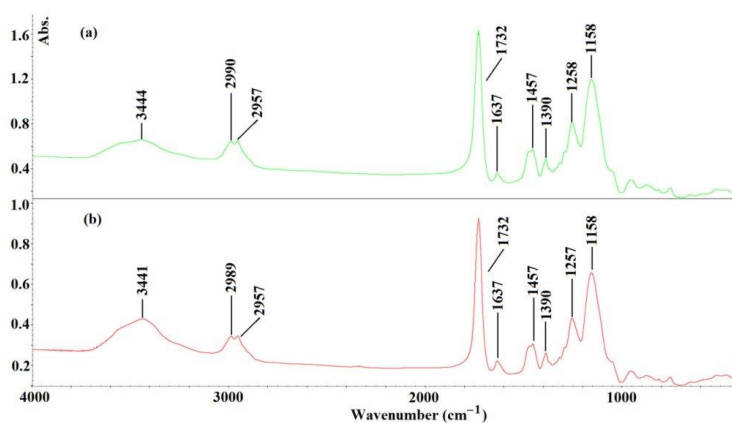


Figure 5. FT-IR spectra of MIP1<sub>h</sub> after synthesis and extraction of template ((a), green line), and MIP1<sub>h</sub> after soaked in the standard solution of BPA and dried ((b), red line).

As can be seen, the characteristic vibration peaks, derived from structural fragments of MIP1<sub>h</sub> after the synthesis and extraction of the template, could be assigned as follows: at 3444 cm<sup>-1</sup> (broad), the -OH stretching vibrations; at 2990 and at 2957 cm<sup>-1</sup>, the stretching vibration of the *sp*<sup>2</sup> and *sp*<sup>3</sup> bonds of the -CH from the cross-linker; at 1732 cm<sup>-1</sup>, the -C=O stretching vibration; at 1637 cm<sup>-1</sup>, the stretching of -C=C bonds; at 1457 cm<sup>-1</sup>, the stretching of -CH<sub>2</sub>-CH<sub>2</sub>; at 1390 cm<sup>-1</sup>, the stretching of -CH<sub>3</sub>; at 1258 cm<sup>-1</sup> and 1158 cm<sup>-1</sup>, the C-O-C stretching vibrations. A very similar pattern of the FT-IR was observed for the MIP1<sub>h</sub> after being soaked in the standard solution of BPA and dried. The only difference noted between the two spectra that were recorded was related to the region of the -OH stretching vibrations. The shift of the broad peak maximum from 3444 cm<sup>-1</sup> to 3441 cm<sup>-1</sup> could be explained by the presence of -B(OH)<sub>2</sub> group in the BPA molecule and the possible existence of hydrogen bonds between the BPA and the residues of the methacrylic acid in the MIP1<sub>h</sub>.

### 3.3. Release Studies

The preliminary desorption studies of BPA were conducted after soaking MIP1<sub>h</sub> and NIP1<sub>h</sub> in the standard solution of BPA at the concentrations of 20 µg L<sup>-1</sup>, 200 µg L<sup>-1</sup>, or 1000 µg L<sup>-1</sup> in the methanol–water system (85:15, *v/v*). Firstly, the following binding capacities were obtained for MIP1<sub>h</sub>: 86.5 ± 3.3 ng g<sup>-1</sup>, 715.0 ± 6.1 ng g<sup>-1</sup>, 6970 ± 112 ng g<sup>-1</sup>, respectively, and for NIP1<sub>h</sub>: 44 ± 0.10 ng g<sup>-1</sup>, 370 ± 5.5 ng g<sup>-1</sup>, 4155 ± 31 ng g<sup>-1</sup>, respectively. The calculated *IFs* were as follows: 1.97 (for a concentration of 20 µg L<sup>-1</sup>), 1.93 (for a concentration of 200 µg L<sup>-1</sup>), and 1.68 (for a concentration of 1000 µg L<sup>-1</sup>). The results confirmed the increase in the binding capacity of MIP1<sub>h</sub> and NIP1<sub>h</sub> with the increased concentration of the standard solution of BPA. The specificity remained similar in the concentration range of BPA between 20–200 µg L<sup>-1</sup> but slightly decreased in a higher concentration of 1000 µg L<sup>-1</sup>. Thus, to evaluate the desorption capabilities of MIP1<sub>h</sub> and NIP1<sub>h</sub>, the samples loaded with the concentration of 1000 µg L<sup>-1</sup> were taken for analysis. Figure 6 presents the desorption profiles, expressed as the percentage of the loaded amount of BPA from MIP1<sub>h</sub> and NIP1<sub>h</sub> to the methanol–water system (85:15, *v/v*) in time.

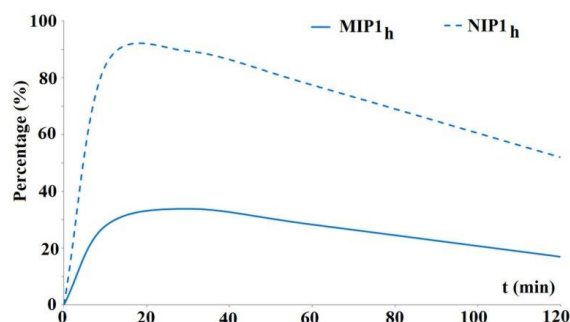


Figure 6. Desorption profiles of BPA from MIP1<sub>h</sub> and NIP1<sub>h</sub> to the methanol–water system (85:15, *v/v*).

As could be seen, the significant difference in the desorption of BPA in the methanol–water system (85:15, *v/v*) from MIP1<sub>h</sub> and NIP1<sub>h</sub> was observed in time. The desorption was fast and proceeded mostly during the first half hour of the experiment with the values of 33.82% for MIP1<sub>h</sub> and 89.46% for NIP1<sub>h</sub>. The lower amount of BPA that was desorbed from MIP1<sub>h</sub> when compared to NIP1<sub>h</sub> could be explained by the presence of the surface modified regions in the polymeric network that were responsible for the adsorption/desorption phenomenon (the so-called ‘tumbling effect’) that slowed down the desorption process of the BPA.

In the next step, the release profiles from the model PBS were performed in various pH values, viz. 2, 5, and 9.5. It is known that the BPA could exist in various ionic forms that depend on the pH of the system. The  $pK_a$  values are as follows: 2.46 ( $pK_{a_1}$ ), 8.46 ( $pK_{a_2}$ ), and 9.76 ( $pK_{a_3}$ ) [29]. Firstly, the binding capacities in the above-mentioned pH values of the BPA from the adjusted methanol–water (85:15,  $v/v$ ) solution were analyzed. The binding capacities were the following for the pH 2:  $370.0 \pm 1.0 \text{ ng g}^{-1}$  for MIP1<sub>h</sub> and  $310 \pm 15 \text{ ng g}^{-1}$  for NIP1<sub>h</sub>; for the pH 5:  $1905 \pm 14 \text{ ng g}^{-1}$  for MIP1<sub>h</sub> and  $1105 \pm 16 \text{ ng g}^{-1}$  for NIP1<sub>h</sub>; for the pH 9.5:  $1345 \pm 53 \text{ ng g}^{-1}$  for MIP1<sub>h</sub> and  $1670 \pm 46 \text{ ng g}^{-1}$  for NIP1<sub>h</sub>. The specificity expressed as the *IFs* were the following: 1.19 for pH 2, 1.72 for pH 5, and 0.81 for pH 9.5. The results suggested that the binding capacity of BPA on the MIP1<sub>h</sub> increased nearly fivefold with the increase in the pH of the adsorption system from pH 2 to pH 5 and then was nearly halved in pH 9.5. In contrast, the binding capacity of BPA on the NIP1<sub>h</sub> increased constantly from an acidic to basic environment of the loading system. The remarkable difference in pH 9.5 was responsible for the lack of specificity of MIP1<sub>h</sub>.

The release profiles of BPA from MIP1<sub>h</sub> and NIP1<sub>h</sub> expressed as the percentage of the loaded amount are presented in Figure 7. For the purpose of this experiment, the loading standard solution of a concentration of  $200 \mu\text{g L}^{-1}$  was applied to emphasize the specificity.

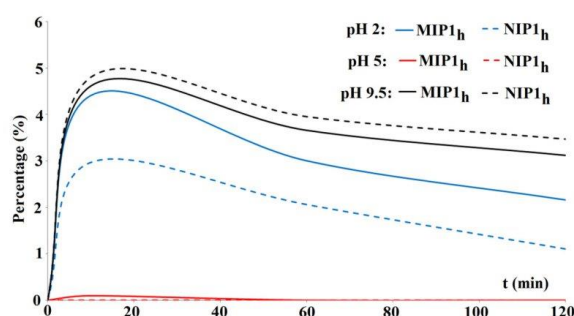


Figure 7. Release profiles of BPA from MIP1<sub>h</sub> and NIP1<sub>h</sub> to PBS.

As can be seen, the percentage of the BPA that was released from the MIP1<sub>h</sub> and NIP1<sub>h</sub> was low (between 0% and 4.81%), and the peak occurred within the first 20 min of the experiment. In the sample adjusted to pH 2, the released amount of the BPA from MIP1<sub>h</sub> was higher than from NIP1<sub>h</sub>. It could be explained by the protonation of the amine group in the BPA molecule and the competitive protonation of the carboxylic residues in the MIP1<sub>h</sub>. In the sample adjusted to pH 5, the released amount of the BPA from MIP1<sub>h</sub> and NIP1<sub>h</sub> was very small. The zwitterion insoluble form of the BPA at pH 5 could explain the result. In the sample adjusted to pH 9.5, the released amount of the BPA from MIP1<sub>h</sub> was lower than from NIP1<sub>h</sub>. The additional interactions of anionic regions of  $-\text{B}(\text{OH})_3^-$  with the polymer network could explain the decrease in release ratio.

#### 3.4. Cytotoxicity Tests

Viability experiments using the MTT assay were conducted using two different cell lines (cancerous and normal) to assess the initial safety of the synthesized honeycomb-like polymer with the most promising properties, MIP1<sub>h</sub>. The V79-4 (normal) and A549 (cancerous) cells were exposed to four different concentrations of MIP1<sub>h</sub> extracts for 20 h at 36.8 °C. The results presented in Figure 8 show a high cell viability and negligible cytotoxicity within the tested range of concentrations, suggesting good biocompatibility of the material under examined conditions and a potential for in vivo applications. For the V79-4 cell line, the viability was above 80% for the entire range of concentrations, and for the A549 cell line, it was above 90%. This is in accordance with the assumptions based on the composition of synthesized material—other MIPs for biomedical applications



synthesized from methacrylic acid and ethylene glycol dimethacrylate have been reported as being low-toxic [36,37].

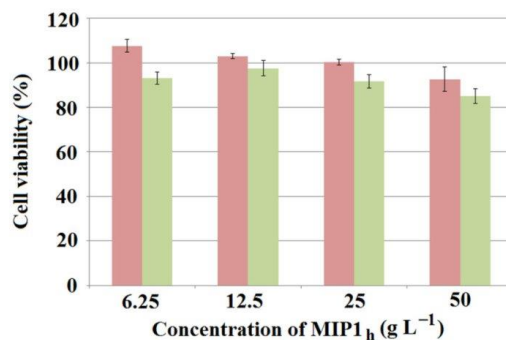


**Figure 8.** The MTT test results on A549 (red bars) and V79-4 (green bars) cell lines, obtained from MIP1<sub>h</sub> extracts within the whole range of examined concentrations.

#### 4. Conclusions

A honeycomb-like MIP composed from methacrylic acid copolymerized with ethylene glycol dimethacrylate was successfully synthesized for specific recognition towards BPA. Theoretical analysis was employed to choose the most suitable monomer, which was further confirmed by experiments on bulk polymer. The specificity of a honeycomb-like MIP compared to a bulk polymer of the same matrix was reduced due to the higher non-specific adsorption caused by higher accessibility of the extended surface of the structure. The increased binding surface was also reflected in a honeycomb-like MIP's higher binding capacity of BPA when compared to a bulk polymer, proving honeycomb-like MIPs a more attractive material for further investigations related to the delivery of boron to the target site. The adsorption properties in different pH were further explained by the theoretical studies. The ordered, porous morphology of honeycomb-like MIPs was confirmed with SEM, and its structure was confirmed by FT-IR, proving that the material of the desired structure was obtained. The release studies in the model PBS revealed that no more than 4.81% of BPA is released from the MIP within two hours, which is a significantly beneficial result when considering the application in BNCT, meaning that the entire composite could be delivered intact to the target site. Cytotoxicity towards A549 and V79-4 cell lines within the tested range of concentrations was considered very low, suggesting the safety of the synthesized MIP for potential in vivo applications. In order to provide a therapeutic dose of boron, the binding capacity of the synthesized material still has to be improved. However, due to the delivery of BPA with a MIP system, and based on the study by Nomoto et al. on a different polymeric delivery system [8], it can be expected that the cellular internalization mechanism will change, and thus, we can assume that the accumulation in tumor cells will be more efficient than in the case of the currently used BPA–fructose complex. To the best of our knowledge, this study presents the first results of a MIP design for boron-containing molecule delivery considered for BNCT application.

**Author Contributions:** Conceptualization, E.B., M.S. (Monika Sobiech), J.G. and P.L.; methodology, E.B., M.S. (Monika Sobiech) and M.S. (Małgorzata Sochacka); software, M.S. (Monika Sobiech); validation, J.G.; formal analysis, M.S. (Monika Sobiech), J.G. and P.L.; investigation, E.B., M.S. (Monika Sobiech) and M.S. (Małgorzata Sochacka); resources, E.B., M.S. (Monika Sobiech), J.G. and P.L.; data curation, E.B., M.S. (Monika Sobiech), J.G. and P.L.; writing—original draft preparation, E.B., M.S. (Monika Sobiech), J.G. and P.L.; writing—review and editing, E.B., M.S. (Monika Sobiech), J.G. and P.L.; visualization, E.B., M.S. (Monika Sobiech) and P.L.; supervision, M.S. (Monika Sobiech), J.G. and P.L.; project administration, P.L.; funding acquisition, E.B. All authors have read and agreed to the published version of the manuscript.



**Funding:** The contribution of Emilia Balcer was realized within the National Centre for Research and Development Project No. POWR.03.02.00-00-I009/17-00 (Radiopharmaceuticals for molecularly targeted diagnosis and therapy, RadFarm. Operational Project Knowledge Education Development 2014–2020 co-financed by the European Social Fund).

**Data Availability Statement:** The data presented in this study are available on request from corresponding author.

**Conflicts of Interest:** The authors declare no conflict of interest.

## References

1. Dymova, M.A.; Taskaev, S.Y.; Richter, V.A.; Kuligina, E.V. Boron Neutron Capture Therapy: Current Status and Future Perspectives. *Cancer Commun.* **2020**, *40*, 406–421. [\[CrossRef\]](#) [\[PubMed\]](#)
2. Barth, R.F.; Mi, P.; Yang, W. Boron Delivery Agents for Neutron Capture Therapy of Cancer. *Cancer Commun.* **2018**, *38*, 35. [\[CrossRef\]](#) [\[PubMed\]](#)
3. Bendel, P.; Wittig, A.; Basilio, F.; Mauri, P.L.; Sauerwein, W. Metabolism of Borono-Phenylalanine–Fructose Complex (BPA–Fr) and Borocaptate Sodium (BSH) in Cancer Patients—Results from EORTC trial 11001. *J. Pharm. Biomed. Anal.* **2010**, *51*, 284–287. [\[CrossRef\]](#)
4. Hu, K.; Yang, Z.; Zhang, L.; Xie, L.; Wang, L.; Xu, H.; Josephson, L.; Liang, S.H.; Zhang, M.-R. Boron Agents for Neutron Capture Therapy. *Coord. Chem. Rev.* **2020**, *405*, 213139. [\[CrossRef\]](#)
5. Kiger, W.S.; Palmer, M.R.; Riley, K.J.; Zamenhof, R.G.; Busse, P.M. Pharmacokinetic Modeling for Boronophenylalanine–Fructose Mediated Neutron Capture Therapy:  $^{10}\text{B}$  Concentration Predictions and Dosimetric Consequences. *J. Neurooncol.* **2003**, *62*, 171–186. [\[CrossRef\]](#) [\[PubMed\]](#)
6. Wongthai, P.; Hagiwara, K.; Miyoshi, Y.; Wiriyaerkmul, P.; Wei, L.; Ohgaki, R.; Kato, I.; Hamase, K.; Nagamori, S.; Kanai, Y. Boronophenylalanine, a Boron Delivery Agent for Boron Neutron Capture Therapy, Is Transported by  $\text{ATB}^{0,+}$ , LAT1 and LAT2. *Cancer Sci.* **2015**, *106*, 279–286. [\[CrossRef\]](#)
7. Mi, P.; Yanagie, H.; Dewi, N.; Yen, H.-C.; Liu, X.; Suzuki, M.; Sakurai, Y.; Ono, K.; Takahashi, H.; Cabral, H.; et al. Block Copolymer-Boron Cluster Conjugate for Effective Boron Neutron Capture Therapy of Solid Tumors. *J. Control. Release* **2017**, *254*, 1–9. [\[CrossRef\]](#)
8. Nomoto, T.; Inoue, Y.; Yao, Y.; Suzuki, M.; Kanamori, K.; Takemoto, H.; Matsui, M.; Tomoda, K.; Nishiyama, N. Poly(Vinyl Alcohol) Boosting Therapeutic Potential of *p*-Boronophenylalanine in Neutron Capture Therapy by Modulating Metabolism. *Sci. Adv.* **2020**, *6*, eaaz1722. [\[CrossRef\]](#)
9. Chauhan, N.P.S.; Hosmane, N.S.; Mozafari, M. Boron-Based Polymers: Opportunities and Challenges. *Mater. Today Chem.* **2019**, *14*, 100184. [\[CrossRef\]](#)
10. BelBruno, J.J. Molecularly Imprinted Polymers. *Chem. Rev.* **2019**, *119*, 94–119. [\[CrossRef\]](#)
11. Janczura, M.; Luliński, P.; Sobiech, M. Imprinting Technology for Effective Sorbent Fabrication: Current State-of-Art and Future Prospects. *Materials* **2021**, *14*, 1850. [\[CrossRef\]](#) [\[PubMed\]](#)
12. Shahhoseini, F.; Azizi, A.; Bottaro, C.S. A Critical Evaluation of Molecularly Imprinted Polymer (MIP) Coatings in Solid Phase Microextraction Devices. *TrAC Trends Anal. Chem.* **2022**, *156*, 116695. [\[CrossRef\]](#)
13. Sobiech, M.; Luliński, P.; Wieczorek, P.P.; Marć, M. Quantum and Carbon Dots Conjugated Molecularly Imprinted Polymers as Advanced Nanomaterials for Selective Recognition of Analytes in Environmental, Food and Biomedical Applications. *TrAC Trends Anal. Chem.* **2021**, *142*, 116306. [\[CrossRef\]](#)
14. Luliński, P. Molecularly Imprinted Polymers Based Drug Delivery Devices: A Way to Application in Modern Pharmacotherapy. A Review. *Mater. Sci. Eng. C* **2017**, *76*, 1344–1353. [\[CrossRef\]](#) [\[PubMed\]](#)
15. Tuwahatu, C.A.; Yeung, C.C.; Lam, Y.W.; Roy, V.A.L. The Molecularly Imprinted Polymer Essentials: Curation of Anticancer, Ophthalmic, and Projected Gene Therapy Drug Delivery Systems. *J. Control. Release* **2018**, *287*, 24–34. [\[CrossRef\]](#)
16. Haupt, K.; Medina Rangel, P.X.; Bui, B.T.S. Molecularly Imprinted Polymers: Antibody Mimics for Bioimaging and Therapy. *Chem. Rev.* **2020**, *120*, 9554–9582. [\[CrossRef\]](#)
17. Hroboňová, K.; Vyboňová, V.; Lomenova, A.; Špačková, A.; Svitková, V. Characterization of Kinetic, Thermodynamic, and Binding Properties of L-Phenylalanine Molecularly Imprinted Polymer. *Monatsh. Chem.* **2022**, *153*, 1037–1047. [\[CrossRef\]](#)
18. Stöber, W.; Fink, A.; Bohn, E. Controlled Growth of Monodisperse Silica Spheres in the Micron Size Range. *J. Colloid Interface Sci.* **1968**, *26*, 62–69. [\[CrossRef\]](#)
19. Janczura, M.; Sobiech, M.; Luliński, P. Insight into the Morphology, Pore Structure and Sorption Properties of 4-hydroxy-3-nitrophenylacetic Acid Imprinted Poly(Acrylic Acid–Co-Ethylene Glycol Dimethacrylate) Sorbent. *Polym. Test.* **2021**, *93*, 106983. [\[CrossRef\]](#)
20. Sobiech, M.; Giebułtowski, J.; Luliński, P. Computational and Experimental Studies of Magnetic Molecularly Imprinted Sorbent with High Specificity towards Aceclofenac. *Microchem. J.* **2023**, *186*, 108272. [\[CrossRef\]](#)
21. Frish, M.J.; Trucks, G.W.; Schlegel, H.B.; Scuseria, G.E.; Robb, M.A.; Cheeseman, J.R.; Scalmani, G.; Barone, V.; Petersson, A.; Nakatsuji, H.; et al. *Gaussian 16*; Gaussian, Inc.: Wallingford, CT, USA, 2016.

22. Martínez, L.; Andrade, R.; Birgin, E.G.; Martínez, J.M. PACKMOL: A Package for Building Initial Configurations for Molecular Dynamics Simulations. *J. Comput. Chem.* **2009**, *30*, 2157–2164. [[CrossRef](#)] [[PubMed](#)]
23. Brooks, B.R.; Brooks, C.L.; Mackerell, A.D.; Nilsson, L.; Petrella, R.J.; Roux, B.; Won, Y.; Archontis, G.; Bartels, C.; Boresch, S.; et al. CHARMM: The Biomolecular Simulation Program. *J. Comput. Chem.* **2009**, *30*, 1545–1614. [[CrossRef](#)] [[PubMed](#)]
24. Dassault Systèmes BIOVIA. *Discovery Studio Modeling Environment*, Release 2021; Dassault Systèmes: San Diego, CA, USA, 2021.
25. Ryckaert, J.-P.; Ciccotti, G.; Berendsen, H.J.C. Numerical Integration of the Cartesian Equations of Motion of a System with Constraints: Molecular Dynamics of n-Alkanes. *J. Comput. Phys.* **1977**, *23*, 327–341. [[CrossRef](#)]
26. Kvamme, B. Thermodynamic Properties and Dielectric Constants in Water/Methanol Mixtures by Integral Equation Theory and Molecular Dynamics Simulations. *Phys. Chem. Chem. Phys.* **2002**, *4*, 942–948. [[CrossRef](#)]
27. Piletsky, S.A.; Karim, K.; Piletska, E.V.; Day, C.J.; Freebairn, K.W.; Legge, C.; Turner, A.P.F. Recognition of Ephedrine Enantiomers by Molecularly Imprinted Polymers Designed Using a Computational Approach. *Analyst* **2001**, *126*, 1826–1830. [[CrossRef](#)]
28. Gul, S.; Shah, N.; Arain, M.B.; Rahman, N.; Rehan, T.; Ul-Islam, M.; Ullah, M.W.; Yang, G. Fabrication of Magnetic Core Shell Particles Coated with Phenylalanine Imprinted Polymer. *Polym. Test.* **2019**, *75*, 262–269. [[CrossRef](#)]
29. Mori, Y.; Suzuki, A.; Yoshino, K.; Kakihana, H. Complex Formation of p-Boronophenylalanine with Some Monosaccharides. *Pigment. Cell Res.* **1989**, *2*, 273–277. [[CrossRef](#)]
30. Zhou, J.; Sheth, S.; Zhou, H.; Song, Q. Highly Selective Detection of L-Phenylalanine by Molecularly Imprinted Polymers Coated Au Nanoparticles via Surface-Enhanced Raman Scattering. *Talanta* **2020**, *211*, 120745. [[CrossRef](#)]
31. Chen, S.; Huang, X.; Yao, S.; Huang, W.; Xin, Y.; Zhu, M.; Song, H. Highly Selective Recognition of L-phenylalanine with Molecularly Imprinted Polymers Based on Imidazolyl Amino Acid Chiral Ionic Liquid. *Chirality* **2019**, *31*, 824–834. [[CrossRef](#)]
32. Widiyanti, P.; Amali, M.A. Aminatun Poly(Ethylene Glycol)Dimethacrylate—Nanofibrillated Cellulose Bionanocomposites as Injectable Hydrogel for Therapy of Herniated Nucleus Pulposus Patients. *J. Mater. Res. Technol.* **2020**, *9*, 12716–12722. [[CrossRef](#)]
33. Zhang, Q.; Yang, X.; Li, P.; Huang, G.; Feng, S.; Shen, C.; Han, B.; Zhang, X.; Jin, F.; Xu, F.; et al. Bioinspired Engineering of Honeycomb Structure—Using Nature to Inspire Human Innovation. *Prog. Mater. Sci.* **2015**, *74*, 332–400. [[CrossRef](#)]
34. Hanemann, T.; Honnef, K. Viscosity and Refractive Index Adjustment of Poly(Methyl Methacrylate-Co-Ethyleneglycol Dimethacrylate) for Application in Microoptics. *Polym. Adv. Technol.* **2015**, *26*, 294–299. [[CrossRef](#)]
35. Killion, J.A.; Geever, L.M.; Devine, D.M.; Kennedy, J.E.; Higginbotham, C.L. Mechanical Properties and Thermal Behaviour of PEGDMA Hydrogels for Potential Bone Regeneration Application. *J. Mech. Behav. Biomed. Mater.* **2011**, *4*, 1219–1227. [[CrossRef](#)] [[PubMed](#)]
36. Cecchini, A.; Raffa, V.; Canfarotta, F.; Signore, G.; Piletsky, S.; MacDonald, M.P.; Cuschieri, A. In Vivo Recognition of Human Vascular Endothelial Growth Factor by Molecularly Imprinted Polymers. *Nano Lett.* **2017**, *17*, 2307–2312. [[CrossRef](#)]
37. Farzaneh, S.; Asadi, E.; Abdouss, M.; Barghi-Lish, A.; Azodi-Deilami, S.; Khonakdar, H.A.; Gharghabi, M. Molecularly Imprinted Polymer Nanoparticles for Olanzapine Recognition: Application for Solid Phase Extraction and Sustained Release. *RSC Adv.* **2015**, *5*, 9154–9166. [[CrossRef](#)]

**Disclaimer/Publisher's Note:** The statements, opinions and data contained in all publications are solely those of the individual author(s) and contributor(s) and not of MDPI and/or the editor(s). MDPI and/or the editor(s) disclaim responsibility for any injury to people or property resulting from any ideas, methods, instructions or products referred to in the content.

### 3.3. Investigation of the Impact of L-Phenylalanine and L-Tyrosine Pre-Treatment on the Uptake of 4-Borono-L-Phenylalanine in Cancerous and Normal Cells Using an Analytical Approach Based on SC-ICP-MS



Article

## Investigation of the Impact of L-Phenylalanine and L-Tyrosine Pre-Treatment on the Uptake of 4-Borono-L-Phenylalanine in Cancerous and Normal Cells Using an Analytical Approach Based on SC-ICP-MS

Emilia Balcer <sup>1,2</sup> , Joanna Giebułtowicz <sup>2,\*</sup> , Małgorzata Sochacka <sup>2</sup> , Anna Ruszczyńska <sup>3</sup> , Magdalena Muszyńska <sup>3,4</sup> and Ewa Bułska <sup>3</sup>

- <sup>1</sup> Radiochemistry Team, Reactor Research Division, Nuclear Facilities Operations Department, National Centre for Nuclear Research, Sołtana 7, Świerk, 05-400 Otwock, Poland; emilia.balcer@ncbj.gov.pl  
<sup>2</sup> Department of Drug Chemistry, Pharmaceutical and Biomedical Analysis, Faculty of Pharmacy, Medical University of Warsaw, Banacha 1, 02-097 Warsaw, Poland; malgorzata.bogucka@wum.edu.pl  
<sup>3</sup> Faculty of Chemistry, Biological and Chemical Research Centre, University of Warsaw, Żwirki i Wigury 101, 02-089 Warsaw, Poland; aruszcz@chem.uw.edu.pl (A.R.); magdalena.muszyńska@pepolska.pl (M.M.); ebulska@chem.uw.edu.pl (E.B.)  
<sup>4</sup> Pro-Environment Polska Sp. z o.o., Żwirki i Wigury 101, 02-089 Warsaw, Poland  
\* Correspondence: joanna.giebułtowicz@wum.edu.pl; Tel.: +48-22-5720630



**Citation:** Balcer, E.; Giebułtowicz, J.; Sochacka, M.; Ruszczyńska, A.; Muszyńska, M.; Bułska, E. Investigation of the Impact of L-Phenylalanine and L-Tyrosine Pre-Treatment on the Uptake of 4-Borono-L-Phenylalanine in Cancerous and Normal Cells Using an Analytical Approach Based on SC-ICP-MS. *Molecules* **2023**, *28*, 6552. <https://doi.org/10.3390/molecules28186552>

Academic Editors: Rafik Karaman, Paola Fossa and Jarkko Rautio

Received: 21 August 2023  
Revised: 4 September 2023  
Accepted: 6 September 2023  
Published: 10 September 2023



**Copyright:** © 2023 by the authors. Licensee MDPI, Basel, Switzerland. This article is an open access article distributed under the terms and conditions of the Creative Commons Attribution (CC BY) license (<https://creativecommons.org/licenses/by/4.0/>).

**Abstract:** Boron has gained significant attention in medical research due to its B-10 isotope's high cross section for the reaction with thermal neutrons, generating ionizing particles that can eliminate cancer cells, propelling the development of boron neutron capture therapy (BNCT) for cancer treatment. The compound 4-borono-L-phenylalanine (BPA) has exhibited potential in BNCT clinical trials. Enhancing BPA uptake in cells involves proposing L-amino acid preloading. This study introduces a novel analytical strategy utilizing ICP-MS and single cell ICP-MS (SC-ICP-MS) to assess the effectiveness of L-tyrosine and L-phenylalanine preloading on human non-small cell lung carcinoma (A549) and normal Chinese hamster lung fibroblast (V79-4) models, an unexplored context. ICP-MS outcomes indicated that L-tyrosine and L-phenylalanine pre-treatment increased BPA uptake in V79-4 cells by  $2.04 \pm 0.74$ -fold ( $p = 0.000066$ ) and  $1.46 \pm 0.06$ -fold ( $p = 0.000016$ ), respectively. Conversely, A549 cells manifested heightened BPA uptake solely with L-tyrosine preloading, with a factor of  $1.24 \pm 0.47$  ( $p = 0.028$ ). BPA uptake remained higher in A549 compared to V79-4 regardless of preloading. SC-ICP-MS measurements showcased noteworthy boron content heterogeneity within A549 cells, signifying diverse responses to BPA exposure, including a subset with notably high BPA uptake. This study underscores SC-ICP-MS's utility in precise cellular boron quantification, validating cellular BPA uptake's heterogeneity.

**Keywords:** 4-borono-L-phenylalanine; boron; boron neutron capture therapy; L-phenylalanine; L-tyrosine; single cell ICP-MS

## 1. Introduction

Cancer is a complex and life-threatening disease characterized by uncontrolled cellular growth and division. Developing effective cancer treatment is of utmost importance, prompting researchers to explore innovative approaches to enhance the effectiveness of cancer therapies. One such approach involves utilizing boron as a cell pre-treatment strategy. Boron has unique properties that have attracted attention in nuclear physics and medicine due to its B-10 isotope's high cross section for the reaction with thermal neutrons, producing heavy ions such as charged lithium nuclei and alpha particles [1]. This specific reaction, involving boron and thermal neutrons, has led to the development of a novel cancer treatment method known as boron neutron capture therapy (BNCT). Although



BNCT has primarily been applied in the treatment of head and neck cancers and melanoma, promising results suggest potential applications beyond these specific cancer types [1].

In clinical trials, a derivative of phenylalanine containing one boron atom per molecule, 4-borono-L-phenylalanine (BPA), has been extensively studied [1]. The transportation of BPA to tumor cells is governed by the active mode of L-amino acid transporters, particularly L-amino acid transporter-1 (LAT-1) [2]. These specific transporters are often overexpressed in various types of cancers due to abnormal tissue growth, leading to an increased supply of amino acids [3]. Consequently, BPA may be recommended for use in BNCT for different cancer types exhibiting overexpression of LAT-1 [4].

The evaluation of new applications of BPA should begin with *in vitro* studies measuring boron uptake in corresponding cell lines. A significant challenge in using BPA in BNCT is its short retention time in tumors [5] due to the antiport mechanism [6]. To enhance BPA uptake, preloading with other L-type amino acids, such as L-DOPA, L-tyrosine, and L-phenylalanine, can be considered [7,8]. However, the results vary depending on the specific cell line or harvested tissue. In the case of L-DOPA and L-tyrosine, pre-treatment either increased boron concentration [8–11] or showed no significant changes [7,12–15], while preloading with L-phenylalanine was reported to inhibit boron uptake [7,16]. To the best of our knowledge, there has been no study on L-amino acid preloading on normal (non-cancerous) cell lines thus far, except for the investigation of L-DOPA pre-treatment on the brain-around-tumor tissue harvested from the biopsy of a high-grade glioma patient [14].

BPA has been evaluated for use in BNCT in various cancer models, including glioblastoma multiforme, head and neck cancer, liver cancer, and lung cancer [1]. The initial research on BNCT and BPA for the treatment of non-small cell lung cancer (NSCLC) emerged in 2014 [17], providing a promising alternative to conventional radiotherapy, which often leads to serious complications [18]. However, BPA has only been tested on the human NSCLC A549 cell line [19–24] as a reference to novel boron carriers, and the effect of preloading with L-type amino acids in the case of lung cancer remains uninvestigated.

It should be stressed that it is crucial to select the appropriate method to analyze the cellular uptake of BPA. Previous studies on boron concentration in cells for BNCT were performed by mass or atomic spectrometry techniques such as inductively coupled plasma mass spectrometry (ICP-MS) [20,22], inductively coupled plasma atomic emission spectrometry (ICP-AES) [25], direct current plasma AES [26], flow-injection electrospray tandem mass spectrometry [27], and secondary ion mass spectrometry [14]. Some reports have also mentioned indirect methods based on alpha particle dosimetry [28]. The most clinically relevant methods of describing biodistribution are magnetic resonance imaging [29] and positron emission tomography, in the case of using F-18 labelled BPA (although it has to be underlined that while similar in structure, it is not chemically identical to BPA) [30]. However, these methods lack the spatial resolution to describe the cellular and subcellular distribution of BPA.

The determination of trace and ultra-trace boron concentrations can be easily performed by ICP-MS, which offers excellent sensitivity and low limits of quantification [31,32]. However, certain challenges can arise, including memory effects and poor washout, which may affect the accuracy of measurements [33,34]. Additionally, C-12 can overlap with the total B-11 concentration in biological samples. Moreover, the biological sample has to be acid-digested or homogenized, and the final result is the average value obtained from a batch sample [35]. The digestion increases the risk of sample loss or contamination, and other errors may occur due to the presence of dead cells. Furthermore, standard ICP-MS measurements commonly assume that each cell accumulates an equal amount of the analyzed element, resulting in the loss of information regarding differentiation within the cell population [36]. In cancer studies, where tumor heterogeneity plays a significant role, obtaining detailed knowledge about drug uptake is essential to understand the molecular mechanisms underlying the investigated therapy [37].

A novel alternative to address these limitations is single cell ICP-MS (SC-ICP-MS). With SC-ICP-MS, individual cells are directly introduced into the plasma for analysis.



Each cell reaching the plasma generates a current spike, with the frequency corresponding to the number of cells and the intensity proportional to the concentration of analyzed elements [38]. Thus, SC-ICP-MS enables the investigation of variations in elemental uptake within a cell population, providing information about cell-to-cell variance, which is not available in standard ICP-MS measurements [39]. What is noteworthy is the possibility of employing SC-ICP-MS to also study the subcellular uptake of elements, which has already been described in the research investigating cis-platin uptake in cell nuclei [39].

While SC-ICP-MS has been applied in various fields, including drug development, cell biology, environmental studies, and metallomics, the analysis of boron has not been reported so far. A number of elements were tested by SC-ICP-MS, including Fe, S, Si, Zn, Pt, Ti, Gd, Au, Ag, As, Mn, Mg, Co, Nd, Eu, Tb, Dy, Ho, Tm, Yb, Lu, and Ir, as reviewed in [40,41].

The studies aimed to provide an approach based on ICP-MS and SC-ICP-MS for determining cellular boron concentration. This approach was employed to investigate the impact of L-phenylalanine and L-tyrosine pre-treatment on the uptake of BPA in both cancerous (NSCLC) and normal cells (lung fibroblasts). The use of SC-ICP-MS in boron analysis holds promise for expanding our understanding of cellular uptake and distributions of boron.

## 2. Results and Discussion

### 2.1. Influence of L-Phenylalanine and L-Tyrosine Pre-Treatment on Boron Concentration

As discussed in the previous section, L-type amino acid pre-treatment of cells may increase the uptake of BPA. To further explore the influence of preloading with L-phenylalanine and L-tyrosine, experiments on A549 and V79-4 cell lines were conducted. The results, represented as the concentration of boron in batch cell samples obtained with the use of conventional ICP-MS, are summarized in Figure 1.

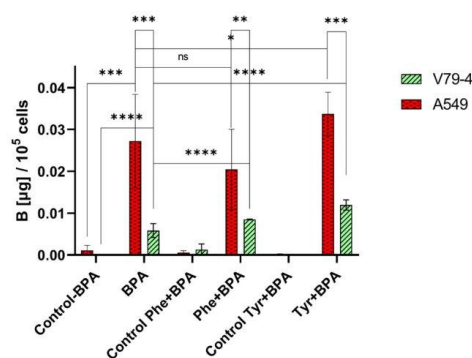


**Figure 1.** Boron accumulation in A549 and V79-4 cells after exposure to BPA and the influence of preloading with L-phenylalanine (Phe) and L-tyrosine (Tyr) on BPA uptake. Boron concentration is expressed as B [μg]/10<sup>5</sup> cells. Data are given as mean ± SD from three independent experiments. Significance level symbols represent the results of unpaired *t*-tests between the studied variants: ns (not significant, *p* > 0.05), \* (*p* ≤ 0.05), \*\* (*p* ≤ 0.01), \*\*\* (*p* ≤ 0.001), and \*\*\*\* (*p* ≤ 0.0001).

In the case of A549 and L-tyrosine pre-treatment, our results correspond with previous literature findings, also describing an enhancement of BPA uptake in other cancerous cell lines. We observed a statistically significant stimulating effect, increasing BPA uptake in cells 1.24 ± 0.47-fold (*p* = 0.028, 5 mM L-tyrosine solution). A similar study investigating the influence of L-tyrosine preloading on the uptake of the BPA analogue, 4-borono-2-[F-18]fluoro-L-phenylalanine, in human hepatocellular carcinoma HuH-7, human colorectal adenocarcinoma CaCo-2, and mouse melanoma B16-F1 cell lines, reported respective increases of boron uptake of 1.34 ± 0.57-fold (2.5 mM L-tyrosine solution), 1.04 ± 0.17-

fold (1 mM L-tyrosine solution), and  $1.57 \pm 0.06$ -fold (2.5 mM L-tyrosine solution), after 60 min of preloading [11]. Some earlier reports also demonstrated nearly two-fold [8] and three-fold [10] increases in BPA uptake after L-tyrosine preloading in rat 9L gliosarcoma cells and B16-F1 mouse melanoma cells, respectively. Since A549 is a cancerous cell line, the amino acid supply is increased and LAT-1 is found to be over-expressed [42]. As described by Aldossari et al. [14], L-tyrosine preloading may stimulate the exchange and transport between the extracellular BPA and intracellular L-tyrosine, which is consistent with our observations. On the other hand, pre-treatment of A549 cells with L-phenylalanine seems to inhibit the uptake of BPA by a factor of  $0.75 \pm 0.86$ , but this result is not statistically insignificant ( $p = 0.068$ ) and thus cannot be confirmed by this study. Previous literature reports described L-phenylalanine as a system L-specific agonist [7] and suggested that a low phenylalanine diet before the beginning of BNCT treatment may be advantageous for patients [43]. However, the inhibiting effect may also be beneficial due to the reduced radiation dose to the normal brain [16]. Nonetheless, as shown by the results of our study, pre-treatment of normal cells with L-phenylalanine may increase BPA uptake, so the dietary recommendation should be evaluated separately for different cancer types.

Similarly, in the case of the normal cell line V79-4, both L-phenylalanine and L-tyrosine pre-treatment exhibited an enhancing effect, resulting in factors of  $1.46 \pm 0.06$  ( $p = 0.000016$ ) and  $2.04 \pm 0.74$  ( $p = 0.000066$ ), respectively. It is most likely due to the increased intracellular accumulation of these L-amino acids, which stimulates the exchange and transport of extracellular BPA. The higher factors in the observed effect compared to the A549 cell line result from a very low uptake of BPA in V79-4 cells without the pre-treatment. This indicates that while normal cells do not exhibit an increased expression of LAT-1, the trans-stimulation of L-amino acids may have a similar effect, as in cancerous cells.

## 2.2. Boron Concentration in Individual Cells by SC-ICP-MS

Based on the results obtained in batch cell samples conducted with conventional ICP-MS measurements, further studies on the preloading effect using SC-ICP-MS were performed using L-tyrosine pre-treatment. The results for the A549 and V79-4 cell lines after exposure to BPA and preloading with L-tyrosine are presented in Figure 2a–f in the form of histograms.

The most distinct observation during the analysis of histograms is the clear diversity in each sample, which corresponds with the genetic heterogeneity of cells, especially in the cancerous cell line. It has been established that cell lines originating from cancer tissues are subjected to transformations such as multiplication, mutation, and chromosomal rearrangement, resulting in the phenotypical and morphological variability within isolated cell lines [44]. That is the case of the nonhomogeneous A549 cell line, which consists of multiple clones [37], as reflected in the presented histograms that show a different cellular response to BPA within the tested population. The results further indicate that even though there is a notable difference in the uptake of BPA in A549 cells compared to V79-4 cells, as described in Section 2.1, only a part of the whole population of cells responds to BPA exposure, and the response varies. After the initial common peak for all samples, there is a visible difference between them after the threshold of 101 ag. Hence this value was chosen as a baseline to compare the separated population of cells, and the results for this highlighted population are summarized in Table 1.

In the case of the A549 samples, the highlighted population represents 39.45% of all detected cells in the BPA exposure group and 40.97% in the BPA exposure with L-tyrosine preloading group. Similarly, in the V79-4 samples, this population constitutes 38.72% of all detected cells in the BPA exposure group and 41.11% in the BPA exposure with L-tyrosine preloading group. In the agreement with predictions, the highlighted population in the control group (exposure to D-fructose solution without BPA) for both cell lines exhibits almost no impulses and constitutes 1.01% (A549) and 2.94% (V79-4) of the entire sample. The less distinct differences between the A549 and V79-4 cell lines than in the case of conventional ICP-MS measurements conducted in the batch cell samples are most

likely due to the aggregation of V79-4 cells, which despite meticulous preparation was not avoidable, causing the possible appearance of signals from more than single cells on the histograms.

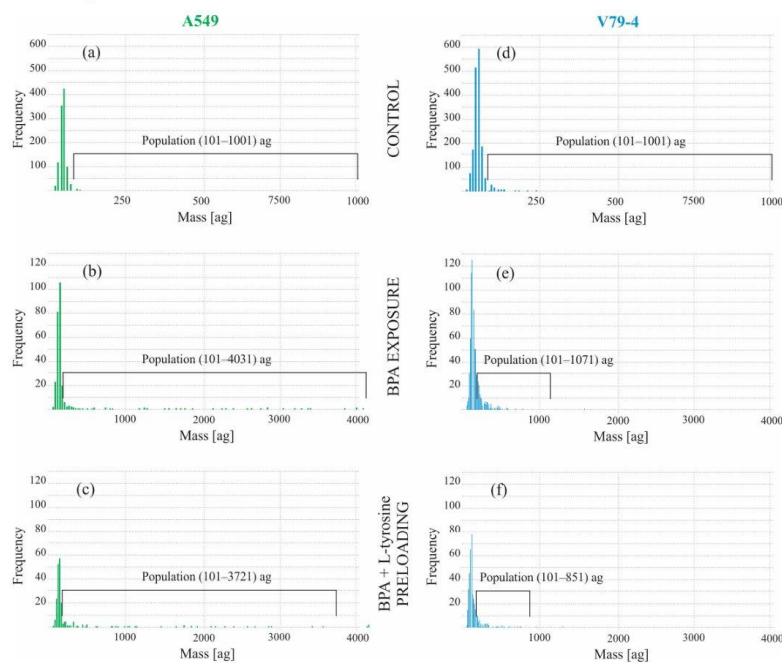


**Figure 2.** The histograms of the number of detected cells for the measured mass of boron in various conditions: (a) control group of A549 cell line, (b) BPA exposure of A549 cell line, (c) BPA + L-tyrosine preloading of A549 cell line, (d) control group of V79-4 cell line, (e) BPA exposure of V79-4 cell line, (f) BPA + L-tyrosine preloading of V79-4 cell line. A chosen population of cells above the baseline of 101 ag is highlighted in each histogram. The 5% of the highest mass signals corresponds to cell aggregates and was subtracted for each sample.

**Table 1.** The SC-ICP-MS results for the highlighted population above the threshold of 101 ag.

Cell line	Percentage of the Highlighted Population in the Entire Sample [%]		Mean Mass [ag] *	
	A549	V79-4	A549	V79-4
Control	1.01	2.94	447	205
BPA exposure	39.45	38.72	719	165
BPA + L-tyrosine preloading	40.97	41.11	619	179

\* The mean masses are calculated by the Syngistix™ (PerkinElmer, Waltham, MA, USA) Single Cell Software (Version 2.5) Module using built-in algorithms.

However, the difference is still visible when comparing the mean mass in the separated population, e.g., 719 ag for A549 cells after BPA exposure and 165 ag for V79-4 cells after BPA exposure. The obtained results provide the first direct observation of the heterogeneity of BPA uptake in both cancerous and normal cell lines and show that a number of A549 cells exhibit an exceptionally high BPA uptake. Based on the collected data, we can conclude that ICP-MS provides the preliminary data on the total content of boron, and SC-ICP-MS measurements provide in-depth information on the BPA uptake. The microscopic evaluation of cells has to be a vital step in order to provide correct data interpretation.



Nonetheless, it would be beneficial to combine SC-ICP-MS with flow cytometry to ensure the lack of interferences from aggregates. However, currently, such combinations are not routinely available.

### 3. Materials and Methods

#### 3.1. Cell Cultivation

The human NSCLC A549 (ATCC® CCL-185™ cell line was provided by the Medical University of Warsaw, Department of Applied Toxicology, Faculty of Pharmacy. The Chinese hamster lung fibroblast V79-4 (ATCC® CCL-93™) cell line was provided by the Department of Environmental Health Science, Faculty of Pharmacy, Medical University of Warsaw. The A549 cell line was cultured in Kaighn's Modification of Ham's F-12 Medium (F-12K, Gibco, Paisley, UK) supplemented with 10% of fetal bovine serum (FBS, Gibco, Paisley, UK), 0.1 mg mL<sup>-1</sup> streptomycin (Gibco, Paisley, UK), and 100 IU mL<sup>-1</sup> penicillin (Gibco, Paisley, UK). The V79-4 cell line was cultured in Dulbecco's Modified Eagle Medium (DMEM, Gibco, Paisley, UK) supplemented with 10% FBS, 0.1 mg mL<sup>-1</sup> streptomycin and 100 IU mL<sup>-1</sup> penicillin. Cells were maintained in a humidified atmosphere of 5% CO<sub>2</sub> in air and 37 °C.

#### 3.2. Cell Pre-Treatment with L-Phenylalanine and L-Tyrosine

A549 and V79-4 cells were seeded in 6-well (10<sup>4</sup> cells/well) plates and allowed to attach and grow for 48 h. After removing the culture medium, the cells were rinsed with warm phosphate-buffered saline (PBS, Gibco, Paisley, UK) and incubated with Hank's balanced salt solution containing calcium and magnesium cations (HBSS, Gibco, Paisley, UK). Alternatively, the cells were incubated in HBSS solution containing 5 mM L-phenylalanine (Sigma Aldrich, Steinheim, Germany) or L-tyrosine (Sigma Aldrich, Steinheim, Germany) at 37 °C for 60 min. Since the aim of the study was to prove the applicability of the proposed novel analytical approach, the conditions of preloading and BPA exposure experiments (concentrations and exposure time of amino acids and BPA) were carefully chosen based on previously described studies investigating the preloading effect on other cancerous cell lines [11,12,15]. After the incubation, the solutions were discarded, and the cells were exposed to BPA (Sigma Aldrich, Steinheim, Germany) according to the procedure described in Section 3.3.

#### 3.3. Cell Exposure to 4-Borono-L-Phenylalanine

A549 and V79-4 cells were seeded in 6-well cell culture plates and cultivated for 48 to 72 h until reaching 80–90% confluency. First, the growth medium was removed, and the cells were washed with warm PBS. Then, the cells were incubated in a 2 mM BPA solution in the form of the D-fructose (LOBA Chemie Vienna, Fischamend, Austria) complex (1 g mL<sup>-1</sup> D-fructose) at 37 °C for 120 min. The control group was incubated in a 1 g mL<sup>-1</sup> D-fructose solution.

#### 3.4. Sample Preparation for ICP-MS and SC-ICP-MS Measurements

After the incubation, the culture medium was first discarded, and the cells were washed with warm PBS. To detach the cells, they were exposed to trypsin (Gibco, Paisley, UK) for 3 and 7 min (V79-4 and A549 cell lines), respectively. Once detached, the cells were diluted with a growth medium and centrifuged at 25 °C for 7 min at 1000 rpm for A549 and 800 rpm for V79-4 cells lines. Subsequently, the medium was removed, and the cells were washed again with PBS and centrifuged under the same conditions. After that, the cells were exposed to 2% formaldehyde solution (Sigma Aldrich, Steinheim, Germany) in PBS and incubated for 10 min at 37 °C. Following the incubation, the cells were centrifuged again using the previously mentioned conditions; the formaldehyde solution was removed, and the cells diluted in PBS were kept refrigerated until the ICP-MS and SC-ICP-MS measurements were performed.



For ICP-MS measurements of boron concentration in batch cell samples, the samples were dissolved in 65% HNO<sub>3</sub> after 2 h of ultrasonic stirring at 50 °C. Transparent solutions were transferred to plastic tubes and filled with deionized water before ICP-MS analysis was conducted, as described in [32]. Since the entirety of each sample was treated with 65% HNO<sub>3</sub> and then measured, any extracellular BPA that may have been present in the sample due to possible leakage from cells was also included in the obtained result.

Preparing single cell samples is crucial for SC-ICP-MS measurements, and the number of cells in suspension must be carefully controlled to ensure that only one cell enters the plasma during the event. Therefore, the samples with the cells were washed a minimum of four times with fresh PBS until no boron was detected in the background. The boron content in the PBS solution after washing was checked before conducting the cell measurements. Subsequently, the cells were diluted to a final concentration of approximately 10<sup>5</sup> cells/mL using PBS. The cells were counted using a haemocytometer (Neubauer improved counting chamber, Fisher Scientific, Vienna, Austria) and a light microscope (Olympus, Tokyo, Japan) with the 40× objective and 2.5× binocular. The cells were measured directly without any additional dilution.

For transport efficiency measurements, colloidal gold nanoparticles LGCQC5050 (LGC Limited, Teddington, UK) and EQ Four Element Calibration Beads (FLUIDIGM, Singapore) solutions were used.

High purity 65% HNO<sub>3</sub> (J. T. Baker, Phillipsburg, NJ, USA or Merck, Darmstadt, Germany) with a final concentration of 1%, NORMATOM 25% ammonia (VWR Chemicals, Gdańsk, Poland) at final concentration 0.25%, Triton X-100 (PerkinElmer, Waltham, MA, USA) at final concentration 0.05%, and Milli-Q water (18.2 MΩ·cm, Merck, Darmstadt, Germany) were used during sample preparation.

### 3.5. Instrumentation

In this study, two spectrometers by PerkinElmer (Waltham, MA, USA) were used: a NexION 300D with a conventional sample introduction system for boron concentration in batch cell samples and a NexION 2000 spectrometer with a software extension for single cell measurements for the concentration of boron in individual cells. Experimental parameters, which were used during the measurements, are presented in Table 2. The working conditions of the spectrometers were optimized daily for maximum sensitivity and stability. An external 5-point calibration was used to obtain quantitative results. The memory effect was minimized by performing washouts between runs and ensuring that the signal reached the baseline after each sample. To control any possible interferences resulting from the presence of C-12 in the sample matrix, two isotopes of boron were measured (B-11 and B-10) in conventional ICP-MS experiments, and all measurements were performed in triplicates.

In the case of SC-ICP-MS experiments, a high efficiency nebulizer (HEN NEB) was applied to operate at a lower sample flow rate, generating smaller droplets and maximizing the signal from a small sample volume. An Asperon<sup>TM</sup> (PerkinElmer, Waltham, MA, USA) spray chamber was used to enhance the transfer of micron-sized objects into the ICP-MS, surpassing traditional introduction systems. Preventing the loss of cells as a result of sticking to the walls of the spray chamber cells was accomplished by the All Matrix Solution (AMS) (PerkinElmer, Waltham, MA, USA) and additional gas flow. The system was also equipped with a syringe-driven Single Cell Micro DX Autosampler (PerkinElmer, Waltham, MA, USA), facilitating the delivery of intact cells into the instrument at a 10 µL min<sup>−1</sup> flow rate.

Analysis was performed using the Syngistix<sup>TM</sup> (PerkinElmer, Waltham, MA, USA) Single Cell Software (Version 2.5) Module that uses algorithms to calculate, among others, transport efficiency (TE), threshold (sum of the mean of each sample signal and 3 times standard deviation), and particle detection limit (PDL), determining the lowest concentration of an element detected in a given SC-ICP-MS measurement. One of the key parameters in SC-ICP-MS analyses is TE. To determine this parameter, a method based on a known number

of particles in two standard solutions was employed: one containing beads and the other containing gold nanoparticles. The bead-containing standard facilitates a more accurate representation of cell size, whereas the nanoparticle standard has certified concentrations, ensuring traceability.

**Table 2.** The experimental parameters for ICP-MS and SC-ICP-MS instruments.

Parameter	ICP-MS	SC-ICP-MS
Instrument	NexION 300D (PerkinElmer)	NexION 2000 (PerkinElmer)
Mass analyzer	Quadrupole	Quadrupole
Measurement Mode	Standard	Standard
Nebulizer	Quartz Mainhardt	HEN Mainhardt
Spray chamber	Quartz cyclonic	Quartz Asperon
Carrier gas	Ar	Ar
Nebulizer gas flow	0.88 L min <sup>-1</sup>	0.40 L min <sup>-1</sup>
Sample introduction	Manually, peristaltic pump	SC Micro DX, syringe pump
Sample Flow Rate	0.2 mL min <sup>-1</sup>	10 µL min <sup>-1</sup>
Dwell time	100 ms	50 µs
AMS gas flow	n/a	0.7 L min <sup>-1</sup>
Measured isotopes *	B-10, B-11	B-10, B-11
Transport Efficiency	n/a	28%
Sample preparation	Digestion and dilution	Dilution with PBS to ~10 <sup>5</sup> cells mL <sup>-1</sup>
<b>Analytical Parameters</b>	<b>Digestion + ICP-MS</b>	<b>Dilution + SC-ICP-MS</b>
Calibration range	(10–100) µg L <sup>-1</sup> in 1% HNO <sub>3</sub>	(1–5) µg L <sup>-1</sup> in PBS
Regression equation **	y = 1526x + 157.13	y = 0.8108x + 0.335
Correlation coefficient, R <sup>2</sup>	0.9999	0.9999
LOD/PDL	20 ng kg <sup>-1</sup>	12 ag/cell
Recovery	100–115%	n/a
Bin size	n/a	10 ag
Threshold	n/a	1.06–3.05

\* The signal monitoring for B-10 and B-11 was similar for both in the case of both methods. Therefore, it was decided to conduct measurements using B-11 due to its higher abundance and, consequently, better sensitivity.

\*\* Regression equation of (i) ICP-MS measurements relates the dependence of intensity expressed in count per second (cps) to concentration (µg), and (ii) SC-ICP-MS relates the dependence of intensity expressed in counts to max flux (µg/event).

### 3.6. Statistics

The statistical analysis was performed to evaluate the significance of the results. The data are presented as the mean ± standard deviation (SD) of boron concentration in batch cell samples determined with conventional ICP-MS and are derived from three independent experiments (*n* = 9). Differences between concentrations were considered significant at *p* < 0.05. Statistical analyses were performed with Statistica 13.3 using unpaired *t*-tests, and GraphPad Prism 9.5.1 software was used for graphs.

## 4. Conclusions

In this work, we successfully employed the SC-ICP-MS technique to measure boron concentration in cell lines exposed to BPA, providing a novel method for determining boron content at the individual cell level and estimating the efficiency of the uptake of boron agents. Pre-treatment with L-tyrosine and L-phenylalanine demonstrated enhanced BPA uptake in the normal cell line. However, in the NSCLC cell line, the enhancement was

only observed for L-tyrosine. Interestingly, the cancerous cell line exhibited significant heterogeneity in boron content. These results confirm the importance of dietary restriction regarding L-phenylalanine content due to its possible influence on BPA uptake in normal cells. For successful employment of SC-ICP-MS in boron uptake studies, the possibility of cell aggregate formation has to be carefully evaluated at the sample preparation stage, and the additional use of flow cytometry could be considered to overcome this issue.

**Author Contributions:** Conceptualization, E.B. (Emilia Balcer), J.G., M.S., A.R., M.M. and E.B. (Ewa Bulska); methodology, E.B. (Emilia Balcer), M.S., A.R. and M.M.; software, A.R. and M.M.; validation, M.M. and A.R.; formal analysis, E.B. (Emilia Balcer), J.G., M.S., A.R. and M.M.; investigation, E.B. (Emilia Balcer), M.S., A.R. and M.M.; resources, E.B. (Emilia Balcer), M.S., A.R. and M.M.; data curation, E.B. (Emilia Balcer), M.S., A.R. and M.M.; writing—original draft preparation, E.B. (Emilia Balcer), J.G., M.S., A.R. and M.M.; writing—review and editing, E.B. (Emilia Balcer), J.G., M.S., A.R., M.M. and E.B. (Ewa Bulska); visualization, E.B. (Emilia Balcer), A.R. and M.M.; supervision, J.G. and E.B. (Ewa Bulska); project administration, J.G.; funding acquisition, E.B. (Emilia Balcer). All authors have read and agreed to the published version of the manuscript.

**Funding:** The contribution of Emilia Balcer was realized within the National Centre for Research and Development Project No. POWR.03.02.00-00-I009/17-00 (Radiopharmaceuticals for molecularly targeted diagnosis and therapy, RadFarm. Operational Project Knowledge Education Development 2014–2020 co-financed by the European Social Fund).

**Institutional Review Board Statement:** Not applicable.

**Informed Consent Statement:** Not applicable.

**Data Availability Statement:** The data presented in this study are available on request from corresponding author.

**Conflicts of Interest:** The authors declare no conflict of interest.

**Sample Availability:** Not applicable.

## References

- Wang, S.; Zhang, Z.; Miao, L.; Li, Y. Boron Neutron Capture Therapy: Current Status and Challenges. *Front. Oncol.* **2022**, *12*, 788770. [CrossRef]
- Wongthai, P.; Hagiwara, K.; Miyoshi, Y.; Wiriyasermkul, P.; Wei, L.; Ohgaki, R.; Kato, I.; Hamase, K.; Nagamori, S.; Kanai, Y. Boronophenylalanine, a Boron Delivery Agent for Boron Neutron Capture Therapy, Is Transported by ATB<sup>0+</sup>, LAT 1 and LAT 2. *Cancer Sci.* **2015**, *106*, 279–286. [CrossRef]
- Seneviratne, D.; Advani, P.; Trifiletti, D.M.; Chumsri, S.; Beltran, C.J.; Bush, A.F.; Vallow, L.A. Exploring the Biological and Physical Basis of Boron Neutron Capture Therapy (BNCT) as a Promising Treatment Frontier in Breast Cancer. *Cancers* **2022**, *14*, 3009. [CrossRef]
- Kanai, Y. Amino Acid Transporter LAT1 (SLC7A5) as a Molecular Target for Cancer Diagnosis and Therapeutics. *Pharmacol. Ther.* **2022**, *230*, 107964. [CrossRef]
- Coghi, P.; Li, J.; Hosmane, N.S.; Zhu, Y. Next Generation of Boron Neutron Capture Therapy (BNCT) Agents for Cancer Treatment. *Med. Res. Rev.* **2023**, *43*, 1809–1830. [CrossRef] [PubMed]
- Nomoto, T.; Inoue, Y.; Yao, Y.; Suzuki, M.; Kanamori, K.; Takemoto, H.; Matsui, M.; Tomoda, K.; Nishiyama, N. Poly(Vinyl Alcohol) Boosting Therapeutic Potential of *p*-Boronophenylalanine in Neutron Capture Therapy by Modulating Metabolism. *Sci. Adv.* **2020**, *6*, eaaz1722. [CrossRef] [PubMed]
- Detta, A.; Cruickshank, G.S. L-Amino Acid Transporter-1 and Boronophenylalanine-Based Boron Neutron Capture Therapy of Human Brain Tumors. *Cancer Res.* **2009**, *69*, 2126–2132. [CrossRef] [PubMed]
- Wittig, A.; Sauerwein, W.A.; Coderre, J.A.; Coderre, J.A. Mechanisms of Transport of *p*-Boronophenylalanine through the Cell Membrane In Vitro. *Radiat. Res.* **2000**, *153*, 173–180. [CrossRef] [PubMed]
- Capuani, S.; Gili, T.; Bozzali, M.; Russo, S.; Porcari, P.; Cametti, C.; D'Amore, E.; Colasanti, M.; Venturini, G.; Maraviglia, B.; et al. L-DOPA Preloading Increases the Uptake of Boronophenylalanine in C6 Glioma Rat Model: A New Strategy to Improve BNCT Efficacy. *Int. J. Radiat. Oncol. Biol. Phys.* **2008**, *72*, 562–567. [CrossRef] [PubMed]
- Papasprou, M.; Feinendegen, L.E.; Müller-Gärtner, H.W. Preloading with L-Tyrosine Increases the Uptake of Boronophenylalanine in Mouse Melanoma Cells. *Cancer Res.* **1994**, *54*, 6311–6314. [PubMed]
- Wingelhofer, B.; Kreis, K.; Mairinger, S.; Muchitsch, V.; Stanek, J.; Wanek, T.; Langer, O.; Kuntner, C. Preloading with L-BPA, L-Tyrosine and L-DOPA Enhances the Uptake of [18F]FBPA in Human and Mouse Tumour Cell Lines. *Appl. Radiat. Isot.* **2016**, *118*, 67–72. [CrossRef] [PubMed]



12. Gielisch, M.; Moergel, M.; Al-Nawas, B.; Kämmerer, P.W. Does Trans-Stimulation of L-Tyrosine Lead to an Increase in Boron Uptake in Head and Neck Squamous Cell Carcinoma Cells? *Appl. Sci.* **2021**, *11*, 7286. [\[CrossRef\]](#)
13. Grunewald, C.; Sauberer, M.; Filip, T.; Wanek, T.; Stanek, J.; Mairinger, S.; Rollet, S.; Kudejova, P.; Langer, O.; Schütz, C.; et al. On the Applicability of <sup>18</sup>F]FBPA to Predict L-BPA Concentration after Amino Acid Preloading in HuH-7 Liver Tumor Model and the Implication for Liver Boron Neutron Capture Therapy. *Nucl. Med. Biol.* **2017**, *44*, 83–89. [\[CrossRef\]](#)
14. Aldossari, S.; McMahon, G.; Lockyer, N.P.; Moore, K.L. Microdistribution and Quantification of the Boron Neutron Capture Therapy Drug BPA in Primary Cell Cultures of Human Glioblastoma Tumour by NanoSIMS. *Analyst* **2019**, *144*, 6214–6224. [\[CrossRef\]](#) [\[PubMed\]](#)
15. Yang, W.; Barth, R.F.; Huo, T.; Kabalka, G.W.; Shaikh, A.L.; Haider, S.A.; Chandra, S. Effects of L-DOPA Pre-Loading on the Uptake of Boronophenylalanine Using the F98 Glioma and B16 Melanoma Models. *Appl. Radiat. Isot.* **2014**, *88*, 69–73. [\[CrossRef\]](#)
16. Watanabe, T.; Tanaka, H.; Fukutani, S.; Suzuki, M.; Hiraoka, M.; Ono, K. L-Phenylalanine Preloading Reduces the <sup>10</sup>B(n,  $\alpha$ )<sup>7</sup>Li Dose to the Normal Brain by Inhibiting the Uptake of Boronophenylalanine in Boron Neutron Capture Therapy for Brain Tumours. *Cancer Lett.* **2016**, *370*, 27–32. [\[CrossRef\]](#)
17. Farias, R.O.; Bortolussi, S.; Menéndez, P.R.; González, S.J. Exploring Boron Neutron Capture Therapy for Non-Small Cell Lung Cancer. *Phys. Med.* **2014**, *30*, 888–897. [\[CrossRef\]](#)
18. Quah, S.C. Boron Neutron Capture Therapy in the Treatment of Lung Cancer. *J. Xiangya Med.* **2018**, *3*, 29. [\[CrossRef\]](#)
19. Nakagawa, F.; Kawashima, H.; Morita, T.; Nakamura, H. Water-Soluble Closo-Doceborate-Containing Pteroyl Derivatives Targeting Folate Receptor-Positive Tumors for Boron Neutron Capture Therapy. *Cells* **2020**, *9*, 1615. [\[CrossRef\]](#)
20. Wang, M.; Tong, Y.; Luo, Q.; Hu, S. Comparative Study on Neutron Irradiation Sensitization Effects of Nucleotide Borate Esters and Several Other Boron Agents. *Radiat. Res.* **2020**, *193*, 249. [\[CrossRef\]](#)
21. Varol, M.; Benkli, K.; Koparal, A.T.; Bostancıoğlu, R.B. Design and Synthesis of Novel Organometallic Complexes Using Boronated Phenylalanine Derivatives as Potential Anticancer Agents. *Drug Chem. Toxicol.* **2019**, *42*, 436–443. [\[CrossRef\]](#)
22. Ueda, H.; Suzuki, M.; Kuroda, R.; Tanaka, T.; Aoki, S. Design, Synthesis, and Biological Evaluation of Boron-Containing Macrocyclic Polyamines and Their Zinc(II) Complexes for Boron Neutron Capture Therapy. *J. Med. Chem.* **2021**, *64*, 8523–8544. [\[CrossRef\]](#)
23. Kondo, N.; Hirano, F.; Temma, T. Evaluation of 3-Borono-L-Phenylalanine as a Water-Soluble Boron Neutron Capture Therapy Agent. *Pharmaceutics* **2022**, *14*, 1106. [\[CrossRef\]](#)
24. Sahni, A.; Qian, Z.; Pei, D. Cell-Penetrating Peptides Escape the Endosome by Inducing Vesicle Budding and Collapse. *ACS Chem. Biol.* **2020**, *15*, 2485–2492. [\[CrossRef\]](#) [\[PubMed\]](#)
25. Linko, S.; Revitzer, H.; Zilliacus, R.; Kortessniemi, M.; Kouri, M.; Savolainen, S. Boron Detection from Blood Samples by ICP-AES and ICP-MS during Boron Neutron Capture Therapy. *Scand. J. Clin. Lab. Inv.* **2008**, *68*, 696–702. [\[CrossRef\]](#)
26. Gibson, C.R.; Staubus, A.E.; Barth, R.F.; Yang, W.; Ferketich, A.K.; Moeschberger, M.M. Pharmacokinetics of Sodium Borocaptate: A Critical Assessment of Dosing Paradigms for Boron Neutron Capture Therapy. *J. Neurooncol.* **2003**, *62*, 157–169. [\[CrossRef\]](#)
27. Basilico, F.; Sauerwein, W.; Pozzi, F.; Wittig, A.; Moss, R.; Mauri, P.L. Analysis Of <sup>10</sup>B Antitumoral Compounds by Means of Flow-Injection into ESI-MS/MS. *J. Mass Spectrom.* **2005**, *40*, 1546–1549. [\[CrossRef\]](#)
28. Takagaki, M.; Mishima, Y. Boron-10 Quantitative Analysis of Neutron Capture Therapy on Malignant Melanoma by Spectrophotometric  $\alpha$ -Track Reading. *Int. J. Radiat. Appl. Instrum. Part D. Nucl. Tracks Radiat. Meas.* **1990**, *17*, 531–535. [\[CrossRef\]](#)
29. Zhu, Y.; Fazal, T. Application of Theranostic Technology in Boron Neutron Capture Therapy. In *Frontiers in Boron-Based Medicinal Chemistry*, 1st ed.; Zhu, Y., Ed.; World Scientific Publishing Co., Pte Ltd.: Singapore, 2023; pp. 90–114. ISBN 9789811267963.
30. Ishiwata, K. 4-Borono-2-<sup>18</sup>F-Fluoro-L-Phenylalanine PET for Boron Neutron Capture Therapy-Oriented Diagnosis: Overview of a Quarter Century of Research. *Ann. Nucl. Med.* **2019**, *33*, 223–236. [\[CrossRef\]](#) [\[PubMed\]](#)
31. Xiao, J.; Vogl, J.; Rosner, M.; Deng, L.; Jin, Z. A Validated Analytical Procedure for Boron Isotope Analysis in Plants by MC-ICP-MS. *Talanta* **2019**, *196*, 389–394. [\[CrossRef\]](#)
32. Adamska, A.; Rumijowska-Galewicz, A.; Ruszczyńska, A.; Studzińska, M.; Jabłońska, A.; Paradowska, E.; Bulska, E.; Munier-Lehmann, H.; Dziadek, J.; Leśnikowski, Z.J.; et al. Anti-Mycobacterial Activity of Thymine Derivatives Bearing Boron Clusters. *Eur. J. Med. Chem.* **2016**, *121*, 71–81. [\[CrossRef\]](#) [\[PubMed\]](#)
33. Sun, D.; Ma, R.; McLeod, C.W.; Wang, X.; Cox, A.G. Determination of Boron in Serum, Plasma and Urine by Inductively Coupled Plasma Mass Spectrometry (ICP-MS). Use of Mannitol-Ammonia as Diluent and for Eliminating Memory Effect. *J. Anal. At. Spectrom.* **2000**, *15*, 257–261. [\[CrossRef\]](#)
34. Liu, T.; He, T.; Shi, Q.; Ni, Q. Rapid Determination of Boron in 61 Soil, Sediment, and Rock Reference Materials by ICP-MS. *At. Spectrosc.* **2019**, *40*, 55–62. [\[CrossRef\]](#)
35. Egger, A.E.; Rappel, C.; Jakupc, M.A.; Hartinger, C.G.; Heffeter, P.; Keppler, B.K. Development of an Experimental Protocol for Uptake Studies of Metal Compounds in Adherent Tumor Cells. *J. Anal. At. Spectrom.* **2009**, *24*, 51–61. [\[CrossRef\]](#) [\[PubMed\]](#)
36. Li, L.; Fan, Y.; Li, Q.; Sheng, R.; Si, H.; Fang, J.; Tong, L.; Tang, B. Simultaneous Single-Cell Analysis of Na<sup>+</sup>, K<sup>+</sup>, Ca<sup>2+</sup>, and Mg<sup>2+</sup> in Neuron-Like PC-12 Cells in a Microfluidic System. *Anal. Chem.* **2017**, *89*, 4559–4565. [\[CrossRef\]](#)
37. Watanabe, N.; Dickinson, D.A.; Krzywanski, D.M.; Iles, K.E.; Zhang, H.; Venglarik, C.J.; Forman, H.J. A549 Subclones Demonstrate Heterogeneity in Toxicological Sensitivity and Antioxidant Profile. *Am. J. Physiol. Lung Cell Mol. Physiol.* **2002**, *283*, L726–L736. [\[CrossRef\]](#)



38. Ho, K.-S.; Chan, W.-T. Time-Resolved ICP-MS Measurement for Single-Cell Analysis and on-Line Cytometry. *J. Anal. At. Spectrom.* **2010**, *25*, 1114. [[CrossRef](#)]
39. Galé, A.; Hofmann, L.; Lüdi, N.; Hungerbühler, M.N.; Kempf, C.; Heverhagen, J.T.; Von Tengg-Kobligk, H.; Broekmann, P.; Ruprecht, N. Beyond Single-Cell Analysis of Metalloids by ICP-MS: Targeting Cellular Substructures. *Int. J. Mol. Sci.* **2021**, *22*, 9468. [[CrossRef](#)]
40. Taylor, A.; Barlow, N.; Day, M.P.; Hill, S.; Martin, N.; Patriarca, M. Atomic Spectrometry Update: Review of Advances in the Analysis of Clinical and Biological Materials, Foods and Beverages. *J. Anal. At. Spectrom.* **2019**, *34*, 426–459. [[CrossRef](#)]
41. Da Silva, A.B.S.; Arruda, M.A.Z. Single-Cell ICP-MS to Address the Role of Trace Elements at a Cellular Level. *J. Trace Elem. Med. Biol.* **2023**, *75*, 127086. [[CrossRef](#)]
42. Salisbury, T.; Arthur, S. The Regulation and Function of the L-Type Amino Acid Transporter 1 (LAT1) in Cancer. *Int. J. Mol. Sci.* **2018**, *19*, 2373. [[CrossRef](#)] [[PubMed](#)]
43. Chandra, S.; Ahmad, T.; Barth, R.F.; Kabalka, G.W. Quantitative Evaluation of Boron Neutron Capture Therapy (BNCT) Drugs for Boron Delivery and Retention at Subcellular-Scale Resolution in Human Glioblastoma Cells with Imaging Secondary Ion Mass Spectrometry (SIMS). *J. Microsc.* **2014**, *254*, 146–156. [[CrossRef](#)] [[PubMed](#)]
44. Freshney, R.I. Transformation and Immortalization. In *Culture of Animal Cells*, 6th ed.; John Wiley & Sons, Inc.: Hoboken, NJ, USA, 2011; pp. 279–297. ISBN 978-0-470-64936-7.

**Disclaimer/Publisher's Note:** The statements, opinions and data contained in all publications are solely those of the individual author(s) and contributor(s) and not of MDPI and/or the editor(s). MDPI and/or the editor(s) disclaim responsibility for any injury to people or property resulting from any ideas, methods, instructions or products referred to in the content.

---

## 4. Podsumowanie i wnioski

Uzyskany przeze mnie nośnik BPA na bazie MIP o określonej strukturze i morfologii, został pomyślnie zsyntezowany z użyciem L-fenyloalaniny w roli szablonu (wybór szablonu podyktowany był podobieństwem strukturalnym do BPA). Podczas przeprowadzonych badań otrzymałam łącznie trzy polimery blokowe i pięć polimerów typu tzw. plastra miodu, wdrukowanych L-fenyloalaniną, oraz odpowiednio trzy i pięć polimerów kontrolnych. Otrzymany materiał scharakteryzowałam pod kątem właściwości adsorpcyjnych wobec BPA, struktury i morfologii, wybierając tym samym MIP o matrycy wykazującej najwyższe wartości pojemności adsorpcyjnej i współczynnika specyficzności. Zbadałam również uwalnianie BPA z otrzymanego optymalnego MIP w układzie symulującym warunki fizjologiczne, potwierdzając, że BPA zaadsorbowana na MIP, jedynie w nieznaczącym stopniu ulega desorpcji w czasie dwóch godzin eksperymentu. Czas ten został wybrany na podstawie danych o czasach infuzji stosowanych w BNCT. Otrzymany wynik oznacza, że BPA może być dostarczana do miejsc zmienionych nowotworowo w formie związanej z MIP. Można tym samym wnioskować, że zapewni to transport całego nośnika do komórek poprzez endocytozę z wykorzystaniem LAT-1. Ponadto, otrzymany MIP wykazywał niską cytotoksyczność *in vitro* wobec dwóch wybranych linii komórkowych, niedrobnokomórkowego raka płuc oraz prawidłowych fibroblastów płuc, wykazując tym samym potencjał i bezpieczeństwo w kontekście dalszych badań tego materiału na modelach *in vivo*.

Badania nad zastosowaniem L-aminokwasowych analogów BPA na tych samych modelach niedrobnokomórkowego raka płuc oraz prawidłowych fibroblastów płuc z użyciem metody ICP-MS wykazały, że przedekspozycyjne narażenie zarówno na L-tyrozynę, jak i L-fenyloalaninę, powoduje istotnie statystycznie zwiększony wychwyt BPA w komórkach prawidłowych. W przypadku komórek nowotworowych, istotnie statystyczny zwiększony wychwyt BPA wystąpił jedynie dla L-tyrozyny. Bez względu na stosowanie narażania przedekspozycyjnego, wychwyt BPA przez komórki nowotworowe pozostawał wyższy niż w przypadku komórek prawidłowych w obrębie porównywanych grup. Przeprowadzone badania wykonałam w trzech powtórzeniach, a każdy wariant podczas jednego powtórzenia testowałam trzykrotnie ( $n = 9$ ). Pomiary z użyciem techniki SC-ICP-MS udowodniły natomiast znaczną heterogenność w zawartości boru pomiędzy pojedynczymi komórkami nowotworowymi jednej próbki, sugerując, że BPA jest wychwytywana w różnym stopniu w obrębie populacji.

---

Wyniki przedstawione w pracy pokazują, że istnieje możliwość poprawienia skuteczności działania stosowanej już w praktyce klinicznej BPA w BNCT. Wskazują także na możliwość zaprojektowania bardziej efektywnego nośnika BPA na bazie MIP i opracowania strategii, która może potencjalnie doprowadzić do poprawy parametrów wytworzonego materiału pod kątem pojemności adsorpcyjnej oraz funkcjonalności. Może być to osiągnięte poprzez ewentualne dodanie elementu magnetycznego lub dodatkowo rozpoznającego wybrany cel molekularny. W celu dalszej ewaluacji MIP jako nośnika BPA, należy przeprowadzić badania dystrybucji oraz toksyczności na modelach *in vivo*. W pracy zaprezentowałam także nową metodę analityczną pomagającą w określeniu zróżnicowania wychwytu BPA w populacji badanych komórek. W kontekście badań nad zastosowaniem L-aminokwasowych analogów BPA na wybranym modelu raka płuc, następnym etapem powinna być weryfikacja nowo opisanej techniki SC-ICP-MS z użyciem innej metody analitycznej, takiej jak ICP-MS, aby potwierdzić otrzymane wyniki ilościowe i jakościowe. Kolejnym ważnym aspektem jest przeprowadzenie badań na modelu zwierzęcym z indukowanym guzem o różnym stopniu zaawansowania i klasyfikacji histologicznej w celu jak najlepszej weryfikacji skuteczności i bezpieczeństwa zaproponowanego protokołu.

---

## 5. Oświadczenia współautorów prac

...Warszawa, 18.09.2023...  
(miejscowość, data)

.....Emilia Balcer.....  
(imię i nazwisko)

### OŚWIADCZENIE

Jako współautor pracy pt. „Molecularly Imprinted Carriers for Diagnostics and Therapy—A Critical Appraisal” oświadczam, iż mój własny wkład merytoryczny w przygotowanie, przeprowadzenie i opracowanie badań oraz przedstawienie pracy w formie publikacji stanowi:

... przegląd piśmiennictwa, przygotowanie manuskryptu i prace edytorskie.....

Mój udział procentowy w przygotowaniu publikacji określám jako...60.. %

Jednocześnie wyrażám zgodę na wykorzystanie w/w pracy jako część rozprawy doktorskiej.

*Emilia Balcer*  
.....  
(podpis oświadczającego)



...Warszawa, 18.09.2023r.  
(miejscowość, data)

.....Monika Sobiech.....  
(imię i nazwisko)

### OŚWIADCZENIE

Jako współautor pracy pt. „Molecularly Imprinted Carriers for Diagnostics and Therapy—A Critical Appraisal” oświadczam, iż mój własny wkład merytoryczny w przygotowanie, przeprowadzenie i opracowanie badań oraz przedstawienie pracy w formie publikacji stanowi:

... przygotowanie manuskryptu i prace edytorskie.....

Mój udział procentowy w przygotowaniu publikacji określam jako...15.. %

Jednocześnie wyrażam zgodę na wykorzystanie w/w pracy jako część rozprawy doktorskiej mgr Emilii Balcer.

.....Monika Sobiech.....  
(podpis oświadczającego)

...Warszawa, 15.09.2023  
(miejscowość, data)

.....Piotr Luliński.....  
(imię i nazwisko)

### OŚWIADCZENIE

Jako współautor pracy pt. „Molecularly Imprinted Carriers for Diagnostics and Therapy—A Critical Appraisal” oświadczam, iż mój własny wkład merytoryczny w przygotowanie, przeprowadzenie i opracowanie badań oraz przedstawienie pracy w formie publikacji stanowi:

...koncepcja pracy, przygotowanie manuskryptu, nadzór nad redagowaniem manuskryptu.....

Mój udział procentowy w przygotowaniu publikacji określám jako...25.. %

Jednocześnie wyrażám zgodę na wykorzystanie w/w pracy jako część rozprawy doktorskiej mgr Emilii Balcer.

  
.....  
(podpis oświadczającego)

---

...Warszawa, 18.09.2023...  
(miejscowość, data)

.....Emilia Balcer.....  
(imię i nazwisko)

### OŚWIADCZENIE

Jako współautor pracy pt. „Molecularly Imprinted Polymer Specific Towards 4-Borono-L-Phenylalanine – Synthesis Optimization, Theoretical Analysis, Morphology Investigation, Cytotoxicity and Release Studies” oświadczam, iż mój własny wkład merytoryczny w przygotowanie, przeprowadzenie i opracowanie badań oraz przedstawienie pracy w formie publikacji stanowi:

....przeprowadzenie badań (synteza polimerów, analiza pojemności adsorpcyjnej, selektywności, badania uwalniania i cytotoksyczności), współudział w interpretacji wyników, analiza danych, przygotowanie manuskryptu.....

Mój udział procentowy w przygotowaniu publikacji określám jako...55.. %

Jednocześnie wyrażám zgodę na wykorzystanie w/w pracy jako część rozprawy doktorskiej.

.....*Emilia Balcer*.....  
(podpis oświadczającego)

...Warszawa, 18.09.2023r.  
(miejscowość, data)

.....Monika Sobiech.....  
(imię i nazwisko)

### OŚWIADCZENIE

Jako współautor pracy pt. „Molecularly Imprinted Polymer Specific Towards 4-Borono-L-Phenylalanine – Synthesis Optimization, Theoretical Analysis, Morphology Investigation, Cytotoxicity and Release Studies” oświadczam, iż mój własny wkład merytoryczny w przygotowanie, przeprowadzenie i opracowanie badań oraz przedstawienie pracy w formie publikacji stanowi:

....przeprowadzenie badań (wykonanie analizy teoretycznej), przygotowanie manuskryptu.....

Mój udział procentowy w przygotowaniu publikacji określłam jako...25.. %

Jednocześnie wyrażam zgodę na wykorzystanie w/w pracy jako część rozprawy doktorskiej mgr Emilii Balcer.

.....Monika Sobiech.....  
(podpis oświadczającego)



---

...Warszawa, 15.09.2023...  
(miejscowość, data)

.....Joanna Giebułtowicz.....  
(imię i nazwisko)


### OŚWIADCZENIE

Jako współautor pracy pt. „Molecularly Imprinted Polymer Specific Towards 4-Borono-L-Phenylalanine – Synthesis Optimization, Theoretical Analysis, Morphology Investigation, Cytotoxicity and Release Studies” oświadczam, iż mój własny wkład merytoryczny w przygotowanie, przeprowadzenie i opracowanie badań oraz przedstawienie pracy w formie publikacji stanowi:

....opracowanie metody analitycznej opartej na LC-MS, nadzór nad wykonaniem analiz, nadzór nad badaniami cytotoksyczności, przygotowanie manuskryptu.....

Mój udział procentowy w przygotowaniu publikacji określám jako...5.. %

Jednocześnie wyrażám zgodę na wykorzystanie w/w pracy jako część rozprawy doktorskiej mgr Emilii Balcer.

  
.....  
(podpis oświadczającego)

...Warszawa, 14.09.2023  
(miejscowość, data)

.....Małgorzata Sochacka.....  
(imię i nazwisko)

### OŚWIADCZENIE

Jako współautor pracy pt. „Molecularly Imprinted Polymer Specific Towards 4-Borono-L-Phenylalanine – Synthesis Optimization, Theoretical Analysis, Morphology Investigation, Cytotoxicity and Release Studies” oświadczam, iż mój własny wkład merytoryczny w przygotowanie, przeprowadzenie i opracowanie badań oraz przedstawienie pracy w formie publikacji stanowi:

....zaprojektowanie badania cytotoksyczności, współuczestniczenie w badaniach.....

Mój udział procentowy w przygotowaniu publikacji określám jako...5.. %

Jednocześnie wyrażám zgodę na wykorzystanie w/w pracy jako część rozprawy doktorskiej mgr Emilii Balcer.

ADJUNKT BADAWCZO-DYDAKTYCZNY  
Zakład Chemii Leków, Analizy  
Farmaceutycznej i Biomedycznej

dr. in. farm. Małgorzata Sochacka

(podpis oświadczającego)

...Warszawa, 15.09.2023  
(miejscowość, data)

.....Piotr Luliński.....  
(imię i nazwisko)

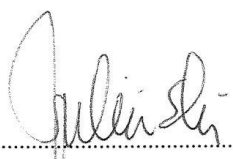
### OŚWIADCZENIE

Jako współautor pracy pt. „Molecularly Imprinted Polymer Specific Towards 4-Borono-L-Phenylalanine – Synthesis Optimization, Theoretical Analysis, Morphology Investigation, Cytotoxicity and Release Studies” oświadczam, iż mój własny wkład merytoryczny w przygotowanie, przeprowadzenie i opracowanie badań oraz przedstawienie pracy w formie publikacji stanowi:

....koncepcja pracy, nadzór nad realizacją prac, interpretacja wyników, przygotowanie manuskryptu.....

Mój udział procentowy w przygotowaniu publikacji określám jako...10.. %

Jednocześnie wyrażám zgodę na wykorzystanie w/w pracy jako część rozprawy doktorskiej mgr Emilii Balcer.

  
.....  
(podpis oświadczającego)

---

...Warszawa, 18.09.2023.....  
(miejscowość, data)

.....Emilia Balcer.....  
(imię i nazwisko)

### OŚWIADCZENIE

Jako współautor pracy pt. „Investigation of the Impact of L-Phenylalanine and L-Tyrosine Pre-Treatment on the Uptake of 4-Borono-L-Phenylalanine in Cancerous and Normal Cells Using an Analytical Approach Based on SC-ICP-MS” oświadczam, iż mój własny wkład merytoryczny w przygotowanie, przeprowadzenie i opracowanie badań oraz przedstawienie pracy w formie publikacji stanowi:

..... przeprowadzenie eksperymentów ekspozycji komórek na badane związki, przygotowanie próbek komórkowych, współudział w pomiarach analitycznych, przygotowanie rysunków, interpretacja i opracowanie wyników, przygotowanie manuskryptu.....

Mój udział procentowy w przygotowaniu publikacji określám jako...55.. %

Jednocześnie wyrażám zgodę na wykorzystanie w/w pracy jako część rozprawy doktorskiej.

.....Emilia Balcer.....  
(podpis oświadczającego)



---

...Warszawa,...15.09.2023..  
(miejscowość, data)

.....Joanna Giebułtowicz.....  
(imię i nazwisko)

### OŚWIADCZENIE

Jako współautor pracy pt. „Investigation of the Impact of L-Phenylalanine and L-Tyrosine Pre-Treatment on the Uptake of 4-Borono-L-Phenylalanine in Cancerous and Normal Cells Using an Analytical Approach Based on SC-ICP-MS” oświadczam, iż mój własny wkład merytoryczny w przygotowanie, przeprowadzenie i opracowanie badań oraz przedstawienie pracy w formie publikacji stanowi:

.....koncepcja pracy, nadzór nad realizacją prac, interpretacja wyników, przygotowanie manuskryptu.....

Mój udział procentowy w przygotowaniu publikacji określłam jako...5.. %

Jednocześnie wyrażam zgodę na wykorzystanie w/w pracy jako część rozprawy doktorskiej mgr Emilii Balcer.

.....*Joanna Giebułtowicz*.....  
(podpis oświadczającego)

...Warszawa, 14.09.2023  
(miejscowość, data)

.....Małgorzata Sochacka.....  
(imię i nazwisko)

### OŚWIADCZENIE

Jako współautor pracy pt. „Investigation of the Impact of L-Phenylalanine and L-Tyrosine Pre-Treatment on the Uptake of 4-Borono-L-Phenylalanine in Cancerous and Normal Cells Using an Analytical Approach Based on SC-ICP-MS” oświadczam, iż mój własny wkład merytoryczny w przygotowanie, przeprowadzenie i opracowanie badań oraz przedstawienie pracy w formie publikacji stanowi:

.....współudział w zaprojektowaniu i przeprowadzeniu eksperymentów ekspozycji komórek na badane związki, przygotowanie manuskryptu.....

Mój udział procentowy w przygotowaniu publikacji określám jako...5.. %

Jednocześnie wyrażám zgodę na wykorzystanie w/w pracy jako część rozprawy doktorskiej mgr Emilii Balcer.

ADJUNKI BADAWCZO-DYDAKTYCZNY  
Zakład Chemii Leków, Analizy  
Farmaceutycznej i Biomedycznej

dr. n. farm. Małgorzata Sochacka

.....  
(podpis oświadczającego)

---

Warszawa, 14 września 2023  
(miejscowość, data)

Anna Ruszczyńska  
(imię i nazwisko)

### OŚWIADCZENIE

Jako współautor pracy pt. „Investigation of the Impact of L-Phenylalanine and L-Tyrosine Pre-Treatment on the Uptake of 4-Borono-L-Phenylalanine in Cancerous and Normal Cells Using an Analytical Approach Based on SC-ICP-MS” oświadczam, że mój wkład merytoryczny w przygotowanie, przeprowadzenie i opracowanie badań oraz przedstawienie pracy w formie publikacji stanowi:

- 1) pomiary analityczne dotyczące oznaczania stężenia boru w przygotowanych wcześniej roztworach zawierających komórki metodą ICP-MS,
- 2) opracowanie wyników dotyczących pomiarów metodą ICP-MS,
- 3) przygotowanie tej części tekstu, która dotyczyła pomiarów ICP-MS oraz udział w redagowaniu tekstu,
- 4) przygotowanie rysunków.

Mój udział procentowy w przygotowaniu publikacji określám jako 15 %

Jednocześnie wyrażám zgodę na wykorzystanie w/w pracy jako część rozprawy doktorskiej mgr Emilii Balcer.

  
.....  
(podpis oświadczającego)

... Warszawa, 18.09.2023....  
(miejscowość, data)

.....Magdalena Muszyńska.....  
(imię i nazwisko)


### OŚWIADCZENIE

Jako współautor pracy pt. „Investigation of the Impact of L-Phenylalanine and L-Tyrosine Pre-Treatment on the Uptake of 4-Borono-L-Phenylalanine in Cancerous and Normal Cells Using an Analytical Approach Based on SC-ICP-MS” oświadczam, iż mój własny wkład merytoryczny w przygotowanie, przeprowadzenie i opracowanie badań oraz przedstawienie pracy w formie publikacji stanowi:

.....pomiarów analitycznych dotyczących oznaczania stężenia boru w przygotowanych wcześniej roztworach zawierających komórki metodą SC-ICP-MS, opracowanie wyników dotyczących pomiarów metodą SC-ICP-MS, przygotowanie tej części tekstu, która dotyczyła pomiarów SC-ICP-MS oraz udział w redagowaniu tekstu i przygotowaniu rysunków.....

Mój udział procentowy w przygotowaniu publikacji określę jako...15.. %

Jednocześnie wyrażam zgodę na wykorzystanie w/w pracy jako część rozprawy doktorskiej mgr Emilii Balcer.

  
(podpis oświadczającego)



---

prof. dr hab. Ewa Bulska  
Centrum Nauk Biologiczno-Chemicznych  
Wydział Chemii  
Uniwersytet Warszawski

Warszawa, 15 września 2023 r.

### OŚWIADCZENIE

Jako współautorka pracy pt. „Investigation of the Impact of L-Phenylalanine and L-Tyrosine Pre-Treatment on the Uptake of 4-Borono-L-Phenylalanine in Cancerous and Normal Cells Using an Analytical Approach Based on SC-ICP-MS” oświadczam, iż mój własny wkład merytoryczny w przygotowanie, przeprowadzenie i opracowanie badań oraz przedstawienie pracy w formie publikacji to udział w przygotowaniu koncepcja pracy, nadzór nad realizacją prac oraz pomoc merytoryczna i redakcyjna na etapie przygotowania manuskryptu.

Mój udział procentowy w przygotowaniu publikacji określam jako 5 %

Jednocześnie wyrażam zgodę na wykorzystanie w/w pracy jako część rozprawy doktorskiej mgr Emilii Balcer.



(podpis oświadczającego)

---

## 6. Bibliografia

1. Dymova, M.A.; Taskaev, S.Y.; Richter, V.A.; Kuligina, E.V. Boron Neutron Capture Therapy: Current Status and Future Perspectives. *Cancer Commun.* **2020**, *40*, 406–421, doi:10.1002/cac2.12089.
2. Barth, R.F.; Mi, P.; Yang, W. Boron Delivery Agents for Neutron Capture Therapy of Cancer. *Cancer Commun.* **2018**, *38*, 35, doi:10.1186/s40880-018-0299-7.
3. Chen, D.; Xu, L.; Wang, Z.; Liu, C. Enriched 10B-Diboron Reagents Synthesis from 10BF<sub>3</sub>. *Chem* **2023**, S2451929423003248, doi:10.1016/j.chempr.2023.06.019.
4. Wang, S.; Zhang, Z.; Miao, L.; Li, Y. Boron Neutron Capture Therapy: Current Status and Challenges. *Front. Oncol.* **2022**, *12*, 788770, doi:10.3389/fonc.2022.788770.
5. Hu, K.; Yang, Z.; Zhang, L.; Xie, L.; Wang, L.; Xu, H.; Josephson, L.; Liang, S.H.; Zhang, M.-R. Boron Agents for Neutron Capture Therapy. *Coord. Chem. Rev.* **2020**, *405*, 213139, doi:10.1016/j.ccr.2019.213139.
6. Wongthai, P.; Hagiwara, K.; Miyoshi, Y.; Wiriyaerkmul, P.; Wei, L.; Ohgaki, R.; Kato, I.; Hamase, K.; Nagamori, S.; Kanai, Y. Boronophenylalanine, a Boron Delivery Agent for Boron Neutron Capture Therapy, Is Transported by ATB<sup>0+</sup>, LAT 1 and LAT 2. *Cancer Sci.* **2015**, *106*, 279–286, doi:10.1111/cas.12602.
7. Kanai, Y. Amino Acid Transporter LAT1 (SLC7A5) as a Molecular Target for Cancer Diagnosis and Therapeutics. *Pharmacol. Ther.* **2022**, *230*, 107964, doi:10.1016/j.pharmthera.2021.107964.
8. Nomoto, T.; Inoue, Y.; Yao, Y.; Suzuki, M.; Kanamori, K.; Takemoto, H.; Matsui, M.; Tomoda, K.; Nishiyama, N. Poly(Vinyl Alcohol) Boosting Therapeutic Potential of *p* - Boronophenylalanine in Neutron Capture Therapy by Modulating Metabolism. *Sci. Adv.* **2020**, *6*, eaaz1722, doi:10.1126/sciadv.aaz1722.
9. Janczura, M.; Luliński, P.; Sobiech, M. Imprinting Technology for Effective Sorbent Fabrication: Current State-of-Art and Future Prospects. *Materials* **2021**, *14*, 1850, doi:10.3390/ma14081850.
10. *Handbook of Molecularly Imprinted Polymers*; Alvarez-Lorenzo, C., Concheiro, A., Eds.; Smithers Rapra: Shrewsbury, UK, 2013; ISBN 978-1-84735-959-9.
11. Haupt, K.; Medina Rangel, P.X.; Bui, B.T.S. Molecularly Imprinted Polymers: Antibody Mimics for Bioimaging and Therapy. *Chem. Rev.* **2020**, *120*, 9554–9582, doi:10.1021/acs.chemrev.0c00428.

- 
12. Wróblewska, A.; Szermer-Olearnik, B.; Pajtasz-Piasecka, E. Nanocząstki o Wysokiej Zawartości Boru Jako Potencjalne Nośniki w Terapii Borowo-Neutronowej\*. *Postępy Hig. Med. Dośw.* **2021**, *75*, 122–132, doi:10.5604/01.3001.0014.7760.
  13. Aldossari, S.; McMahon, G.; Lockyer, N.P.; Moore, K.L. Microdistribution and Quantification of the Boron Neutron Capture Therapy Drug BPA in Primary Cell Cultures of Human Glioblastoma Tumour by NanoSIMS. *Analyst* **2019**, *144*, 6214–6224, doi:10.1039/C9AN01336A.
  14. Detta, A.; Cruickshank, G.S. L-Amino Acid Transporter-1 and Boronophenylalanine-Based Boron Neutron Capture Therapy of Human Brain Tumors. *Cancer Res.* **2009**, *69*, 2126–2132, doi:10.1158/0008-5472.CAN-08-2345.
  15. Wittig, A.; Sauerwein, W.A.; Coderre, J.A.; Coderre, J.A. Mechanisms of Transport of *p*-Borono-Phenylalanine through the Cell Membrane *In Vitro*. *Radiat. Res.* **2000**, *153*, 173–180, doi:10.1667/0033-7587(2000)153[0173:MOTOPB]2.0.CO;2.
  16. Capuani, S.; Gili, T.; Bozzali, M.; Russo, S.; Porcari, P.; Cametti, C.; D'Amore, E.; Colasanti, M.; Venturini, G.; Maraviglia, B.; et al. L-DOPA Preloading Increases the Uptake of Borophenylalanine in C6 Glioma Rat Model: A New Strategy to Improve BNCT Efficacy. *Int. J. Radiat. Oncol. Biol. Phys.* **2008**, *72*, 562–567, doi:10.1016/j.ijrobp.2008.06.1493.
  17. Papaspyrou, M.; Feinendegen, L.E.; Müller-Gärtner, H.W. Preloading with L-Tyrosine Increases the Uptake of Boronophenylalanine in Mouse Melanoma Cells. *Cancer Res.* **1994**, *54*, 6311–6314.
  18. Wingelhofer, B.; Kreis, K.; Mairinger, S.; Muchitsch, V.; Stanek, J.; Wanek, T.; Langer, O.; Kuntner, C. Preloading with L-BPA, L-Tyrosine and L-DOPA Enhances the Uptake of [18F]FBPA in Human and Mouse Tumour Cell Lines. *Appl. Radiat. Isot.* **2016**, *118*, 67–72, doi:10.1016/j.apradiso.2016.08.026.
  19. Gielisch, M.; Moergel, M.; Al-Nawas, B.; Kämmerer, P.W. Does Trans-Stimulation of L-Tyrosine Lead to an Increase in Boron Uptake in Head and Neck Squamous Cell Carcinoma Cells? *Appl. Sci.* **2021**, *11*, 7286, doi:10.3390/app11167286.
  20. Grunewald, C.; Sauberer, M.; Filip, T.; Wanek, T.; Stanek, J.; Mairinger, S.; Rollet, S.; Kudejova, P.; Langer, O.; Schütz, C.; et al. On the Applicability of [18F]FBPA to Predict L-BPA Concentration after Amino Acid Preloading in HuH-7 Liver Tumor Model and the Implication for Liver Boron Neutron Capture Therapy. *Nucl. Med. Biol.* **2017**, *44*, 83–89, doi:10.1016/j.nucmedbio.2016.08.012.

- 
21. Yang, W.; Barth, R.F.; Huo, T.; Kabalka, G.W.; Shaikh, A.L.; Haider, S.A.; Chandra, S. Effects of L-DOPA Pre-Loading on the Uptake of Boronophenylalanine Using the F98 Glioma and B16 Melanoma Models. *Appl. Radiat. Isot.* **2014**, *88*, 69–73, doi:10.1016/j.apradiso.2014.01.002.
  22. Watanabe, T.; Tanaka, H.; Fukutani, S.; Suzuki, M.; Hiraoka, M.; Ono, K. L-Phenylalanine Preloading Reduces the  $^{10}\text{B}(\text{n}, \alpha)^7\text{Li}$  Dose to the Normal Brain by Inhibiting the Uptake of Boronophenylalanine in Boron Neutron Capture Therapy for Brain Tumours. *Cancer Lett.* **2016**, *370*, 27–32, doi:10.1016/j.canlet.2015.10.004.
  23. Wang, M.; Tong, Y.; Luo, Q.; Hu, S. Comparative Study on Neutron Irradiation Sensitization Effects of Nucleotide Borate Esters and Several Other Boron Agents. *Radiat. Res.* **2020**, *193*, 249, doi:10.1667/RR15473.1.
  24. Ueda, H.; Suzuki, M.; Kuroda, R.; Tanaka, T.; Aoki, S. Design, Synthesis, and Biological Evaluation of Boron-Containing Macrocyclic Polyamines and Their Zinc(II) Complexes for Boron Neutron Capture Therapy. *J. Med. Chem.* **2021**, *64*, 8523–8544, doi:10.1021/acs.jmedchem.1c00445.
  25. Basilico, F.; Sauerwein, W.; Pozzi, F.; Wittig, A.; Moss, R.; Mauri, P.L. Analysis Of  $^{10}\text{B}$  Antitumoral Compounds by Means of Flow-Injection into ESI-MS/MS. *J. Mass Spectrom.* **2005**, *40*, 1546–1549, doi:10.1002/jms.909.
  26. Linko, S.; Revitzer, H.; Zilliacus, R.; Kortensniemi, M.; Kouri, M.; Savolainen, S. Boron Detection from Blood Samples by ICP-AES and ICP-MS during Boron Neutron Capture Therapy. *Scand. J. Clin. Lab. Inv.* **2008**, *68*, 696–702, doi:10.1080/00365510802100831.
  27. Gibson, C.R.; Staubus, A.E.; Barth, R.F.; Yang, W.; Ferketich, A.K.; Moeschberger, M.M. Pharmacokinetics of Sodium Borocaptate: A Critical Assessment of Dosing Paradigms for Boron Neutron Capture Therapy. *J. Neurooncol.* **2003**, *62*, 157–169, doi:10.1023/A:1023288905708.
  28. Galé, A.; Hofmann, L.; Lüdi, N.; Hungerbühler, M.N.; Kempf, C.; Heverhagen, J.T.; Von Tengg-Kobligk, H.; Broekmann, P.; Ruprecht, N. Beyond Single-Cell Analysis of Metallodrugs by ICP-MS: Targeting Cellular Substructures. *Int. J. Mol. Sci.* **2021**, *22*, 9468, doi:10.3390/ijms22179468.
  29. Da Silva, A.B.S.; Arruda, M.A.Z. Single-Cell ICP-MS to Address the Role of Trace Elements at a Cellular Level. *J. Trace Elem. Med. Biol.* **2023**, *75*, 127086, doi:10.1016/j.jtemb.2022.127086.